Structural and biochemical characterisation of *O*-acetylserine sulphydrylase (CysK) from *Neisseria gonorrhoeae*

A thesis
submitted in partial fulfilment
of the requirements for the degree
of

Master of Science (Research) in Cellular and Molecular Biology

At

The University of Waikato

by

Jack McGarvie

THE UNIVERSITY OF
WAIKATO
Te Whare Wānanga o Waikato

2021

Abstract

Neisseria gonorrhoeae is the causative bacteria of the sexually transmitted infection (STI), gonorrhoea. Rapid emergence of antibiotic resistant strains of *N. gonorrhoeae* has given rise to almost untreatable gonorrhoea over the last few decades. There is an urgent need for development of new antimicrobial treatments for gonorrhoea infection. Synthesis of the amino acid cysteine is a promising new target for the development of new antimicrobials. Cysteine plays a vital role in protein folding and function, and synthesis of glutathione for protection against oxidative stress during infection.

The final step of the two-step cysteine biosynthesis pathway is catalysed by the enzyme *O*-acetylserine sulphydrylase (OASS). Most bacteria have two isoforms of OASS, OASS-A/CysK that utilises sulphide and *O*-acetylserine for the synthesis of cysteine and OASS-B/CysM that utilises thiosulphate. *N. gonorrhoeae* has just one OASS isoform (annotated as CysK) in its genome. *N. gonorrhoeae* displays unique differences in its sulphate acquisition pathway for cysteine biosynthesis, yet little is known about these pathways in *N. gonorrhoeae*. We propose CysK is a potential antimicrobial target. This thesis biochemically characterises the structure and function of CysK to determine its role in cysteine biosynthesis. Kinetic characterisation demonstrates that CysK has *O*-acetylserine sulphydrylase activity and displays positive cooperativity with respect to substrates, *O*-acetylserine and sulphide. Sulphide shows partial allosteric inhibition, and the enzyme does not use thiosulphate as a substrate. The structure of CysK was solved to 2.49 Å by X-ray crystallography and shows CysK belongs to the tryptophan synthase β superfamily and adopts a homodimeric structure consisting of two monomers. The structure supports positive cooperativity as co-factor binding residues are in inactive and active conformations in each monomer of the dimer, respectively. Many CysK enzymes form complexes with the first enzyme in the two-step cysteine synthesis pathway, CysE. It appears CysE and CysK from *N. gonorrhoeae* are unable to form a complex, indicating an alternate pathway for regulation of sulphur flux and cysteine production. Attempts to investigate the *in vivo* role of CysK were inconclusive.

The research presented in this thesis represents a major leap in our understanding of the uncharacterised cysteine biosynthesis pathway in *N. gonorrhoeae*. Data presented here is the basis for future work using the kinetics and structure of CysK to guide computational inhibitor design, to identify lead compounds for CysK inhibition, and thereby development of new antimicrobials for treatment of extensively drug resistant gonorrhoea.

Acknowledgements

I would like to thank my super supervisor Dr. Joanna Hicks. Thank you for your never-ending support and guidance during my masters. You were always available to answer my questions and to help me solve any issues I encountered, despite your extreme workload, whether it was a quick 5 minute zoom call or even a passing conversation in the hallway when you were on your way to teaching.

I would also like to thank Annmaree Warrender for being a fantastic supervisor over my time as a summer research student. You taught me the appropriate lab etiquette and procedure and introduced me to the exciting world of research. Your constant help and patience with my incessant questions was awesome and I would not have coped in the lab environment without your oversight. You helped me develop the confidence to work independently and problem solve on the spot, which I am ever grateful for.

Thank you to the past and present members of the Proteins and Microbes lab group: Dr Judith Burrows, Dr Emma Summers, Dr Erica Prentice, Dr Adele Williamson, Professor Vic Arcus, Carlin, Andrew, Keely, Emily, Liz, Jolyn, Bronwyn, Daniel, Meghan, Stacy, Hannah, Ricki, Ashleigh-Amanda, Allen, Rudi, Marion, Dr Olivia Patty, Dr Greg Jacobson and Dr. Ray Cursons. My years in this lab so far have been fun, inspiring and exciting thanks to all of you. A special thank you in particular to Keely, Annmaree, Emily and Carlin for your invaluable insights, constant help and support during my research. I would also like to thank Shaun and Savannah for enduring the frustrations of MSc research with me and helping me maintain my sanity.

Thank you to the University of Waikato for my MSc Research Scholarship and the Sir Edmund Hillary Senior Leadership Scholarship.

Lastly, a huge thank you to my family for their unwavering support and pride in what I do. Thank you for constantly reading my assignments, proposals and being interested in my research (despite not always understanding it). Your love and encouragement has kept me going on many a long night.

Table of Contents

List of Figures

List of Tables

List of Equations

Glossary

A	alanine, amino acid
ABC	ATP-binding cassette
Ala	alanine, amino acid
AMR	antimicrobial persistence
APS^1	adenosine 5'-phosphosulphate
APS^2	ammonium persulphate
Arg	arginine, amino acid
Asn	asparagine, amino acid
Asp	aspartate, amino acid
ASU	asymmetric unit
ATP	adenine tri-phosphate
AWH	(3-((Z)-((Z)-5-(4-Fluorobenzylidene)-3-methyl-4-oxothiazolidin-2-ylidene) amino) benzoic Acid)
C	cysteine, amino acid
CDC	centre for disease control and prevention
CEACAM	carcinoembryonic antigen cell adhesion molecule
Cl^-	chloride ion
CSC	cysteine synthase complex
C-terminal	carboxy terminus
CysE	serine acetyltransferase
CysK	*O*-acetylserine sulphydrylase-A
CysM	*O*-acetyserine sulphydrylase-B
D	aspartate, amino acid

DNA	deoxyribose nucleic acid
DTT	dithiothreitol
DUS	DNA uptake sequence
ESC	extended-spectrum cephalosporin
F	phenylalanine, amino acid
FPLC	fast protein liquid chromatography
FWD	forward sequence
G	glycine, amino acid
GC	gonococcus
GCB	gonococcus base
Gln	glutamine, amino acid
Glu	glutamate, amino acid
Gly	glycine, amino acid
h	hill constant
His	histidine, amino acid
I	isoleucine, amino acid
IC_{50}	concentration of inhibitor where activity is reduced to 50%
Ile	isoleucine, amino acid
IMAC	immobilised metal affinity chromatography
IPTG	isopropylthio-B-D-galactosidase
K	lysine, amino acid
K_{av}	gel phase distribution co-efficient
k_{cat}	enzyme rate constant
k_{cat}/K_M	catalytic efficiency constant

kDa	kilodalton
K_{half}	Michaelis constant
K_i	inhibitor constant
K_M	Michaelis constant
KO	knockout
LB	Luria Bertani
Leu	leucine, amino acid
LOS	lipooligosaccharide
Lys	lysine, amino acid
M	methionine, amino acid
MFS	major facilitator superfamily
min	minutes
MOPs	3-(*N*-morpholino)propanesulfonic acid
MQ	milliQ ultrapure water
MW	molecular weight
N	asparagine, amino acid
Na_2S	sodium sulphide
nm	nanometer
NOD	nucleotide-binding oligomerisation domain
NRA	no reducing agent
N-terminal	amino terminus
OAS	*O*-acetylserine
OASS	*O*-acetylserine sulphydrylase
OMVs	outer membrane vesicles

Opa	opacity-associated
P	proline, amino acid
PAGE	polyacrylamide gel electrophoresis
PAPS	phosphoadenosylphosphosulphate
PCR	polymerase chain reaction
PDB	protein databank
Phe	phenylalanine, amino acid
PLP	pyridoxal 5'-phosphate
PMNs	polymorphonuclear neutrophils
Pro	proline, amino acid
Q4	quenching buffer
REV	reverse sequence
ROS	reactive oxygen species
rpm	revolutions per minute
RSAP	reductive sulphate assimilation pathway
S	serine, amino acid
S^{2-}	sulphide ion
SAT	serine acetyltransferase
sbp	sulphate binding protein
SDS	sodium dodecyl sulphate
sec	seconds
Ser	serine, amino acid
STI	sexually transmitted infection
T	threonine, amino acid

TAE	tris-acetate-EDTA
TCA	trichloroacetic acid
TEMED	tetramethylethylenediamine
Thr	threonine, amino acid
TLRs	toll-like receptors
TNB	5-thio-2-nitrobenzoate
tNCS	translational non-crystallographic symmetry
Tris	tris(hydroxymethyl)aminomethane
Trp	tryptophan, amino acid
Tyr	tyrosine, amino acid
US	United States
v	rate
v/v	volume per volume
Val	valine, amino acid
Vmax	maximum reaction rate
w/v	weight per volume
WHO	World Health Organisation
XDS	X-ray detector software

Chapter 1

Introduction

1.1 Introduction

Neisseria gonorrhoeae is the causative agent of the sexually transmitted infection (STI) gonorrhoea (Hill *et al.*, 2016; Wi *et al.*, 2017). *N. gonorrhoeae* is a Gram-negative, diplococcus (referred to as gonococcus, GC), obligate human pathogen primarily transmitted through sexual contact (Hill *et al.*, 2016). Records of the contagious nature of *N. gonorrhoeae* can be seen in biblical times, indicating gonorrhoea to be one of the oldest recorded human diseases (Edwards & Apicella, 2004). More than 60 million cases of gonorrhoea were reported annually in 1996 (Gerbase *et al.*, 1998), with numbers increasing to an estimated over 85 million cases worldwide in 2016, making it the third most prevalent STI worldwide (Rowley *et al.*, 2019). Alongside this, an increasing number of strains have developed antimicrobial resistance (AMR) to every available antibiotic used for its treatment (Wi *et al.*, 2017). Due to the combination of both increasing prevalence and increasing AMR, the World Health Organisation (WHO) has labelled *N. gonorrhoeae* as a high priority pathogen (WHO, 2017). All three of these factors have created an increased demand for the development of new antimicrobial agents to treat this disease in the future. Targeting and prevention of amino acid biosynthesis in bacteria is one such new and promising avenue for this development. The amino acid cysteine is not only crucial for protein folding and function, and protection from oxidative stress during infection, but its biosynthesis is the primary pathway for sulphur acquisition in bacterial cells (Hatzios & Bertozzi, 2011; Takumi & Nonaka, 2016; Ren *et al.*, 2017; Anderson *et al.*, 2019). Therefore, making cysteine biosynthesis a promising target for development of new antimicrobial drugs. This pathway, however, remains uncharacterised in *N. gonorrhoeae*. This research investigates the enzyme CysK *O*-acetylserine sulphydrylase (CysK), which is involved in the final step of cysteine biosynthesis, as a potential antimicrobial target in *N. gonorrhoeae.*

1.2 Pathogenesis of Gonorrhoea

N. gonorrhoeae has evolved alongside humans for millennia, resulting in its host restriction to humans, and thus its obligate human pathogenicity (Landig *et al.*, 2019). The ability of *N. gonorrhoeae* to mitigate host immune responses through a variety of mechanisms heavily contribute to its pathogenic success. *N. gonorrhoeae* infects a variety

of mucosal surfaces such as the urethra, the endocervix, the ectocervix, the nasopharynx, conjunctiva (inside of eyelids and the white surface of eyes) and the rectum with the urogenital epithelia (urethra, endocervix and ectocervix) being the most common sites of infection (Edwards & Apicella, 2004; Edwards & Butler, 2011; Hill *et al.*, 2016; Wi *et al.*, 2017; Landig *et al.*, 2019; Rowley *et al.*, 2019). It is also common for new-born babies to contract *N. gonorrhoeae* infection in their anus, nasopharynx and eyes from mothers with gonorrhoea (Sandstrom, 1987).

Gonorrhoeal infection begins with colonisation of the mucosal membrane, via adhesion to the epithelial cells through four established adhesins; (1) the major outer membrane protein, porin, (2) two types of opacity-associated (Opa) proteins, Opa_{50} and Opa_{52}, (3) a major glycolipid of the outer membrane of gonococcus (GC), lipooligosaccharide (LOS) which lacks the repeating O-antigen of lipopolysaccharide, and (4) long polymers of pilin proteins that protrude from the GC surface, type IV-A pili (Edwards & Butler, 2011). The mode of adhesion used by GC is dependent on specific cell type, site of infection, and gender (Edwards & Apicella, 2004). Once initial adhesion occurs, the gonococci begin to form micro-colonies on non-ciliated columnar epithelial cells 1 – 2 hours after infection (Hill *et al.*, 2016). From this stage, the general process involves the pilus-mediated attachment of the GC to the CD46 host cell-surface receptors. This begins once the micro-colonies reach a cell density of 100+ GC (Figure 1.1) (Hill *et al.*, 2016). Tighter binding to the host cells is mediated via PilE depolymerisation of pilus structures which is followed by Opa binding to CEACAM receptors (Figure 1.1) (Hill *et al.*, 2016). Actin polymerisation and rearrangement is induced within the host cells. This results in bacterial endocytosis into host cells, transcellular transcytosis or trafficking of bacteria to the basolateral side of cells where they are exocytosed into the subepithelial layer (Figure 1.1) (Hill *et al.*, 2016). GC isolated from the male urethra show co-expression of pili and at least one of several Opa proteins. In women however, Opa expression varies depending on the stage of the menstrual cycle, and the consumption of oral contraceptives (Hill *et al.*, 2016). The adhesion process GC undertakes is thus dependent upon the nature of its host. In some infections, *N. gonorrhoeae* is able to remain inside mucosal cells, in a dormant state, avoiding activation of the immune system (Hopper *et al.*, 2000).

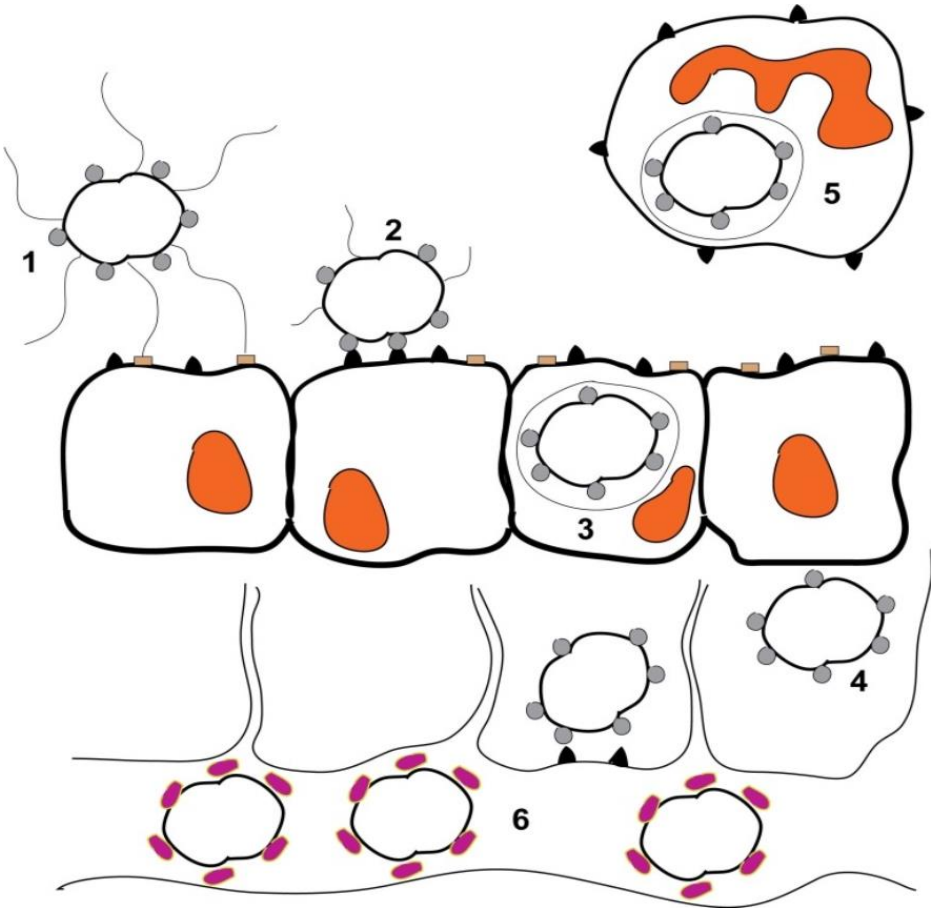

Figure 1.1: Schematic representation of a *N. gonorrhoeae* infection. (1) Piliated, Opa-expressing gonococci interact with the mucosal epithelium. The thin, hair-like pilus appendages provide the initial contact with receptors on the surface of the mucosal cells. (2) Pili are then retracted which allows for more intimate, Opa-mediated attachment of the bacteria with the CD66 antigens located on the mucosal cells. (3) Following Opa-mediated attachment, the bacteria are engulfed and are internalised into the mucosal cells. (4) Following internalisation, some bacteria can transcytose to the basolateral side of the mucosal epithelium. (5) Depending upon which Opa protein is being expressed, gonococci can also reside and survive inside of neutrophils. (6) Following transcytosis, gonococci can enter the bloodstream where heavy sialylation of lipooligosaccharide (LOS) renders the bacteria serum resistant. Figure from (Hill *et al.*, 2016).

Upon attachment to mucosal cells, or entrance into the sub-epithelial layer, an immune response is triggered (Hill *et al.*, 2016). This immune response involves recruitment of pro-inflammatory cytokines and neutrophils to the infection site, leading to the observable symptoms of GC infection, localised inflammation and pustular discharge (Ramsey *et al.*, 1995; Fisette *et al.*, 2003; Hill *et al.*, 2016; Anderson *et al.*, 2019). This initial infection causes uncomplicated cervicitis in women, and urethritis in men, both of which present observable symptoms and are local infections (Unemo & Shafer, 2014). However, in many cases, *N. gonorrhoeae* is in a persistent state, presenting an asymptomatic subclinical infection where no immune response is triggered (Workowski & Berman, 2011). Asymptomatic subclinical infections result in persistent GC infection. This affects women disproportionately to men, occurring in 50% of cases compared to 10% respectively (Workowski & Berman, 2011).

Persistent bacteria are a subpopulation of bacteria that differentiate to become dormant and significantly decrease their rate of division (Kussell *et al.*, 2005; Balaban, 2011). This improves the bacteria's ability to survive environmental stresses such as nutrient starvation or antibiotic treatments (Kussell *et al.*, 2005; Balaban, 2011). Bacteria in this persistent state have a higher tolerance to antibiotics as they downregulate the replication and division cellular processes that are targeted by antibiotics, sometimes completely avoiding antibiotic exposure (Lewis, 2010; Balaban, 2011; Maisonneuve & Gerdes, 2014). This persistence is different to antibiotic resistant phenotypes, which prevent antibiotics from binding to their targets (Lewis, 2010). Once environmental stresses have attenuated, the dormant subpopulation can upregulate its cellular growth pathways, actively dividing, thus repopulating their environment (Balaban, 2011).

Untreated asymptomatic GC infections can over time enter a carrier state. In the carrier state, apparently healthy individuals carry the disease and are able to transmit the infection, or it can allow GC to ascend into the upper urogenital tract leading to more complicated infections (Hopper *et al.*, 2000; Edwards & Apicella, 2004; Edwards & Butler, 2011). Complications include pelvic inflammatory disease, salpingitis (acute inflammation of the fallopian tubes) and endometritis, all of which can lead to infertility or an ectopic pregnancy (where pregnancy occurs outside the uterus and is often life-threatening) (Hopper *et al.*, 2000; Fisette *et al.*, 2003; Edwards & Apicella, 2004; Edwards & Butler, 2011; Rowley *et al.*, 2019). In rare cases, certain strains are capable of dissemination, crossing the endothelium, resulting in septic arthritis, pustular skin lesions, and bacteraemia (presence of bacteria in the blood stream, which can cause serious harm to the body and spread to other organs) (Hopper *et al.*, 2000; Fisette *et al.*, 2003; Edwards & Apicella, 2004; Hill *et al.*, 2016; Rowley *et al.*, 2019). Nasopharyngeal infections are of particular concern, due to their asymptomatic nature and hypothesised role as one of the main routes for acquisition of antimicrobial resistant genes (Unemo & Shafer, 2014). *N. gonorrhoeae* is naturally transformable, readily accepting DNA, such as antibiotic resistant plasmids, from the environment into its chromosome, even if these plasmids are present during periods of persistence (Ochman *et al.*, 2000). The ability to naturally transform, plays a large role in the antigenic variation generated by *N. gonorrhoeae.* This allows evasion of the immune systems recognition of the pathogen, thus allowing multiple infections to occur in an individual over their lifetime (Stern *et al.*, 1986; Criss *et al.*, 2005; Hill *et al.*, 2016).

1.3 Surfacing of antibiotic resistant *Neisseria gonorrhoeae*

The WHO has labelled *N. gonorrhoeae* as a high priority pathogen due to the rapid surfacing of antibiotic resistant strains (WHO, 2017). *N. gonorrhoeae* has the highest levels of AMR across all STIs. Over the last 70 to 80 years, *N. gonorrhoeae* has become increasingly resistant to an extensive range of antibiotic classes including: fluoroquinolones, macrolides, sulphonamides, penicillins, tetracyclines, and early generation cephalosporins (Unemo & Shafer, 2014; Wi *et al.*, 2017; Bodie *et al.*, 2019). The only remaining empirical monotherapy for gonorrhoeal treatment is the injectable extended-spectrum cephalosporin (ESC) ceftriaxone. However, treatment failures and *in vitro* resistance to cefixime and ceftriaxone alongside high-level clinical resistance to all ESCs has been found in many countries (Unemo & Shafer, 2014; Wi *et al.*, 2017). Combined with the possibility of *N. gonorrhoeae* developing AMR to any monotherapy antibiotic, it was thought that monotherapy was no longer an option (Unemo & Shafer, 2014; Bodie *et al.*, 2019; Unemo *et al.*, 2020). Thus, to combat AMR development, particularly to ceftriaxone as the only effective monotherapy antibiotic, dual-therapy of the ESC ceftriaxone combined with the oral antibiotic azithromycin was recommended (Unemo & Shafer, 2014; Kidd & Workowski, 2015; Wi *et al.*, 2017; Unemo *et al.*, 2020). However, AMR to ceftriaxone and azithromycin is on the rise, on a global scale (Unemo & Shafer, 2014; Eyre *et al.*, 2018; Fifer *et al.*, 2018; Bodie *et al.*, 2019; George *et al.*, 2019; Cyr *et al.*, 2020). In 2018, strains of *N. gonorrhoeae* that were completely resistant to both ceftriaxone and azithromycin were isolated in the UK (Eyre *et al.*, 2018; Jennison *et al.*, 2019). These cases resulted in three days of hospitalisation with last resort intravenous antibiotic treatment for the patients. There have been no cases of treatment resistant gonorrhoea in New Zealand, however, ceftriaxone and azithromycin resistance have been detected in several district health boards (Lee *et al.*, 2018). Antimicrobial susceptibility of 400 New Zealand *N. gonorrhoeae* was tested in a recent study, revealing around 4 and 10% of isolates had decreased susceptibility to ceftriaxone and azithromycin respectively (Lee *et al.*, 2018). Combined with the increasing incidence of gonorrhoea infection in New Zealand and across the globe (Lee *et al.*, 2018; Rowley *et al.*, 2019), the possibility of ceftriaxone and azithromycin resistant gonorrhoea emergence in New Zealand is ever increasing.

As a result of increasing evidence of strains resistant to dual-therapy and azithromycin in particular, the United States (US) Centre for Disease Control and Prevention (CDC) updated its treatment guidelines in 2020, recommending monotherapy with ceftriaxone

(Cyr *et al.*, 2020). Subsequently, the 'super-bug' status, alongside *N. gonorrhoeae's* labelling as a 'high priority pathogen' by the WHO demonstrates the urgent need for research to develop both vaccines to reduce the spread of gonorrhoea, and new antimicrobial agents for treatment of AMR gonorrhoea infections (WHO, 2017). New antimicrobial targets for the design of new antibiotics are in critical demand. One such approach, is targeting the pathways and mechanisms essential for infection and survival of *N. gonorrhoeae.*

The sulphur assimilation and cysteine biosynthetic pathways play an integral role in survival of many persistent pathogens and as such provide a new and promising area for antimicrobial research (Campanini *et al.*, 2014). This avenue has been investigated for development of antimicrobials for treatment of pathogens such as the tuberculosis causing bacterium, *Mycobacterium tuberculosis,* or the acute gastroenteritis causing bacterium, *Salmonella typhimurium* (Campanini *et al.*, 2014). We hypothesise these pathways are also a valid target in *N. gonorrhoeae.*

1.4 Oxidative stress and the role of L-cysteine in *N. gonorrhoeae*

The primary method of environmental inorganic sulphur acquisition in almost all bacteria requires L-cysteine biosynthesis. Cysteine residues play a vital role in protein folding, structure and therefore function, through the disulphide bonds they form (Takumi & Nonaka, 2016). Cysteine is also used to form an array of vital biomolecules such as biotin, co-enzyme-A and iron sulphur clusters (Kredich, 2008; Takumi & Nonaka, 2016; Hicks & Mullholland, 2018). Cysteine is also utilised for producing reducing agents thioredoxin and glutathione, which are essential for mitigating intracellular oxidants (Carmel-Harel & Storz, 2000; Kredich, 2008; Hicks & Mullholland, 2018).

One of the primary challenges for bacteria, in particular pathogenic bacteria, is surviving the hostile host environment and evading the host immune system, both of which *N. gonorrhoeae* is proficient in (Quillin & Seifert, 2018). *N. gonorrhoeae* inhabits an environment of unrelenting oxidative stress and is constantly under pressure of oxidative killing from the host (Seib *et al.*, 2006). Thus, making mechanisms to mitigate this oxidative stress of extreme importance. There are two main sources of oxidative stress *N. gonorrhoeae* is exposed to; oxidative stress produced by commensal *Lactobacillus* species, and the host immune system. The immune system exerts this oxidative killing

mechanism primarily through polymorphonuclear neutrophils (PMNs) (Seib *et al.*, 2006; Quillin & Seifert, 2018).

Lactobacilli are one of the most prevalent micro-flora of the female urogenital tract (Larsen & Monif, 2001). *Lactobacillus* species have been shown to inhibit *N. gonorrhoeae* colonisation of the urogenital tract (Larsen & Monif, 2001; Seib *et al.*, 2006). *Lactobacillus* species secrete lactate, which lowers pH, promoting aerobic respiration, which leads to endogenous production of reactive oxygen species (ROS) (Seib *et al.*, 2006). *Lactobacilli* also secrete hydrogen peroxide, which is shown to inhibit growth of *N. gonorrhoeae* at a more acidic pH (Larsen & Monif, 2001; Seib *et al.*, 2006). It was also found that *Lactobacillus* and *Candida* species may co-colonise the female urogenital tract (Larsen & Monif, 2001). In addition, *Candida* species were found to produce gliotoxin, a substance that supresses the growth of *N. gonorrhoeae* (Hipp *et al.*, 1974; Larsen & Monif, 2001).

Oxidative stress from the host immune system begins with colonisation of the surface of cell epithelia. During colonisation, *N. gonorrhoeae* releases outer membrane vesicles (OMVs) and LOS, which bind to nucleotide binding oligomerisation domain (NOD) and toll-like receptors (TLRs) on dendritic cells and macrophages (Fisette *et al.*, 2003; Liu *et al.*, 2006; Quillin & Seifert, 2018). Upon binding, a signalling cascade results in release of chemokines and cytokines (Fisette *et al.*, 2003; Liu *et al.*, 2006; Hill *et al.*, 2016; Quillin & Seifert, 2018). Release of the cytokines recruits PMNs to the site of infection (Edwards & Apicella, 2004; Hill *et al.*, 2016; Quillin & Seifert, 2018). PMNs phagocytose *N. gonorrhoeae*, using antibacterial peptides, proteases and neutrophil mediated oxidative burst (rapid release of ROS). The oxidative burst results in superoxide anion formation, which leads to further ROS (Seib *et al.*, 2006; El-Benna *et al.*, 2016; Quillin & Seifert, 2018). Phagocytosis is an effective method for killing most bacteria, however, *N. gonorrhoeae* has evolved the ability to survive this process, mitigating the oxidative burst and replicating within the PMNs (Simons *et al.*, 2005). The purulent excretion, which is characteristic of gonorrhoea infection, is largely comprised of PMNs infected with *N. gonorrhoeae* (Hill *et al.*, 2016). For *N. gonorrhoeae* to be capable of

mitigating this oxidative stress, an effective intracellular reducing system is required. Most of the compounds that comprise this system are derived from L-cysteine.

One such compound is glutathione, which is synthesised by glutathione reductase. Glutathione's role in the cell is to regulate the redox balance when encountering free radicals released by the host cell and to prevent unwanted oxidation of cellular contents (Meister & Anderson, 1983; Pinto *et al.*, 2013). Therefore, glutathione levels are one of the main oxidative stress mitigating mechanisms encountered during infection. Glutathione synthesis systems are present in *N. gonorrhoeae* (Hicks & Mullholland, 2018), however, there is a distinct lack of glutathione transportation systems (Seib *et al.*, 2006). Given the lack of transporters, glutathione synthesis in *N. gonorrhoeae* is dependent on the cysteine biosynthetic pathway (Hicks & Mullholland, 2018).

1.5 Sulphate assimilation and cysteine biosynthesis in *Neisseria* species

The *de novo* biosynthesis of L-cysteine has been extensively studied and is conserved across bacteria, protozoa and higher plant species (Mino & Ishikawa, 2003; Jeelani *et al.*, 2017). This is the main pathway for these organisms to acquire environmental inorganic sulphur (Nozaki *et al.*, 1999; Jeelani *et al.*, 2017). *Neisseria meningitidis* and *N. gonorrhoeae* share a large degree of genome similarity (90%) (Hicks & Mullholland, 2018), however, there are key differences between these two pathogenic *Neisseria* species. Namely, sulphate acquisition and cysteine synthesis pathways, which will be discussed in this section.

1.5.1 Active sulphate transport

Cysteine biosynthesis begins with the import of sulphur into the cell, and subsequent reduction via the reductive sulphate assimilation pathway (RSAP) (Campanini *et al.*, 2014). There are two main families of sulphate transporter proteins responsible for the uptake of inorganic sulphate into microbial cells, the major facilitator superfamily (MFS) and the ATP-binding cassette (ABC) superfamily (Kertesz, 2001; Guédon & Martin-Verstraete, 2007). These transporters actively import sulphate into the cell. Genomic analysis of pathogenic *Neisseria* species (*N. meningitidis* and *N. gonorrhoeae*) showed

that *N. gonorrhoeae* only has one sulphate uptake system, from the ABC transporter superfamily (Figure 1.2) (Hicks & Mullholland, 2018).

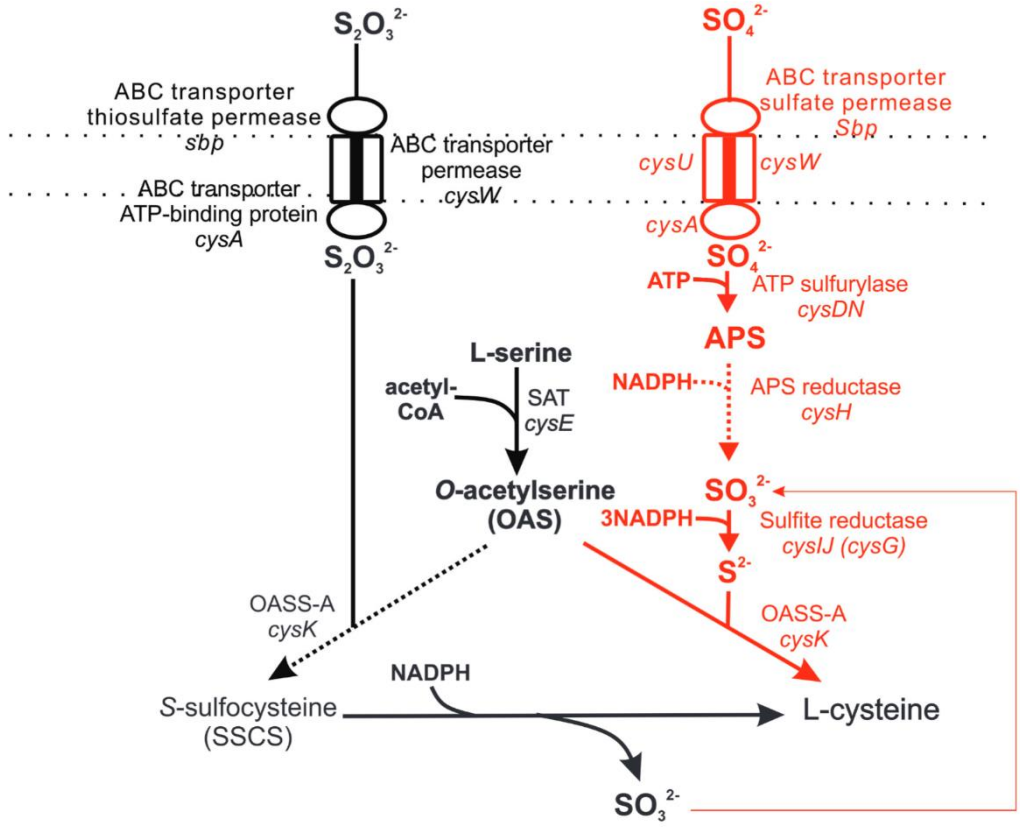

Figure 1.2: Sulphate acquisition and cysteine biosynthetic pathways in *Neisseria* species. The sulphate reduction pathway absent in *N. gonorrhoeae* is shown in red. Red and black pathways are functional in *N. meningitidis.* Differences between *Neisseria* species and other bacterial species are shown by two dotted lines. Figure from (Hicks & Mullholland, 2018).

This is composed of a transporter permease (*cysW*), an ATP-binding protein (*cysA*), periplasmic sulphate-binding protein (*sbp*) and a sulphate permease (*cysU*) (Kertesz, 2001; Hicks & Mullholland, 2018). The sulphate permease (*cysU*) is present in both *Neisseria* species except for the FA1090 *N. gonorrhoeae* strain (Hicks & Mullholland, 2018). The sbp transporter has previously been shown to transport sulphate (Kredich, 2008) and given that *N. gonorrhoeae* is able to grow with thiosulphate as a sole source of sulphur (Le Faou, 1984), this indicates that sbp is able to transport thiosulphate in *N. gonorrhoeae* (Hicks & Mullholland, 2018).

1.5.2 Sulphate Reduction

After importation into the cell, sulphate is prepared for incorporation into L-cysteine through successive reduction of sulphide (Figure 1.2). In *E. coli,* sulphate is first reduced to adenosine 5'-phosphosulphate (APS[1]) by the multi-enzyme complex ATP sulphydrylase (CysDN) (Sekowska *et al.*, 2000). In most bacteria, APS[1] is reduced to

phosphoadenosylphosphosulphate (PAPS) by ATP-kinase (CysC), and is subsequently reduced by PAPS reductase (CysH), to sulphite and phosphoadenosylphosphate (PAP) (Sekowska *et al.*, 2000; Kredich, 2008). However, in *Neisseria* species, both reduction of APS^1 to PAPS, and subsequent reduction to PAP is carried out by a single enzyme, APS^1 reductase (which is also denoted as CysH). This is therefore a single step reaction from APS^1 reduced directly to sulphite (Figure 1.2) (Rusniok *et al.*, 2009). The final step of the sulphate reduction pathway involves reduction of sulphite to sulphide by the sulphite reductase (CysIJ) (Kredich, 2008). Sulphide is then incorporated with *O*-acetylserine to form L-cysteine (Figure 1.2).

Genome analysis of *Neisseria* species revealed the variance in completeness and arrangement of the sulphate reduction pathway (Hicks & Mullholland, 2018). In *N. meningitidis*, both import and reduction genes are controlled by a single operon *cysGHDNJI*. However, in all *N. gonorrhoeae* strains examined by Hicks and Mullholland (2018), a 3.5 kb deletion between *cysG* and *cysN* genes, has removed *cysH* and *cysD* from this operon (Figure 1.3) (Hicks & Mullholland, 2018). These genes are not found anywhere else in the *N. gonorrhoeae* genome (Hicks & Mullholland, 2018). The sulphite reductase encoding genes, *cysIJ*, are present in the *N. gonorrhoeae* genome, however, they are non-functional due to an in-frame stop codon present in each coding sequence (Figure 1.3) (Hicks & Mullholland, 2018). *cysD* deletion would prevent *N. gonorrhoeae* from reducing sulphate to APS^1, alongside *cysH* deletion preventing subsequent reduction of APS^1 to sulphite. The in frame stop codons in *cysIJ* would prevent reduction of sulphite to sulphide. The combination of these deletions and in frame stop codons renders this pathway of sulphate reduction non-functional in *N. gonorrhoeae*. Investigation of the sulphur requirements of *Neisseria* species, demonstrated the inability of *N. gonorrhoeae* to grow on sulphate as its sole source of sulphur (Le Faou, 1984). This is consistent with the non-functional sulphate reduction pathway in *N. gonorrhoeae* described above. Other commensal species and some strains of *N. meningitidis*, however, can grow on sulphate as a sole sulphur source. Previous growth experiments demonstrated *N. gonorrhoeae's* ability to grow on media supplemented with thiosulphate, in the absence of L-cysteine (Le Faou, 1984). The requirement for L-cysteine, being met by thiosulphate links to the non-functional sulphite reducing pathway and suggests that the ABC transporter complex is able to import both thiosulphate and sulphate (Hicks & Mullholland, 2018).

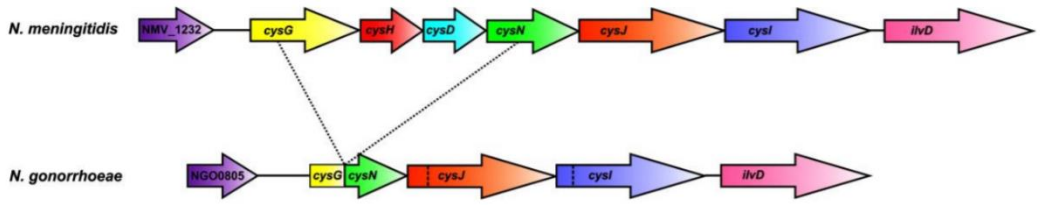

Figure 1.3: Comparison of the sulphate reduction operons from *N. meningitidis* and *N. gonorrhoeae*. Dotted lines show a deletion between *cysG* and *cysN* in *N. gonorrhoeae*, resulting in a deletion between *cysG* and *cysN* in *N. gonorrhoeae*. This causes deletion of *cysH* and *cysD* and the partial truncation of *cysG* and *cysN*. Direction of arrows indicates direction of transcription. Dashed lines show stop codons in pseudogenes of *N. gonorrhoeae*. Figure from (Hicks & Mullholland, 2018).

1.5.3 L-Cysteine and L-Cystine transport

It is well established that *de novo* cysteine biosynthesis is well conserved across bacteria and many other species, however, bacteria can also obtain L-cysteine directly from the environment. Under oxidative conditions, L-cysteine is more commonly found in its oxidised form L-cystine (a disulphide bond is formed between two L-cysteine molecules) (Korshunov *et al.*, 2020). In *Neisseria* species, L-cysteine and L-cystine are actively imported into the cell via ABC-transporters. *N. gonorrhoeae* has ABC transporters for both L-cysteine (*ngo2011-2014*), and L-cystine (*ngo0372-0374*) (Figure 1.4) (Bulut *et al.*, 2012; Hicks & Mullholland, 2018). Interestingly, in *N. meningitidis*, homology searches of the genome showed the presence of only the L-cystine transporter *nmb0786-0789* (Figure 1.4). The cystine ABC transporter operon in *N. meningitidis* shows 97% identity to the *ngo0372-0374* L-cystine ABC transporter operon indicating similar modes of cystine transport in both species (Hicks & Mullholland, 2018). *N. gonorrhoeae* and *N. meningitidis* genome comparisons (90% sequence homology), however, demonstrated complete deletion of the L-cysteine ABC transporter operon from *N. meningitidis*. Further research indicated these genes were not present anywhere in the *N. meningitidis* genome (Hicks & Mullholland, 2018). This suggests *N. meningitidis* relies on L-cystine import and *de novo* cysteine biosynthesis to meet its L-cysteine demands, or otherwise, has an alternate transporter for L-cysteine (Hicks & Mullholland, 2018). This difference may be due to variance in cysteine/cystine availability in the host infection sites of *N. gonorrhoeae* and *N. meningitidis*.

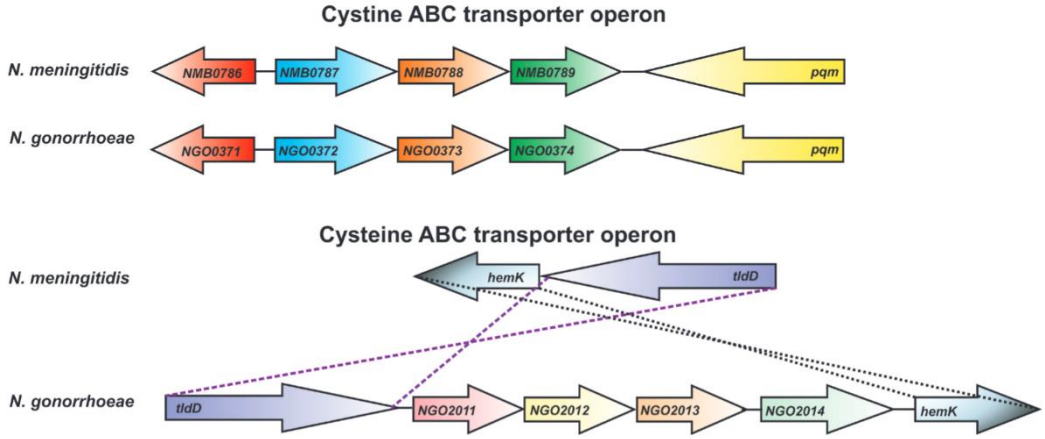

Figure 1.4: Comparison of L-cysteine and L-cystine ABC transporters in *N. gonorrhoeae* and *N. meningitidis*. The complete cystine ABC transporter is present in both *Neisseria* species (top). The cysteine ABC transporter operon present in only *N. gonorrhoeae* (bottom). Directions of arrows indicate direction of transcription. Dashed lines represent areas of homology. Figure from (Hicks & Mullholland, 2018).

Importation of L-cysteine and L-cystine from the environment is well conserved across many species of bacteria, particularly in pathogens. This provides an advantage over *de novo* synthesis of L-cysteine, as importation is a less energy dependent process (Takahashi *et al.*, 2018). However, transportation alone would not be ideal in an oxidative environment, such as the infection sites of both *N. gonorrhoeae* and *N. meningitidis*, or a cysteine/cystine deplete environment, therefore justifying the need for *de novo* biosynthesis of L-cysteine.

1.5.4 Cysteine biosynthesis

The cysteine biosynthesis pathway is a two-step reaction, catalysed by two enzymes, serine acetyltransferase (SAT) and *O*-acetylserine sulphydrylase (OASS), denoted as CysE and CysK/CysM (OASS isoforms), respectively. First, CysE catalyses the acetylation of L-serine, forming *O*-acetylserine and CoA (Figure 1.5). In the final step, *O*-acetylserine undergoes a CysK catalysed condensation reaction with sulphide to form L-cysteine (Figure 1.5). This two-step pathway is regulated at its first step by feedback inhibition with L-cysteine (Figure 1.5).

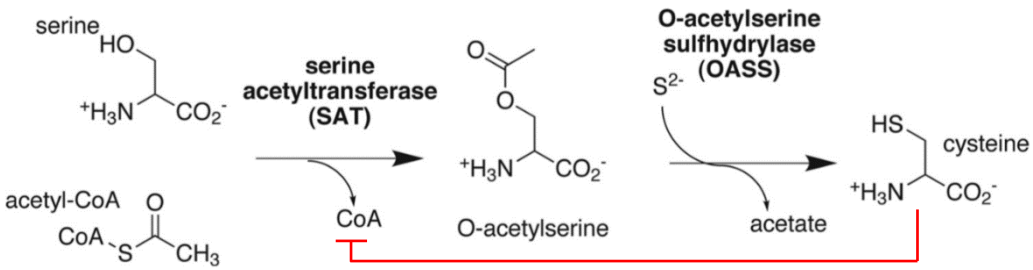

Figure 1.5: Cysteine biosynthesis pathway. CysE denoted as SAT and CysK denoted as OASS. Red line indicates cysteine feedback inhibition of CysE. Figure adapted from (Yi et al., 2013)

CysE is a member of the left-handed parallel β-helix family that catalyse the committed step in the *de novo* synthesis of L-cysteine in both plants and bacteria (Johnson *et al.*, 2005). CysE has been identified as an essential gene in *N. gonorrhoeae* (Remmele *et al.*, 2014) and while it is non-essential in *N. meningitidis*, the *cysE* deletion strain has impaired growth in media (Capel *et al.*, 2016). The cysteine feedback inhibition of CysE is well conserved across bacteria and is the primary method for prevention of high concentrations of L-cysteine, which are toxic to bacteria (Takumi & Nonaka, 2016; Benoni *et al.*, 2017b).

OASS belongs to the tryptophan synthase β superfamily and the β-family of pyridoxal 5'-phopshate (PLP) dependent enzymes making it a PLP dependent enzyme (Mino & Ishikawa, 2003; Guédon & Martin-Verstraete, 2007; Takumi & Nonaka, 2016). PLP is utilised as a cofactor in the active site of the enzyme. OASS has two isoforms, OASS-A (CysK) and OASS-B (CysM) (Kredich, 2008). Most bacteria have both CysK (OASS-A) and CysM (OASS-B) isoforms for cysteine biosynthesis using sulphide or thiosulphate respectively. *S. typhimurium* is one such example, where both OASS isoforms are present, however, CysK (OASS-A) was shown to be expressed in excess of CysM (OASS-B) under aerobic conditions, and vice versa under anaerobic conditions (Tai *et al.*, 1993). CysM differs from CysK, as it can directly utilise thiosulphate to produce S-sulphocysteine, which is then reduced to L-cysteine (Tai *et al.*, 1993). Interestingly, *Neisseria* species are unique in that they only have one OASS isoform. This has greatest homology to CysK (OASS-A) and is hypothesise to utilise sulphide for cysteine biosynthesis (Hicks & Mullholland, 2018). This raises interesting questions regarding the role of CysK in *N. gonorrhoeae*, with the bacterium's inability to reduce sulphate to sulphide and its reliance on thiosulphate for cysteine biosynthesis, a substrate that is usually utilised by the alternate OASS isoform CysM. While *cysK* is not an essential gene for pathogenic *Neisseria* species (Remmele *et al.*, 2014), it has been shown to be important for colonisation of epithelial cells in *N. meningitidis* and when knocked out results in both decreased fitness and increased susceptibility to antibiotics (Turnbull & Surette, 2010; Capel *et al.*, 2016).

1.6 Regulation of cysteine biosynthesis

1.6.1 Transcriptional regulation of sulphate acquisition and cysteine biosynthesis

Transcriptional regulation of the cysteine regulon is controlled by the master regulator CysB, a homotetramer, and a member of the LysR family of transcription factors (Jovanovic *et al.*, 2003; Hicks & Mullholland, 2018). The CysB N-terminal domain contains a helix-turn-helix motif which allows DNA binding to occur (Lochowska *et al.*, 2004). The CysE product OAS is unstable and rapidly non-enzymatically forms the isoform *N*-acetylserine, both of which cause CysB to positively regulate the sulphate acquisition and cysteine biosynthesis genes, however, *N*-acetylserine produces a markedly higher response (Ostrowski & Kredich, 1989; Hryniewicz & Kredich, 1991). It is proposed that binding of *N*-acetylserine causes a conformational change in CysB, which then binds to CysB binding regions and recruits RNA polymerase (Hicks & Mullholland, 2018). CysB has been shown to upregulate expression of sulphate acquisition genes *cysJIH*, *cysK*, and *cysP*, alongside negatively autoregulating its own transcription through binding upstream of its own promoter (Ostrowski & Kredich, 1989, 1991; Lochowska *et al.*, 2004). The DNA binding repeat for CysB (CCGTTG-N_{17}-CAACGG) was found in the *cysB* promoter region in both *N. gonorrhoeae* and *N. meningitidis* (Hicks & Mullholland, 2018). However, these binding sites could not be confirmed at the start of either the cysteine biosynthesis or the sulphate reduction regulon genes in *N. gonorrhoeae*. This could be a consequence of low conservation of the CysB binding sequences.

Transcriptional regulation of both the cysteine regulon and the sulphate acquisition pathway are of particular importance to pathogenic bacteria, as successful infection depends on the ability of the pathogen to rapidly adapt and overcome host defences. Alongside this, *cysB* has been identified as an essential gene in *N. gonorrhoeae* (Remmele *et al.*, 2014). CysB transcriptional regulation has control over many sulphate acquisition genes including that of *cysK* and thus, also has complete control over expression of the CysK protein.

1.6.2 The cysteine synthase complex

Feedback inhibition of CysE is not the only method through which sulphur flux throughout the cysteine biosynthesis pathway is regulated. The other mechanism for regulating sulphur flux in this pathway is the formation of the cysteine synthase complex (CSC). The complex is composed of the two enzymes that catalyse the two step cysteine biosynthesis pathway, CysE and CysK. Gel filtration chromatography and fluorescence studies have shown that this complex consists of a 3:2 protomer ratio, consisting of one CysE hexamer and two CysK dimers (Figure 1.6) (Kredich *et al.*, 1969; Johnson *et al.*, 2005; Benoni *et al.*, 2017b; Hicks & Mullholland, 2018).

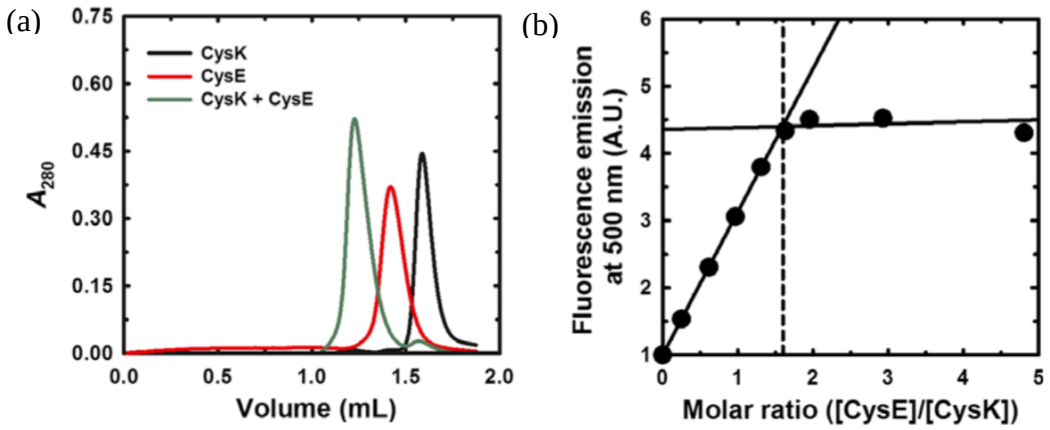

Figure 1.6: Analysis of the cysteine synthase complex from E. coli. (a) Gel filtration chromatograph of CSC, CysE and CysK. (b) Formation of the CSC through monitoring PLP emission at 500 nm with increasing [CysE:CysK] molar ratio. Figure adapted from (Benoni et al., 2017b).

This complex was first discovered during the purification of CysK and CysE from *S. typhimurium* (Kredich & Tomkins, 1966; Kredich *et al.*, 1969). Further evidence of CSC formation has been found in other bacterial species, including *E. coli* (Mino *et al.*, 2000; Benoni *et al.*, 2017b), *Haemophilus influenzae* (Huang *et al.*, 2005), and *M. tuberculosis* (Schnell *et al.*, 2007), as well as some plant species (Yi *et al.*, 2013). In this formation, the C-terminal tail of CysE inserts into the active site of CysK to inhibit its activity.

Formation of the CSC is essentially controlled by sulphur availability. When the complex is formed, CysE loses sensitivity to feedback inhibition by L-cysteine, and catalytic activity increases as a result of reduced substrate inhibition by L-serine (Benoni *et al.*, 2017b). With high availability of sulphur to the cell, the CSC is stabilised by bisulphide, conversely, when sulphur availability is low, *O*-acetylserine (OAS) accumulates, signalling sulphur starvation and dissociation of the complex (Zhao *et al.*, 2006; Benoni

et al., 2017b). Dissociation of the CSC can occur at µM OAS concentrations (upwards of 50µM OAS) (Kredich *et al.*, 1969; Wang & Leyh, 2012), OAS is then able to non-enzymatically isomerise to *N*-acetylserine, which can bind to transcriptional regulator CysB, promoting expression of sulphate acquisition genes (Jovanovic *et al.*, 2003; Kredich, 2008; Wang & Leyh, 2012). In contrast to the CSC formations effect on CysE, CysK becomes almost completely inhibited (Saito *et al.*, 1995).

Binding of the CysE C-terminal peptide into CysK's active site has been confirmed through fluorescent spectroscopy peptide binding studies, where a blue shift in emission (500 nm) is observed by PLP, the co-factor of CysK (Campanini *et al.*, 2014). The CSC is an important regulator of the cysteine biosynthesis pathway and has yet to be characterised in *N. gonorrhoeae*.

The CSC structure has not yet been established, however, there is a crystal structure of CysK from *H. influenzae,* with a 10 amino acid C-terminal peptide bound in the active site (Huang *et al.*, 2005). The key residues required for binding were determined via screening a tetrapeptide library. Binding ability was monitored by CysK activity and PLP fluorescence (Campanini *et al.*, 2014). It was determined that a C-terminal isoleucine (Ile) is essential for binding and inhibition of CysK. This residue is well conserved across CSC forming organisms, including *S. typhimurium, H. influenzae* and *E. coli* (Huang *et al.*, 2005; Salsi *et al.*, 2011; Benoni *et al.*, 2017b).

Previous research using Clustal Omega (Madeira *et al.*, 2019), generated a sequence alignment of CysE bacterial homologues that was analysed using ESPript 3.0 (Robert & Gouet, 2014). This analysis concluded that CysE from *N. gonorrhoeae* had moderate sequence similarities to other CysE homologues (57%, however, with a 97% similarity to *N. meningitidis* being the exception) (Oldham, 2020). The C-terminus four peptide fragment, GDGI was well conserved across three species with DFMI being the conserved peptide sequence in *Neisseria* species (Oldham, 2020). The conservation of this terminal Ile indicates potential formation of the CSC in *N. gonorrhoeae.* It has also been confirmed that the CysK active site serves as the anchor for the formation of the CSC (Campanini *et al.*, 2015). Given the complete inhibition of CysK by the CSC formation and key differences in sulphur acquisition and cysteine biosynthesis shown in other bacterial species, characterisation both CysK and the CSC in *N. gonorrhoeae* would provide

further insight into elucidating the sulphur assimilation and synthesis of L-cysteine in *N. gonorrhoeae*.

1.7 *O*-acetylserine sulphydrylase/CysK

1.7.1 Structural characteristics of CysK

O-acetylserine sulphydrylase (OASS), CysK, is a pyridoxal 5'phosphate (PLP) dependent enzyme belonging to the OASS belongs to the tryptophan synthase β superfamily (Fold type II) (Takumi & Nonaka, 2016). Characteristic of this, the lysine (Lys) residue key to forming a Schiff base with the aldehyde group of PLP is located closer to the N-terminus of each monomer, while the loop region that binds to the phosphate group of PLP is closer to the C-terminus of each monomer (Liang *et al.*, 2019). Another important distinction, the active site of the enzyme is made up of residues all from one subunit, compared to the fold type I family where the active site is made of residues combined from different subunits (Liang *et al.*, 2019). CysK is a homodimer comprised of two subunits, each of approximately 315 amino acid residues, composed of two domains, an N-terminal domain (formed predominantly by residues 1-145) and a C-terminal domain (formed predominantly by residues 146-315) (Rabeh & Cook, 2004). Each domain consists of an α/β fold with a central twisted β-sheet surrounded by α-helices

Figure 1.7) (Rabeh & Cook, 2004). Crossover of N-terminus residues (13-34) into the C-terminal domain form the first two strands of these central β-sheets (Rabeh & Cook, 2004). The active site of each subunit is located deep within the protein at the interface of the N-terminal and C-terminal domains.

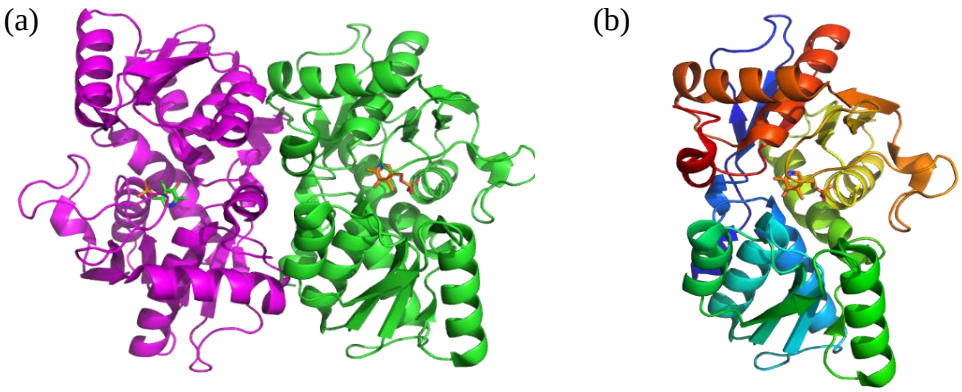

Figure 1.7: Cartoon representation of the *S. typhimurium* CysK structure (PDB # 2J3C). (a) Structure of the CysK dimer, with monomers coloured purple and green respectively. Bound PLP shown in licorice-stick format in green and orange respectively. (b) Structure of the CysK monomer, coloured from N-terminus (blue) to C-terminus (red). The central twisted β-sheet is surrounded by α-helices in both domains. Entry to the active side is seen on the left of the monomer. Figures generated in PyMOL.

Combination of improved stability and an allosteric anion-binding site at the dimer interface give purpose to the formation of the dimeric structure CysK forms (Rabeh & Cook, 2004).

To date there are 34 bacterial CysK structures deposited in the Protein Data Bank (PDB). Both structural and functional conservation of CysK is found across gram-negative bacteria and plant species, independent of sequence similarities (Benoni *et al.*, 2017a). Within the active site, the PLP cofactor is in Schiff base linkage with the amino group of Lys-41 (Figure 1.8), whilst its pyridine ring is supported at the back by Valine (Val)-40. Main and side chain functional groups within the Glycine (Gly)-176-Threonine (Thr)-180 loop, anchor the 5'-phosphate of PLP (Figure 1.8) (Rabeh & Cook, 2004). The amide nitrogen and Schiff base nitrogen of the Asparagine (Asn)-71 residue can hydrogen bond with the O-3' of PLP. The asparagine loop alongside Glutamine (Gln)-142 bind the substrate carboxylate group in the external Schiff base (Rabeh & Cook, 2004). Serine (Ser)-272 is within hydrogen bonding distance of PLP's pyridine nitrogen (Figure 1.8).

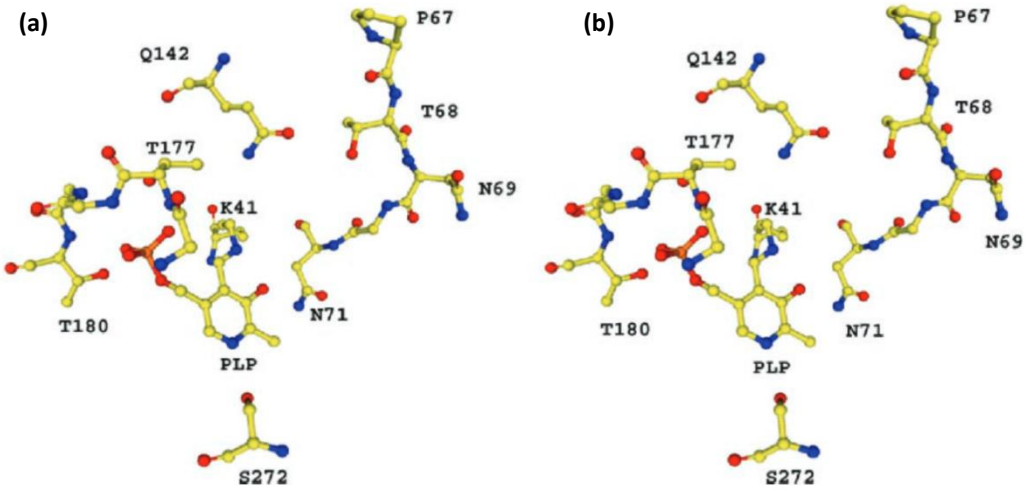

Figure 1.8: Active site residues of CysK. (a) Threonine loop (T177-T180) which interacts with 5'-phosphate of PLP seen on the left. (b) Asparagine loop (residues 68-72) seen on the right. Cofactor PLP is visible at the bottom of the active site cleft. Schiff base linkage between C-4' of PLP and Lys-41 can be seen. Ser-272 is within hydrogen bonding distance of N-1 of the pyridine ring in PLP. Side chain of Asparagine (Asn)-71 interacts with O-3' of PLP. Figure taken from (Rabeh & Cook, 2004).

Consensus sequence analysis of CysK enzymes has indicated 5'-phosphate PLP anchoring by a Gly-Thr loop (GTGGT) is conserved across 10 bacterial species ranging from residues 166-170 to residues 191-195 (Joshi *et al.*, 2019). The exact same GTGGT motif is found in the *N. gonorrhoeae* CysK sequence at residues Gly-179-Thr-183 (Figure 3.13). The Schiff base linkage forming Lys-41 found in *S. typhimurium* is also conserved across 11 bacterial species ranging from residue position 35-58. This lysine is analogous to Lys-44 in *N. gonorrhoeae.* The asparagine that hydrogen bonds to O-3' of PLP, and the asparagine loop alongside the Gln-142 that bind the carboxylate group of the substrate

are also conserved across 11 bacterial species and are found in *N. gonorrhoeae* at residues Asn-74 and Gln-145, respectively. Ser-272 which hydrogen bonds with PLP's pyridine nitrogen is also conserved across these 11 bacterial species and is found in *N. gonorrhoeae* at Ser-267. The active site residues Thr69-Thr73 and Gly228-Ala231 are conserved across nine bacterial species and are found in *N. gonorrhoeae* at Thr71-Thr75 and Gly223-Ala226, respectively. The presence of these similarly positioned and conserved residues involved in the active site and cofactor binding in CysK indicates similar structure and function of the previously uncharacterised *N. gonorrhoeae* CysK enzyme to other CysK enzymes found in literature.

However, structural characteristics will only partially elucidate *N. gonorrhoeae* CysK's function and role in the sulphur acquisition and cysteine biosynthesis pathways. The kinetic mechanism will help further characterise the function of *N. gonorrhoeae* CysK.

1.7.2 CysK kinetic mechanism

The kinetics of CysK homologues have been studied extensively in both bacteria and plant species. As CysK uses two substrates in its reaction to produce L-cysteine, there are two possible catalytic mechanisms for its action: sequential and ping-pong. Many studies in literature have already determined the CysK reaction mechanism to be bi-bi ping-pong (also known as a non-sequential mechanism) (Rabeh & Cook, 2004; Joshi *et al.*, 2019). The ping-pong mechanism involves release of one of the products before all substrates have bound to the enzyme, generating an enzyme intermediate in the process (Ulusu, 2015). The bi-bi ping-pong mechanism utilised by CysK begins with diffusion of OAS into the active site, and an elimination reaction occurs, removing acetate, forming the intermediate α-aminoacrylate. Nucleophilic attack of sulphide results in formation of L-cysteine (Figure 1.9) (Joshi *et al.*, 2019).

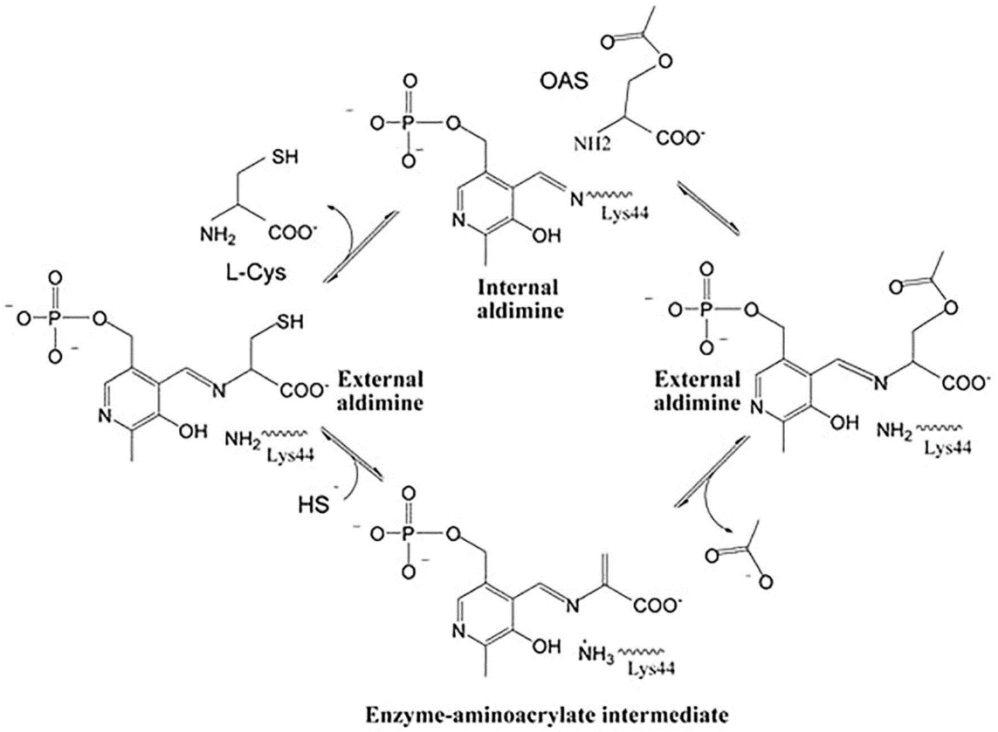

Figure 1.9: *Mycobacterium tuberculosis* CysK catalytic mechanism. Figure from (Joshi et al., 2019).

This mechanism has been identified in CysK from both *S. typhimurium* and *M. tuberculosis* (Rabeh & Cook, 2004; Joshi *et al.*, 2019), indicating *N. gonorrhoeae* may utilise the same mechanism of cysteine production.

1.8 CysK as a drug target

Given the importance of the cysteine biosynthesis pathway in pathogen virulence and overcoming oxidative stress, targeting this pathway has become of particular interest in development of new antimicrobials. Mammals synthesise L-cysteine through reverse-transulphurisation of methionine obtained in the diet, thus, the lack of cysteine biosynthesis and a reductive sulphate acquisition pathway, makes this pathway a particularly promising target for drug development (Stipanuk *et al.*, 2006; Hicks & Mullholland, 2018). Development of inhibitors for targeting CysK isoforms in pathogenic bacteria, including *S. typhimurium* (Spyrakis *et al.*, 2013), *H. influenzae* (Salsi *et al.*, 2010) and *M. tuberculosis* (Jean Kumar *et al.*, 2013) has already begun.

A transcriptomic study showed that *cysK* is not an essential gene for *N. gonorrhoeae* (Remmele *et al.*, 2014). This transposon-mediated mutagenesis study was conducted in the presence of cysteine, and under these conditions the first enzyme (CysE) in the two-step cysteine biosynthesis pathway was essential, yet curiously the second enzyme (CysK) was not. This demonstrates that L-cysteine requirements for *N. gonorrhoeae*

cannot be met solely from environmental import of L-cysteine, and is supported by *N. gonorrhoeae* being able to grow in the absence of cysteine and the presence of thiosulphate (Le Faou, 1984). However, CysK is important for colonisation of epithelial cells in *N. meningitidis* and when deleted results in both decreased fitness and increased susceptibility to antibiotics (Turnbull & Surette, 2010; Capel *et al.*, 2016).

Although CysK has been evaluated as a drug target in *S. typhimurium, H. influenzae,* and *M. tuberculosis*, cysteine biosynthesis has not been investigated in *N. gonorrhoeae. N. gonorrhoeae* lacks the necessary transporters for glutathione uptake and therefore, relies on the precursor cysteine for synthesis of glutathione (Seib *et al.*, 2006). Although *N. gonorrhoeae* has cysteine and cystine transporters, it is likely *N. gonorrhoeae* relies on *de novo* cysteine biosynthesis to maintain high intracellular glutathione concentrations given the essential nature of both *cysB* and *cysE*. Given CysK is the final step in the *de novo* biosynthesis of L-cysteine, this places high importance on elucidating its function in the pathogenicity of *N. gonorrhoeae.*

Although *N. gonorrhoeae* cannot grow on sulphate as its lacks the enzyme required for reducing sulphate to sulphide (due to genome deletions and in frame stop codons), it is able to grow on thiosulphate as the sole source of sulphur. We suggest that *N. gonorrhoeae* has a different, yet functional cysteine biosynthesis pathway from other *Neisseria* species, and as a function of that pathway, a dual-functioning CysK which utilises both thiosulphate and sulphide for the final step in the synthesis of cysteine. Genome searches and sequence comparisons identified and annotated a likely functional *O*-acetylserine sulphydrylase in *N. gonorrhoeae* strain FA1090 and MS11.

1.9 Research objectives

The aim of this research is to characterise a key enzyme in the *N. gonorrhoeae* cysteine biosynthesis pathway, *O*-acetylserine sulphydrylase/CysK. Characterisation of the biochemical and biophysical properties of CysK from *N. gonorrhoeae* will guide future research into the development of new antimicrobials and will improve our understanding of the pathogenicity of *N. gonorrhoeae*. The following objectives were set to achieve this:

Objective 1:
Investigate the *O*-acetylserine sulphydrylase activity and peptide inhibition of CysK from *N. gonorrhoeae.*

Objective 2:
Determine the three-dimensional structure of CysK using protein crystallisation and X-ray diffraction.

Objective 3:
Characterise the cysteine synthase complex of *N. gonorrhoeae.*

Objective 4:
Create genetic knockouts of the *cysK* gene from *N. gonorrhoeae* to test the essentiality of the CysK protein.

Chapter 2

Materials and Methods

2.1 Cloning of *cysK* for expression in *Escherichia coli*

The *cysK* gene NGO_0340 was codon optimised for *E. coli* and ordered from Geneart (Thermo Fisher) (Appendix A.1). The synthetic *cysK* construct was cloned into expression vector pET28b-PstI with a C-terminal hexahistidine-tag, between PstI and XhoI restriction sites by Dr Joanna Hicks (The University of Waikato). The NGO_0340 pET28b plasmid was checked by DNA sequencing before transformation into *E. coli* BL21 (DE3) for protein expression. Positive transformants were selected for by growing overnight at 37°C, Luria-Bertani (LB) agar (Appendix A.2) supplemented with 50 $\mu g.ml^{-1}$ kanamycin

2.2 Long term storage of BL21 CysK expression strains

Seeder cultures were prepared from positive transformants, by inoculating a single colony from a transformation plate into LB broth (10 ml) supplemented with kanamycin (50 $\mu g.ml^{-1}$) and incubated at 37 °C, shaking at 200 rpm, overnight. Glycerol stocks were prepared from seeder cultures, by adding 0.5 ml of seeder culture to 0.5 ml sterile 50% glycerol (w/v) and stored at -80 °C.

2.3 CysK expression cultures

Large scale expression cultures were prepared by inoculating the 10 ml seeder culture (prepared as per section 2.2) into 1 L LB broth, supplemented with kanamycin (50 $\mu g.ml^{-1}$). Cultures were incubated at 37 °C, 200 rpm until the culture reached mid-log phase (optical density at A_{600} = 0.5-0.7), at which point protein expression was induced by the addition of 1 ml of 0.75 M isopropylthio-β D-galactosidase (IPTG, final concentration 0.75 mM). Cultures were incubated overnight at 22 °C, 200 rpm. Expression cultures were centrifuged at 4,600 g for 20 min at 4 °C, after which the supernatant was discarded. The remaining cell pellet was resuspended in 15 ml lysis buffer (50 mM potassium phosphate pH 7.0, 200 mM NaCl, 20 mM imidazole). The resuspended culture was transferred to a 50 ml falcon tube and centrifuged for a further 20 min at 4,600 g, 4 °C. After centrifugation, the supernatant was discarded, and the pellet was stored at -80°C.

2.4 Purification of CysK

CysK was isolated and purified using immobilised metal affinity chromatography (IMAC) and gel filtration chromatography. Protein solubility was assessed using SDS-PAGE gel electrophoresis. Oligomeric state was measured using gel filtration chromatography and native-PAGE gel electrophoresis.

2.4.1 Immobilised metal affinity chromatography

Frozen CysK cell pellets (section 2.3) were thawed at room temperature. Cell pellets were resuspended by vortexing in 12.5 ml lysis buffer (50 mM Potassium phosphate pH 7.0, 200 mM NaCl, 20 mM imidazole), 625 µL of 2mM PLP was added (for final concentration of 0.1 mM) and one cOmplete^{TM}, Mini, EDTA-free Protease Inhibitor Cocktail tablet (Roche, Switzerland) was added to inhibit cellular proteases. Cells were lysed on ice using a QSONICA Q700 sonicator using programme 2 with a 1/4" microtip probe (12.5-25 ml volume). Programme 2 involves alternating 2 second bursts at 12% power with 2 second intervals of no sonication for a total of 1.5 min. The sonicated lysate was centrifuged at 13 000 g for 20 min at 4 ºC. The supernatant was filtered through 1.2, 0.45 and 0.2 µm filters. IMAC purification was carried out using either an AKTÄ Purifier fast protein liquid chromatography (FPLC) system (GE Life Sciences) or an NGC FPLC system (BioRad). The same method for IMAC and gel filtration was used for either FPLC system. The filtered supernatant was manually loaded onto a HisTrap^{TM} HP 5 ml column (GE Life Sciences) that was preequilibrated in lysis buffer. The column was attached to the FPLC and washed with 20 ml lysis buffer at 2 ml.min^{-1} to remove unbound proteins. A gradient of elution buffer (50 mM potassium phosphate pH 7.0, 200 mM NaCl, 1 M imidazole) was gradually increased to 50%, over 25 ml, to elute the HexaHis-tagged CysK.

2.4.2 Gel filtration chromatography

At room temperature (22 °C), 1 ml of a single IMAC peak fraction containing CysK was loaded onto an Enrich 650 analytical gel filtration column (Bio-Rad Laboratories, USA), preequilibrated in gel filtration buffer (50 mM Potassium phopshate pH 7.0, 100 mM NaCl) with a flow rate of 1 ml.min^{-1}. An IMAC protein fraction was manually loaded into the injection loop of the FPLC for injection onto the column. After sample injection, 28 ml gel filtration buffer was run at 1 ml.min^{-1} through the column. Fractions of eluted protein were collected, nanodropped and diluted with gel filtration buffer to 1.6 mg.ml^{-1} in 1 ml. 50% glycerol (1 ml) was added to diluted protein (2 ml, final concentration of

0.8 mg.ml^{-1} CysK) and stored at -80 ºC. These CysK stocks (2ml, 0.8 mg.ml^{-1}) were later thawed and 80 µL aliquoted into 1.5 ml tubes and stored at -80 ºC.

2.4.3 SDS-PAGE gel electrophoresis

SDS-PAGE gels were composed of both a resolving and stacking layer, at 12 and 5% polyacrylamide, respectively. All gels were made in house in a multi-gel caster (Hoefer). The resolving layer was prepared by mixing the "Resolving layer" components listed in Table 2.1, and filling the gel caster, leaving a three cm gap at top of the gel plate. A thin layer of isopropanol was then applied to the top of the gel and was left until the resolving layer had polymerised ~30 min. Once set, the isopropanol layer was carefully removed, the stacking layer was prepared by combining "Stacking Layer" components listed in Table 2.1 and filling to the top edge of the gel caster. A ten well comb was inserted into the top of each gel, before leaving to set at room temperature ~30 min. Gels were stored wrapped in wet tissue at 4 °C for up to four weeks. Protein samples were prepared for gel-loading by mixing 15 µL sample with 5 µL 4x SDS loading dye (also known as Quench, Q4) (Appendix B.3). 20 µl of sample was loaded per well, along with 10 µl of Precision Plus Protein^{TM} ladder (Bio-Rad Laboratories, USA) per gel. The gels were run in 1 x Tris-Glycine SDS-PAGE running buffer (Appendix B.3) at 100 V, until the loading dye migrated past the stacking gel where it was increased to 150 V. The gel was stopped when the dye migrated to the end of the resolving gel. Protein bands were visualised by staining in Coomassie Fairbanks stain (Appendix B). Gels and stain were heating by microwaving for 30 s, followed by five min incubation at room temperature with agitation. Stained gels were rinsed with distilled water and left in destaining solution (10% acetic acid) overnight. Destained gel bands were visualised using an Omega Lum™ gel imager (Aplegen, USA).

Table 2.1: Components for five SDS-PAGE gels. Ammonium persulphate (APS^2) stock solution was prepared fresh weekly.

Component	12% Resolving layer (ml)	8% Stacking layer (ml)
Resolving buffer (1.5 M Tris pH 8.8)	7.5	-
Stacking buffer (1 M Tris pH 6.8)	-	1.6
30% Polyacrylamide/Bis (375:1) (v/v)	12.0	2.125
10% SDS (w/v)	0.30	0.125
10% APS^2 (w/v)	0.15	0.063
10% TEMED	0.015	0.0063
MQ H_2O	10.05	8.50

2.4.4 Measuring the oligomeric state of CysK

Previously, the Enrich650 gel filtration column (Bio-Rad Laboratories, USA) was calibrated in gel filtration buffer (50 mM Tris pH 8.0, 200 mM NaCl) using Gel Filtration Standards (Bio-Rad Laboratories, USA), by Dr Joanna Hicks (Appendix B). The molecular weight of CysK was calculated taking the peak elution volume (V_e) and calculate the K_{av} gel phase distribution co-efficient using Equation 2.1, where V_o is the column void volume and V_c is the total column volume: The calibration standard curve relating K_{av} and molecular weight was used to determine the molecular weight of CysK from the calculated K_{av}.

Equation 2.1: Formula for calculating gel phase distribution co-efficient

$$K_{av} = \frac{V_e - V_o}{V_c - V_o}$$

2.4.5 Measuring protein concentration Nanodrop™

Protein concentration was determined by Nanodrop™ 2000 (Thermofisher, USA) measuring absorbance at 280 nm. Protein concentration was calculated using Beer-Lambert law (Equation 2.2), where absorbance readings were corrected by dividing the Nanodrop™ reading (1 Abs = 1 mg.ml^{-1}) by the molar absorption co-efficient of the CysK protein, (Ɛ = 0.590 L mol^{-1}/cm^{-1}) as determined by ProtParam (Gasteiger *et al.*, 2005).

Equation 2.2: Beer-Lambert equation. A= absorbance, Ɛ = molar absorption co-efficient (L mol^{-1} /cm^{-1}), l = pathlength (cm) and c = concentration (molL^{-1}).

$$A = \varepsilon c l$$

2.5 Kinetic Assay Parameters

CysK was purified by IMAC and gel filtration chromatography as per sections 2.4.1 and 2.4.2. Protein concentration was measured by absorbance at 280 nm using a NanodropTM (section 2.4.5). CysK protein used in the first assay sets was purified the same day. After glycerol stabilisation and freezer storage, all CysK enzyme used in subsequent assays was from the 0.8 µg freezer stocks stored at -80 ºC. All assays were carried out in MOPs buffer (100mM MOPs). Substrates *O*-acetylserine (OAS) and sodium sulphide (Na_2S) were freshly prepared for each set of assays (Appendix B3). Enzyme stocks (80 µL of 0.8 mg.ml^{-1}, 0.02 nM, CysK monomer 32.726 kDa) from the freezer were thawed at room temperature ~2 mins before assays were begun.

2.5.1 Assay parameters

Assay data was collected using MOPs buffer (100mM MOPs). Assays were carried out in Axygen 96-well PCR microplates, with a reaction volume of 75 µL, final volume 310 µL.

Table 2.2: CysK activity assays with varying *O*-acetylserine concentrations. Concentrations of substrate were varied by adjusting the volume of substrate 50 mM stock added, unless the volume to be added was less than 3 µl, then a 5 mM stock was used. This was done to prevent inaccuracy of pipetting at extremely low volumes. The amount of enzyme used for each reaction was kept constant (1.6 $mg.ml^{-1}$).

Component	Volume (µL)
***O*-acetylserine (5/50mM, substrate)**	3-30
Sodium sulphide (50mM, substrate)	10.5
MOPs (100mM, initial reaction)	32.5-62.5
CysK (0.8 $mg.ml^{-1}$, Enzyme)	2
TCA (20%)	15
DTT (200mM)	16.5
MOPs (100mM, reduction step)	3.5
Acid Ninhydrin	100
Glacial Acetic acid	100
Total (95 ºC incubation step)	310
Ethanol (Ice cold, 100%)	100
Reaction mixture	100
Total (measuring step)	200

Table 2.3: CysK activity assays with varying sodium sulphide concentrations. Concentrations of substrate were varied by adjusting the volume of substrate 50 mM stock added, unless the volume to be added was less than 3 µl, then a 5 mM stock was used. This was done to prevent inaccuracy of pipetting at extremely low volumes. The amount of enzyme used for each reaction was kept constant (1.6 $mg.ml^{-1}$).

Component	Volume (µL)
***O*-acetylserine (50mM, substrate)**	15
Sodium sulphide (5/50mM, substrate)	3-45
MOPs (100mM, initial reaction)	13-58
CysK (0.8 $mg.ml^{-1}$, Enzyme)	2
TCA (20%)	15
DTT (200mM)	16.5
MOPs (100mM, reduction step)	3.5
Acid Ninhydrin	100
Glacial Acetic acid	100
Total (95 ºC incubation step)	310
Ethanol (100%, Ice cold)	100
Reaction mixture	100
Total (measuring step)	200

All substrate stocks were prepared in MQ H_2O. All components for the assays, except MOPs, acetic acid, ethanol and the enzyme were made fresh just before assays were conducted. OAS stocks were made fresh due to the rapid conversion of *O*-acetylserine to *N*-acetylserine (Campanini *et al.*, 2005). *O*-acetylserine was purchased as a powder from Sigma Aldrich (MW = 183.59 $g.mol^{-1}$) and stored as a powder at -20 ºC according to manufacturer's instructions. Sodium sulphide stocks were made fresh to prevent any possible error in activity that could be caused by substrate degradation. Sodium sulphide was purchased as a fragmented solid from Sigma Aldrich (MW = 142.02 $g.mol^{-1}$) and stored at 4 ºC according to manufacturer's instructions. DTT was made fresh as it has a very short half-life (Stevens *et al.*, 1983). DTT was purchased as a fragmented solid from Sigma Aldrich (MW = 154.253 $g.mol^{-1}$) and stored at 4 ºC according to manufacturer's instructions. TCA was made fresh to prevent any possible error in activity that could be caused by degradation of TCA. TCA was purchased as a clear crystalline solid from Sigma Aldrich (MW = 163.38 $g.mol^{-1}$) and stored at 4 ºC according to manufacturer's instructions.

O-acetylserine sulphydrylase activity of CysK was monitored via absorbance measurements of L-cysteine at 560 nm using an adapted method from (Gaitonde, 1967). Absorbance at 560_{nm} was recorded across five stopped assay time points (0, 2.5, 5, 7.5 and 10 mins) using a Thermo Scientific Multiskan GO spectrophotometer (ThermoScientific, USA). Absorbance readings were subsequently corrected for by subtracting any absorbance from blank samples and converted to cysteine produced (mM) using the cysteine standard curve determined during a summer research project (Appendix B.2). Cysteine produced for each varied substrate concentration condition was plotted and the catalytic rates (cysteine produced $mM.min^{-1}$) for each were derived from linear regression analysis of the first five minutes of the stopped assay reactions (unless otherwise stated).

OAS, sodium sulphide and MOPs were added in appropriate volumes for each reaction condition to individual wells in the 96-well plate. The enzyme was added directly to the side of the wells. Finally, the reaction was initiated via 30 second centrifugation at 3000 rpm, 4 ºC (Heraeus Multifuge 3SR Plus centrifuge). The 96-well plate was covered (Platemax CyclerSeal Sealing Film, PCR-TS) and incubated for 10 mins at 37 ºC. Each reaction was stopped by addition of 15 µl TCA (w/v) at 0, 2.5, 5, 7.5 and 10 minutes accordingly. 16.5 µL of 200mM DTT (final concentration 30 mM) and 3.5 µL of 100mM

MOPs were added to each well and incubated at room temperature for 30 mins. 100 µL of acid ninhydrin and 100 µL of acetic acid were added to each well and incubated for 5 mins, at 95 ºC. The plate was cooled by incubating on ice for 5 mins, and 100 µL ice cold ethanol and 100 µL of each reaction mixture were added to a flat bottomed 96-well plate. Absorbance was measured at 560_{nm} (Thermo scientific, Multiskan GO). Enzyme rates were plotted using GraphPad Prism (version 8.2.0, Windows, GraphPad Software, La Jolla California USA). All datapoints were collected in duplicate, unless otherwise stated.

2.6 Kinetic analysis

The K_M and V_{max} were calculated for each substrate by varying the concentration of the substrate of interest, while keeping the other substrate at a saturating concentration, so it is not rate limiting. Saturating conditions are defined as concentrations 2 x K_M, and greater. *O*-acetyl-L-serine Michaelis Menten curves were collected over a range of *O*-acetyl-L-serine concentrations (0.2-10 mM). Sodium sulphide Michaelis Menten plots were collected over a range of sodium sulphide concentrations (0.2-12 mM). Both Michaelis Menten plots were collected at fixed saturating conditions (10mM OAS and 7mM Na_2S) of the other substrate.

K_M and V_{max} were determined by non-linear regression fit of the Michaelis Menten equation (Equation 2.3), the allosteric sigmoidal equation (Equation 2.4), the substrate inhibition equation (Equation 2.5) or the allosteric sigmoidal with substrate inhibition equation (Equation 2.6) (using GraphPad Prism (version 8.2.0, Windows, GraphPad Software, La Jolla California USA,).

Equation 2.3: The Michaelis Menten equation. S = substrate, K_M = Michaelis constant, v = rate, v_{max} = theoretical maximum rate.

$$v = \frac{V_{max}[S]}{K_M + [S]}$$

Equation 2.4: The allosteric sigmoidal equation. S = substrate, K_{half} = Michaelis constant, v = rate, v_{max} = theoretical maximum rate, h = hill constant.

$$v = \frac{V_{max}[S^h]}{K_{half} + [S^h]}$$

Equation 2.5: The substrate inhibition equation. S = substrate, K_M = Michaelis constant, v = rate, v_{max} = theoretical maximum rate, K_i = dissociation constant for substrate binding in a situation where two substrates can bind to the enzyme.

$$v = \frac{V_{max}[S]}{(K_m + S(\frac{1+S}{K_i}))}$$

Equation 2.6: The allosteric sigmoidal with substrate inhibition equation. S = substrate, K_M = Michaelis constant, v = rate, v_{max} = theoretical maximum rate, h = hill constant, K_i = dissociation constant for substrate binding in a situation where two substrates can bind to the enzyme.

$$v = \frac{v_{max}[S^h]}{(K_m^h + \left(S\left(1 + \frac{S}{K_i}\right)\right)^h)}$$

Enzyme catalytic efficiency was determined by calculating the catalytic constant (k_{cat}) and the specificity constant k_{cat}/K_M. k_{cat} is a measure of the amount of product formed over time, per unit of enzyme (s^{-1}). This is calculated by dividing the V_{max} rate ($M.s^{-1}$) by the molar concentration of dimeric enzyme. The catalytic efficiency k_{cat}/K_M ($M^{-1}s^{-1}$) was calculated by dividing the k_{cat} (s^{-1}) by the K_M (M). Catalytic efficiency values were calculated for each substrate.

2.7 Thiosulphate substrate assays

Thiosulphate substrate assays were conducted using a modified method from section 2.5.1. The key modification was substitution of thiosulphate for sodium sulphide in the reaction. Thiosulphate was added at low to high varied concentrations (final reaction concentration, 1-50 mM).

2.8 CysK inhibition assays

The CysE C-terminal tetrapeptide (DFMI) was ordered from Thermo scientific (MW = 523.54 $g.mol^{-1}$) as a white powder and stored at 4 ºC according to manufacturer's instructions. CysE tetrapeptide was suspended in 1 ml of potassium phosphate gel filtration buffer (Appendix B.1) to a stock of 2 $mg.ml^{-1}$ (3820.15 pmol), which was further diluted to stocks of 0.2, 0.02 and 0.002 $mg.ml^{-1}$ (382, 38.2 and 3.82 pmol respectively) and stored at -21 ºC (Appendix B.4).

CysE C-terminus tail four peptide inhibitor assays were measured using a modified method from section 2.5.1. Modifications included the addition of the CysE C-terminus tail four peptide inhibitor (total inhibitor added, 0.08-191 pmol); using thawed 2 $mg.ml^{-1}$ stock or diluted stocks if volume added dropped below 2µL; to appropriate volumes of thawed CysK for pre-incubation of the enzyme with the peptide. OAS concentration was held at 1 mM instead of 10 mM as OAS is known to cause dissociation of the cysteine synthase complex at very low concentrations. The reaction was initiated via addition of the pre-incubated stock and centrifugation.

2.9 Crystallisation of CysK

2.9.1 Protein purification

CysK protein was expressed and purified following methods in sections 2.3 and 2.4 respectively using crystallisation buffers in Appendix B.2. Protein concentration was determined by Nanodrop^{TM} as per section 2.4.5.

2.9.2 High throughput crystallisation screens

High throughput crystallisation screens were set up by Annmaree Warrender to identify promising crystallisation conditions that could be further optimised to produce crystals suitable for X-ray diffraction. The following screens: Index^{TM}-HR2-144, PEGRxHT^{TM}-HR2-086, CrystalHT^{TM}-HR2-130 and the SaltRxHT^{TM}-HR2-136 (Hampton Research, U.S.A.), were used. Screens were set up in low profile 96-2 well INTELLI-PLATE and were set up using the Mosquito crystallisation robot (TTP LabTech Ltd., USA). Each crystallisation condition had a reservoir solution (crystallisation solution) of 100 µl and 200 nl sitting drops of a 1:1 ration of protein (40 mg.ml^{-1}) and crystallisation solution. Screens were checked weekly for crystal formation using a dissection microscope (Nikon SMZ800).

2.9.3 Hanging drop fine screens

Purified protein was concentrated to 40 mg.ml^{-1} and stored on ice for a short period of time, as prolonged incubation at room temperature led to precipitation. Promising crystallisation conditions from high throughput screens were further optimised by Annmaree Warrender through scaling up to hanging drop fine screens. 24 well VDX trays were set up with crystallisation solution volumes of 500 µl or 1000 µl from concentrated stock solutions. Hanging drops were prepared by mixing a 1:1 ratio (1:1 µl or 2:2 µl) of mother liquor and concentrated protein solution on a siliconised cover slip, before inverting drop-side down, over a well, lined with silicone grease. For each condition, crystallisation parameters such as pH, drop size and the concentration of protein and precipitant were optimised. Crystallisation drops were checked for crystal growth under a dissection microscope, daily for one week and weekly thereafter.

The fine screen that reproduced crystals from the robot screen was based on a condition from the CrystalHT^{TM} robot screen (HR2-130, Hampton Research): 0.1 M HEPES sodium, pH 7.5, 2% polyethylene glycol 400 (v/v), 2.0 M Ammonium sulphate. Trays were set up as above. The hanging-drop the crystal looped from was from condition 0.1

M HEPES pH 7.5, 4% polyethylene glycol 400 (v/v), 2.5 M ammonium sulphate. Drop composition was 1:1 (mother liquor: protein concentrate) in a final volume of 2 µl. All crystals were grown at 18 °C.

2.9.4 Crystal preparation for X-ray diffraction

Each crystal was transferred using a cryo-loop, to a cryo-protectant solution, consisting of the crystallisation solution with the addition of 15% glycerol (v/v) as a cryo-protectant. Crystals were then flash cooled in liquid nitrogen. Crystals were stored short-term in liquid nitrogen (one to two days) before data collection.

2.10 Data collection

X-ray diffraction data was collected at the Australian Synchrotron (Melbourne, Victoria) on the MX2 beamline (McPhillips *et al.*, 2002), equipped with an EIGER x 16M detector (Dectris, Switzerland). Data were collected over 360 ° rotation of the crystal over 360 sec, at 80% beam attenuation.

2.11 Data processing

2.11.1 Indexing, integration and scaling

The CysK diffraction images were indexed, integrated and scaled, using XDS (Kabsch, 2010). Datasets 0016 and 0017 were the best of three datasets obtained from the crystal diffraction. Unit cell dimensions of 0017 were changed to match 0016 and the space group changed from sg 19 ($P2_12_12_1$) to sg 4 ($P2_1$) via rerun of XDS (Kabsch, 2010). The Original space group was found to be incorrect as the resulting model had unexpectedly high R_{work} and R_{free} values. Datasets 0016 and 0017 were scaled together using XDS (Kabsch, 2010) and reflections merged using AIMLESS (Evans & Murshudov, 2013) from the CCP4 suite (Winn *et al.*, 2011). Data quality was assessed through AIMLESS (Evans & Murshudov, 2013). FreeR flag dataset (5% of dataset reflections not to be used in refinement and used to compute R_{free}) was generated in AIMLESS.

2.11.2 Detection of twinning and non-crystallographic symmetry

Data was analysed for evidence of twinning and translational non-crystallographic symmetry (tNCS) in AIMLESS from the CCP4 suite (Winn *et al.*, 2011; Evans & Murshudov, 2013) and *phenix.xtriage* from the PHENIX suite.

2.12 Structural analysis

2.12.1 Matthew's coefficient

The total number of monomers in the asymmetric unit was determined by calculating the solvent content using the Matthew's coefficient (Matthews, 1968) program, as a part of the CCP4 program suite (Winn *et al.*, 2011).

2.12.2 Molecular replacement

The structure of CysK from *M. tuberculosis* (3ZEI) was retrieved from the protein data bank (PDB). A single monomer was extracted from this file, in PyMOL (The PyMOL Molecular Graphics System, Version 2.3.2 Schrödinger, LLC) and water and ligands were removed. This *M. tuberculosis* monomer with no ligands and water was used in molecular replacement carried out using *phenix.phaser* (McCoy *et al.*, 2007), from the PHENIX suite (Adams *et al.*, 2010).

2.12.3 Model building and refinement

The model was initially built and refined using the program *phenix.autobuild* (Terwilliger *et al.*, 2008) from the PHENIX suite (Adams *et al.*, 2010). The resulting structure was further built manually using the program COOT (Emsley & Cowtan, 2004). For manual building and refinement in COOT, the 2Fo-Fc and Fo-Fc electron density maps, were set to 1σ and 3σ, respectively. After each round of structure manipulation, *phenix.refine* and *phenix.autobuild* were used to run rounds of real-space refinement (Terwilliger *et al.*, 2008).

2.12.4 Structural analysis

Images of the model and maps were generated using programmes PyMOL (The PyMOL Molecular Graphics System, Version 2.3.2 Schrödinger, LLC) and COOT (Emsley & Cowtan, 2004). Comparing structures was conducted through calculating root mean square distances (r.m.s.d) using alignment tool in PyMOL. The surface area and buried residue calculations for the trimer/hexamer interfaces were carried out using PDBePISA (Krissinel & Henrick, 2007). ENDscript 3.0 was used to identify secondary structural features (Robert & Gouet, 2014), alongside visual inspection in PyMOL.

2.13 Cysteine synthase complex formation

The protocol for forming the cysteine synthase complex (CSC) was based on a method by (Benoni *et al.*, 2017b). CysK as per section 2.4 and CysE were purified individually before being used for CSC formation.

2.13.1 Purification of CysE

CysE was purified using IMAC and gel filtration chromatography as per section 2.4.1 and 2.4.2 with minor modifications by Keely Oldham. CysE pellets were resuspended and purified as per section 2.2.4 in Keely Oldham's thesis (Oldham, 2020), buffer compositions found in appendix B.2.

2.13.2 Formation of the cysteine synthase complex

2.13.2.1 Monitoring cysteine synthase complex formation by gel filtration chromatography

CysK was freshly purified as per section 2.4.1 and 2.4.2 and CysE was freshly purified as per section 2.13.1. A 1 ml solution of CysE 6 µM: CysK 4 µM (monomer ratios) was manually injected into the injection loop of the FPLC for injection into the Enrich 650 analytical gel filtration column (Bio-Rad Laboratories, USA), preequilibrated in gel filtration buffer (50 mM Potassium phopshate pH 7.0, 100 mM NaCl) with a flow rate of 1 $ml.min^{-1}$. After sample injection, 28 ml gel filtration buffer was run at 1 $ml.min^{-1}$ through the column. Fractions were collected and run on a 12% SDS PAGE gel. This was repeated with a CysE 4 µM: CysK 0.05 µM 1 ml solution, without fractions being run on a 12% SDS PAGE gel.

2.13.2.2 Monitoring cysteine synthase complex formation by fluorescent spectroscopy

CysK was freshly purified as per section 2.4.1 and 2.4.2 (buffers used were pH 8.0 rather than 7.0), and CysE was freshly purified using gel filtration chromatography as per the method in section 2.13.1. 300 µl of CysK was added to a quartz cuvette and an excitation wavelength scan from 350-550_{nm} was completed using a fluorometer (alphatech, F-7000 Fluorescence Spectrophotometer) determining the excitation wavelength to be 400nm. An emission wavelength scan from 350-600_{nm} determined the emission wavelength to be 494.6_{nm}. 75 µl CysE was added to the quartz cuvette to give a CysK 4: CysE 1 monomeric ratio and the emission wavelength was measured at the time of addition and two minutes after. More CysE was subsequently added to give ratios CysK:CysE, 2:1, 1:1 and 2:3, all

of which the emission wavelength was measured in the same manner stated above using a fluorometer (alphatech, F-7000 Fluorescence Spectrophotometer). Emission peaks, the apex wavelength and the corresponding intensities were obtained using FL Solutions 2.1 for F-7000 and spectra plotted using GraphPad Prism (version 8.2.0, Windows, GraphPad Software, La Jolla California USA).

2.13.2.3 Cysteine synthase complex formation using the CysE C-terminal tetrapeptide

CysK and the CysE C-terminus tetrapeptide inhibitor were thawed. 350 µl of 0.8 $mg.ml^{-1}$ CysK was added to a quartz cuvette and an excitation wavelength scan from 350-550_{nm} was completed using a fluorometer (alphatech, F-7000 Fluorescence Spectrophotometer) determining the excitation wavelength to be 386.2_{nm}. An emission wavelength scan from 350-600_{nm} determined the emission wavelength to be 471_{nm}. 5.7 µl of 0.2 $mg.ml^{-1}$ CysE tetrapeptide (final quantity of peptide added, 2176.563 pmol) was added to 350 µl of 0.8 $mg.ml^{-1}$ CysK (final quantity of enzyme added, 8706 pmol) in a quartz cuvette (creating a 4:1 molar ratio of CysK monomer to peptide) and the emission wavelength measured at addition of the peptide and 2 mins after using a fluorometer (alphatech, F-7000 Fluorescence Spectrophotometer). An additional 5.7 µl of 0.2 $mg.ml^{-1}$ CysE C-terminus tail four peptide inhibitor was added (giving a 2:1 ratio of CysK to peptide) and emission wavelength measured as above using a fluorometer (alphatech, F-7000 Fluorescence Spectrophotometer). 11.4 µl of 0.2 $mg.ml^{-1}$ CysE C-terminus tail four peptide inhibitor was subsequently added to give various molar ratios (CysK:CysE peptide, 1:1, 1:2, 1:3, 1:4, 1:5), and emission wavelengths measured at addition of peptide and 2 mins after for each molar ratio. All measurements were taken whilst mixing occurred in the cuvette. Emission peaks, the apex wavelength and the corresponding intensities were obtained using FL Solutions 2.1 for F-7000 and spectra plotted using GraphPad Prism (version 8.2.0, Windows, GraphPad Software, La Jolla California USA).

2.14 *cysK* genomic deletion in *Neisseria gonorrhoeae*

2.14.1 Agarose gel electrophoresis

Agarose gels were made as per Appendix C and a 10 well comb was inserted into the top of the gel, before leaving to set at room temperature ~30 mins. After PCR, 10 µl of each PCR product were mixed with 2 µl of 6x loading dye (Appendix C) using a pipette. Mixed samples were loaded into a 1% agarose gel (HydraGene LE Agarose) made with 1x TAE Buffer (Appendix C) and run in a dedicated OWL electrophoresis tank (ThermoFisher

Scientific) containing 1x TAE (Appendix C) with a LighteningVolt OSP250-L electrophoresis machine (Biolab scientific) at 100V for 40 minutes at room temperature. Samples were run together with 7 µl of Invitrogen 1kb+ ladder (Appendix C). The gel was imaged using an Omega Lum™ gel imager (Aplegen, USA).

2.14.2 PCR to check for homologous recombination

The DNA template for homologous recombination was designed using Geneious Prime (Biomatters) to contain 150 bp of flanking sequence (corresponding to 150 bp upstream and downstream of the *cysK* gene respectively) either side of a kanamycin resistance gene (*kanR*). The DNA construct was ordered as a Geneblock from Twist Bioscience (USA). Lyophilised DNA was resuspended in TE buffer to a final concentration of 20 $ng.\mu l^{-1}$ for use as a DNA template in subsequent PCR reactions. Primers were designed using Geneious Prime (Biomatters) to amplify the entire DNA construct (CysK KO FWD: 5'-TTGTCACTGAAGCGGGAAGG-3' and CysK KO REV: 5'-CCTTCCCGCTTCAGTGACAA-3') and ordered from IDT (USA). Primers were resuspended in TE buffer to 100 µM and working stocks made by diluting in MQ water to 10 µM.

PCR master mix was set up as follows: 20 µl Hotfire Pol MasterMix, 3 µl CysK PCR Forward primer (10 mM), 3 µl CysK PCR Reverse primer (10 mM), 69 µl Ultra Distilled H_2O were added together into a 1.5 ml Eppendorf tube. 19 µl of this mixture was removed and added to a PCR tube and 1 µl of Ultra distilled H_2O was added to produce a negative control. 4 µl of DNA template (CysK KanR KO ordered from TWIST and resuspended in 1x TE buffer) was added to the master mixture. 20 µl of master mix with the DNA template was aliquoted into four PCR tubes. The five PCR tubes were added to BioRad DNA Engine using the following cycling conditions:

PCR Protocol

95 ºC	15 min	
95 ºC	20 sec	⌈
55 ºC	30 sec	| Repeat 29x
72 ºC	1.5 min	⌊
72 ºC	10 min	

PCR products were purified using a Roche-applied-science DNA purification kit according to manufacturer's instructions and run on an agarose gel to check purity as per section 2.14.1.

2.14.3 Measuring Nucleic acid (DNA) concentration Nanodrop™

Nucleic acid concentration was determined by Nanodrop™ 2000 (Thermofisher, USA).

2.14.4 *N. gonorrhoeae* plate transformations

Purified PCR DNA products were pooled and combined with Ultra Distilled water to a final concentration of 20 ng.µl^{-1} in 50 µl. Two 10 µl amounts of PCR product were spotted onto GCB agar (Appendix C) and left to soak in to the agar and dry. This was repeated onto New York agar (Fort Richards, New Zealand). An *N. gonorrhoeae* colony was taken from fresh GCB agar and streaked across the plates through each spot of DNA and incubated at 37 ºC for 48 hours. Single colonies that grew within the spotted DNA circles from both GCB and New York agar were streaked onto GCB agar supplemented with 50 µg.ml^{-1} kanamycin and incubated at 37 ºC for 48 hours to select for integration of the DNA construct into the *N. gonorrhoeae* chromosome.

Chapter 3

Results and Discussion

3.1 Kinetic characterisation of *O*-acetylserine sulphydrylase/CysK from *N. gonorrhoeae* enzyme

3.1.1 CysK kinetic analysis and enzyme mechanism

O-acetylserine sulfhydrylase (CysK/ OASS-A, EC:2.5.1.47) is a key enzyme in the biosynthesis of cysteine in bacteria and plants. It catalyses the final step of the two-step cysteine biosynthesis reaction (Figure 1.2). OASS is a member of the tryptophan synthase β-superfamily (Fold type II) and the β-family of PLP dependent enzymes (Mino & Ishikawa, 2003; Guédon & Martin-Verstraete, 2007; Takumi & Nonaka, 2016). Many bacteria have two OASS isoforms; OASS-A/CysK and OASS-B/CysM. Both isoforms catalyse the same reaction, with OASS-A using sulphide and *O*-acetylserine to synthesis cysteine and OASS-B using thiosulphate in place of sulphide to give cysteine thiosulfonate as a product.

The kinetic mechanism of OASS-A is bi-bi ping-pong with a stable aminoacrylate intermediate. OAS binds to the internal aldimine of the enzyme and acetate is released as the first product forming the aminoacrylate intermediate. Bisulphide enters the active site attacking as the second substrate, and L-cysteine is released as the final product (Figure 1.10) (Rabeh & Cook, 2004; Joshi *et al.*, 2019). OASS-A activity is inhibited by binding to serine acetyltransferase (the first enzyme in the two-step pathway) to form the cysteine synthase complex (CSC) across many species (Saito *et al.*, 1995; Zhao *et al.*, 2006; Benoni *et al.*, 2017b). The OASS-B isoform does not bind to serine acetyltransferase and therefore does not form the cysteine synthase complex (Zhao *et al.*, 2006).

Given the elucidated mechanism, inhibition and family similarities in CysK enzymes across species, we predict that CysK from *N. gonorrhoeae* will have *O*-acetylserine sulfhydrylase activity. CysK is being characterised as a new antimicrobial target for other bacterial pathogens and (Salsi *et al.*, 2011; Franko *et al.*, 2018; Joshi *et al.*, 2019) given the rapid emergence of antimicrobial resistance in *N. gonorrhoeae* we propose that CysK

is a good target for new antimicrobial design for treatment of antimicrobial-resistant *N. gonorrhoeae*.

Inhibitor design relies on a detailed understanding of enzyme structure and mechanism. This section biochemically characterises CysK to understand the enzyme kinetics and mechanism of action.

3.1.2 Expression and purification of CysK

To successfully characterise CysK from *N. gonorrhoeae*, active and soluble protein was purified. Prior to the start of this MSc research, Dr Joanna Hicks had cloned *cysK* from *N. gonorrhoeae* into the expression plasmid pET28b for expression with a C-terminal His-tag in *E. coli* (Section 2.3 and 2.4).

CysK was successfully purified by IMAC and gel filtration chromatography as per method 2.4. The IMAC purification chromatogram in Figure 3.1a shows CysK elutes at ~20% elution buffer (200 mM of imidazole). The corresponding SDS-PAGE gel of the IMAC fractions, demonstrates that the majority of contaminating *E. coli* protein present in the supernatant is removed during IMAC purification (Figure 3.1b). This results in relatively pure CysK protein of approximately 33 kDa (Figure 3.1b, blue arrow) consistent with the predicted molecular weight of the CysK monomer (32.726 kDa, calculated as per section 2.4.4). Fractions containing IMAC purified CysK (Figure 3.1, green bar) were measured for protein concentration and used for gel filtration purification (Figure 3.2a) as per section 2.4.2.

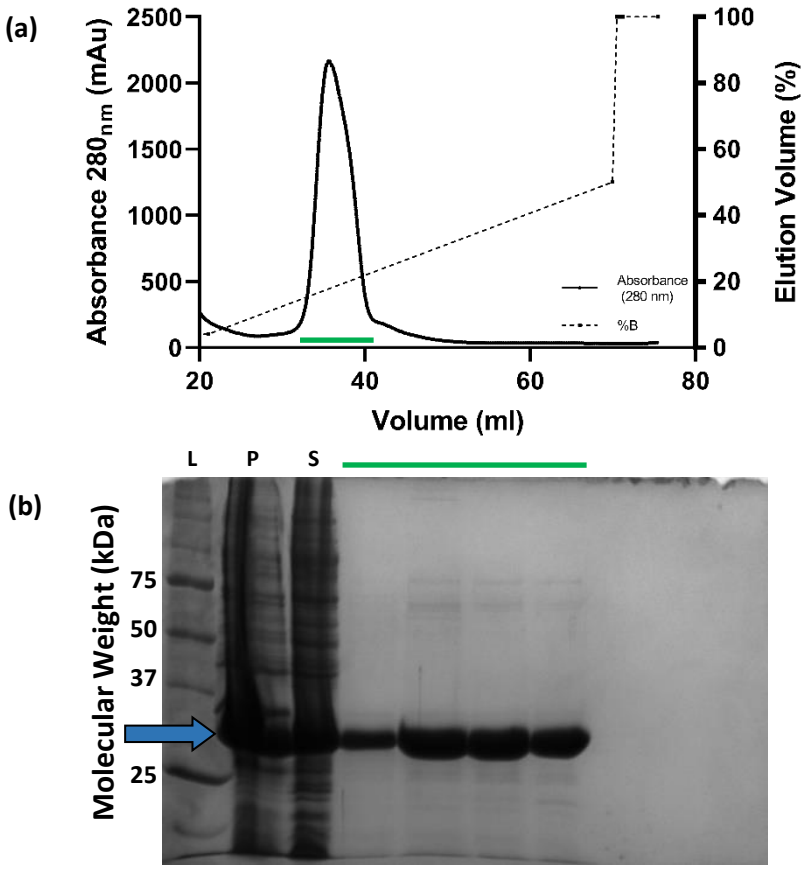

Figure 3.1: IMAC Purification of CysK. (a) IMAC chromatogram of A_{280} nm shows volume (ml) (X-axis), absorbance 280_{nm} (left Y-axis) and concentration of elution buffer (%B) (right Y-axis). Data from protein loading between 0-20 ml has been excluded for scaling purposes. (b) 12% SDS-PAGE gel of CysK IMAC purification. CysK protein (32.726 kDa) is labelled with a blue arrow and is present in all samples (the insoluble pellet (P), the soluble supernatant (S), and the IMAC fractions (green bar)). Molecular weights of Precision Plus Protein Standards (L) in kDa are labelled. Purification was carried out at room temperature.

IMAC-purified CysK underwent a final purification step via gel filtration chromatography (section 2.4.2). CysK eluted as a single peak from an Enrich 650 analytical gel filtration column with an elution volume of 14.2 ml (Figure 3.2a, purple bar). Using the Enrich 650 calibration curve (Appendix B.2), the apparent molecular weight from the elution volume is 52.862 kDa. The predicted molecular weight of the CysK monomer is 32.726 kDa, which suggests that CysK elutes as a dimer (52.862/32.726 = 1.62). No protein was present in the void volume of the column (10.56 ml) indicating that CysK did not aggregate and remained soluble during purification. The corresponding SDS-PAGE gel of the gel filtration column show pure CysK protein of approximately 33 kDa (Figure 3.2).

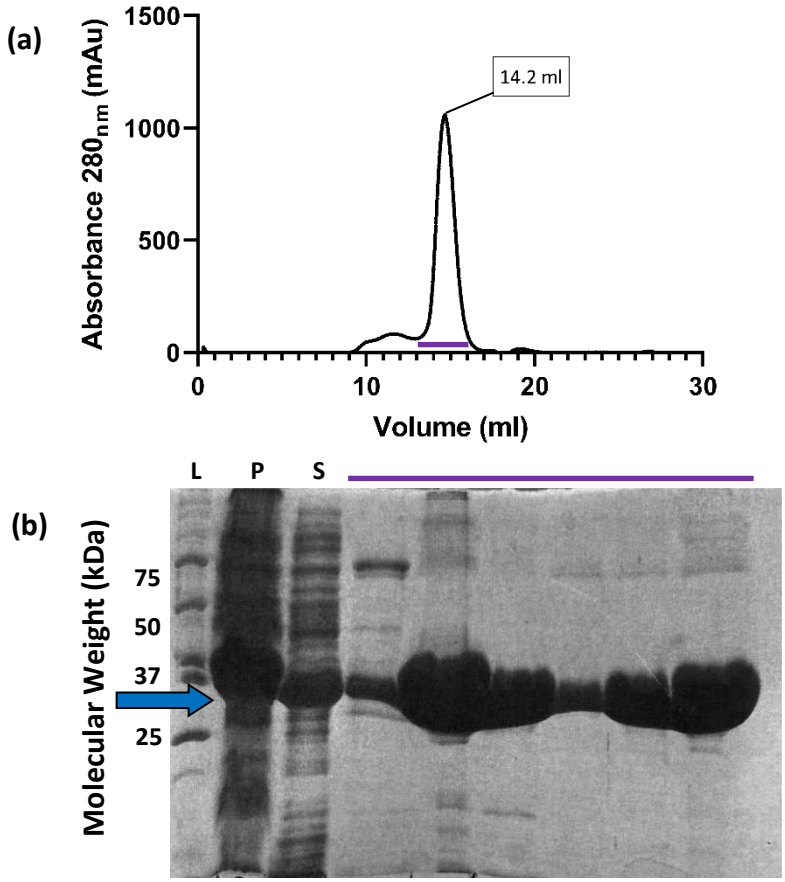

Figure 3.2: Gel filtration purification of CysK. (a) Enrich 650 gel filtration chromatogram shows elution of a large peak at 14.2 ml. (b) 12% SDS-PAGE gel shows high yield and purity of CysK (purple bar). CysK protein (32.726 kDa) is labelled with a blue arrow and is present in all samples (the insoluble pellet (P), the soluble supernatant (S), and the Gel Filtration fractions (purple bar)). Molecular weights of Precision Plus Protein Standards (L) in kDa are labelled. Purification was carried out at room temperature.

3.1.3 Assay optimisation

I developed an assay to measure the enzyme activity of CysK from *N. gonorrhoeae* based on a method for quantifying cysteine produced in a stopped assay (Gaitonde, 1967). Acid ninhydrin reacts with cysteine forming a pink chromophore measurable at 560 nm, indicative of the amount of cysteine present in a reaction.

All assays were carried out in MOPs buffer (100 mM, pH 7) at 37 ºC. Assays were set up as per section 2.5.1. No NaCl was present during purification of the enzyme, or in assay buffers as chloride ions inhibit activity of CysK (Burkhard *et al.*, 2000; Campanini *et al.*, 2005). All raw data collected is listed in Appendix B.5.

3.1.3.1 Optimisation of enzyme (CysK) concentration

Initially, trial assays were completed to determine an appropriate concentration of CysK to use in collecting kinetic data. Enzyme concentration was optimised to obtain steady

state (linear rate) across varied OAS and Na_2S concentrations. Assays were set up using 3 mM Na_2S and 50 mM OAS based on saturating substrate concentrations for CysK from *Arabidopsis thaliana* (Bonner *et al.*, 2005). Na_2S is used for supply of the required S^{2-} ion in the cysteine biosynthesis reaction. The following concentrations of CysK were trialled: 0.0058, 0.058, 0.58, 5.8 and 58 $mg.ml^{-1}$. Each enzyme concentration's absorbances were measured in duplicate and incubated for 15 minutes at 37 ºC. A concentration of 0.58 µg was optimal for obtaining steady state rates for use in future kinetic assays (Figure 3.3).

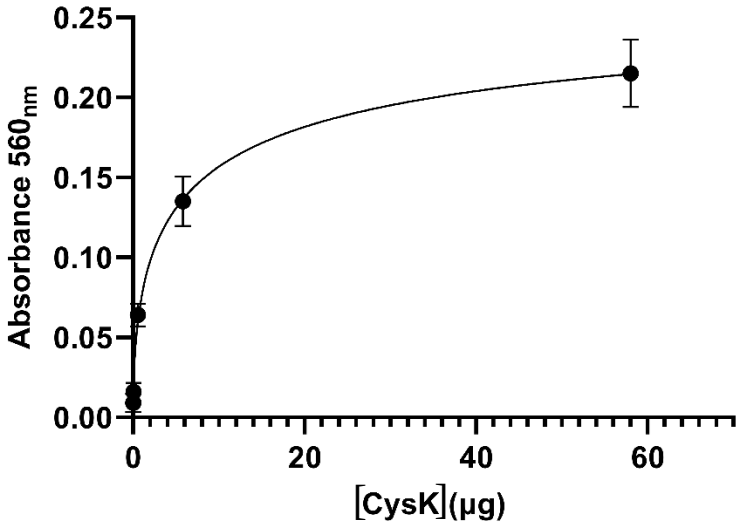

Figure 3.3: Determination of CysK concentration for use in kinetic assays. Concentrations of CysK measured include: 0.0058, 0.058, 0.58, 5.5 and 58 µg. Duplicates for each concentration were collected. Error bars represent standard error.

3.1.3.2 Optimisation of enzyme storage

Following the lack of activity seen in week old CysK enzyme, the literature was interrogated for possible solutions for increasing stability, therefore maintaining long term activity of the enzyme. It is well documented for addition of 50% (v/v) glycerol to enzyme aliquots significantly improves stability the enzyme upon freezing (Vagenende *et al.*, 2009). Thus, glycerol was incorporated for -80 ºC freezer storage. Two 1 ml aliquots of 0.8466 $mg.ml^{-1}$ CysK, 25% (v/v) glycerol final concentration were made and stored at -80 ºC. An aliquot was thawed and CysK activity measured using 10 mM OAS and 1.5 mM Na_2S (Bonner *et al.*, 2005) at 0.8466 $mg.ml^{-1}$ and 1.6932 $mg.ml^{-1}$ CysK concentration. Absorbance readings indicated no freeze/thaw effect decreasing the activity of CysK (Table 3.1), resulting in storage of CysK aliquots (~ 0.8 $mg.ml^{-1}$) in 25% (v/v) glycerol at -80 ºC.

Table 3.1: CysK glycerol (0.8 mg.ml^{-1}, in final concentration 25% glycerol) aliquot activity testing assay

Blank	0.8466 mg.ml^{-1} (1 µl)	1.6932 mg.ml^{-1} (2 µl)
0.040	0.200	0.382
0.043	0.175	0.293

3.1.3.3 Optimisation of reducing agent

Initial activity assays were conducted by varying the concentration of Na_2S from 0.004-1.5 mM based on concentrations used by (Bonner *et al.*, 2005), holding the OAS final concentration at 10mM (saturating). Initial assay data (Appendix B.5) indicated no activity. Dithiothreitol (DTT, 100 mM, pH 7) was made fresh, 10 µl was added post-assay and incubated at room temperature for 30 minutes to reduce any cystine present to cysteine, as cystine is not detected by the acid ninhydrin method.

To alleviate the 30-minute room temperature incubation with DTT, the DTT reducing agent was replaced by a new reducing agent TCEP (Tris (2-carboxyethyl) phosphine hydro-chlorine). TCEP is known to effectively reduce substances in 5 min when added at a 1.5 times concentration to the substance being reduced and is able to be stored at room temperature for longer periods of time before oxidising (Hampton Research Solutions for Crystal Growth; Thermo Fisher Scientific, 2013).

Assays where the concentration of Na_2S was varied between 0.004-1.5 mM were performed using TCEP added to the assay reaction at a final concentration of 8mM, however, the results were inconclusive as absorbance readings (Appendix B.5) for each reaction condition indicated no activity, reading the same as both the blank and negative control conditions. CysK activity was tested without the presence of a reducing agent, indicating the enzyme was still active and TCEP optimisation was necessary (Appendix B.5).

Five different reaction conditions were set up to measure the ability of TCEP to reduce cystine to cysteine using a solution of 5 mM cysteine that had been left at room temperature for 14 days therefore converting to cystine. Reaction conditions included: no cysteine, no TCEP and addition of 8 mM TCEP (final concentration) after incubation for 30 sec, 5 min and 10 min, respectively. No enzyme or substrates were included in these assays, so we could observe the effect of the TCEP reducing agent vs no reducing agent. Results showed the reaction with no TCEP added had the highest absorbance (indicating

the highest cysteine concentration) and irregular, significantly lower absorbance readings were observed in all three 8 mM TCEP conditions, regardless of incubation time (Appendix B.5). With TCEP added as a reducing agent, we would expect these samples to have the highest absorbance and increase over time, indicating a higher cysteine:cystine ratio.

Therefore, the TCEP activity test was repeated with minor modifications. TCEP was added at a final concentration of 50 mM and the pH of the cysteine solution was adjusted to pH 2. Eight different assay conditions were set up to measure the ability of TCEP to reduce cystine to cysteine using a solution of 5 mM cystine (a 5 mM cysteine solution that had been left at room temperature for 14 days therefore oxidising to cystine). Reaction conditions included: no cysteine, no TCEP and 50 mM TCEP with incubation for 30 sec, 5 min and 10 min respectively, and 50mM TCEP with a fresh 5 mM solution of cysteine. Again, no enzyme or substrates were included in these assays. Surprisingly, the fresh L-cysteine did not react with the acid ninhydrin added, giving absorbance readings equivalent to the blank samples. The cystine solution however, produced a similar pattern observed previously (Appendix B.5), the condition with no TCEP gave the highest absorbance reading, whilst the conditions with TCEP gave irregular and significantly lower absorbance readings.

Subsequently, assays without TCEP present and 6.32 µg of CysK were conducted to determine the approximate amount of cysteine produced using the cysteine standard curve (Appendix B.2). Following this, three sets of assays with 9.17, 2.478 and 1.626 µg of CysK respectively were conducted using final concentration 30 mM TCEP (Appendix B.5). These were all inconclusive, giving irregular absorbance readings with extremely high standard deviations making it impossible to draw accurate conclusions.

Review of the literature surrounding TCEP in these cysteine determination assays, indicated three issues. Desulphurisation of cysteine containing compounds occurs in the presence of TCEP when heated to 60 ºC, resulting in conversion of cysteine to alanine (Wang *et al.*, 2010). TCEP is also unstable in phosphate buffers (Thermo Fisher Scientific, 2013) and cannot be used in the presence of high protein concentration (defined as 6 mM +) (Melnikova *et al.*, 2019). The CysK enzyme is purified in a potassium phosphate buffer and the assay method has an incubation step at 95 ºC that is significantly higher

than 60 ºC. We therefore hypothesised that the lack of enzyme activity in our assays was due to the conversion of cysteine to alanine during the 5 min 95 ºC incubation step, which would be unable to react with the acid ninhydrin reagent to produce the pink chromophore that absorbs at 560 nm. Therefore, comparisons of different reducing agents in activity assays were compared to determine which reducing agent should be used in cysteine determination assays. Six reaction conditions were trialled: 30 mM TCEP, 30 mM DTT, no reducing agent (NRA) and blanks for each reducing agent condition (blanks had no enzyme added). Assays were conducted at saturating substrate concentrations of 10 mM OAS and 10 mM Na_2S with 2.4 µg of CysK. Higher concentrations of CysK were used in these reducing agent assays to allow for higher cysteine production hopefully making comparisons between reducing agents more stated. Reactions were set up without the addition of reducing agent and once all reactions were stopped by addition of 20% TCA, the reducing agents were added (TCEP, DTT and NRA) to a final concentration of 30 mM (addition of MOPS buffer in the NRA condition). All conditions were incubated at room temperature, and the assay method followed as per section 2.5.1. Absorbance readings indicated a stark contrast between the reducing abilities of TCEP and DTT in these assays (Table 3.2), with TCEP absorbance readings approximately half that of the DTT reducing agent absorbance readings, the NRA also had higher absorbance readings compared to TCEP (Table 3.2). Thus, it was established that DTT would be used in all cysteine determination assays from this point.

Table 3.2: Reducing agent efficacy testing absorbance readings at 560_{nm}. TCEP, DTT and NRA tested as reducing agents.

	Reaction 1	**Reaction 2**
TCEP (blank)	0.048	0.050
DTT (blank)	0.051	0.052
NRA (blank)	0.047	0.049
TCEP (30 mM)	0.513	0.531
DTT (30 mM)	1.153	0.961
NRA	0.669	0.619

3.1.3.4 Final assay optimisation

The assay method was redesigned accommodating the use of 100 mM DTT to give a final concentration of 30 mM in the reducing step as per section 3.1.3.3. Assays were set up as per section 2.5.1 with minor modifications outlined below. The addition of 39 µl 100 mM DTT to all reactions resulting in 130 µl final volume.

Preliminary results were more promising than previous assays, showing consistent activity across different varied OAS concentration conditions, however, outliers were still present with blank activity compared to their duplicates (Appendix B.5). After the 95 ºC incubation step, the reaction solution overflowed over the reaction wells. To alleviate these outliers and the overflow, three modifications to the method were introduced. (1) The concentration of the DTT stock solution was doubled to 200 mM, changing the DTT and MOPs volume added to 16.5 and 3.5 µl respectively with a final volume of 110 µl. This change in volume prevented overflow during the 95 ºC incubation step, therefore preventing potential loss of cysteine produced during the reaction. (2) The concentration of Na_2S was increased from 1 mM to 10mM to ensure saturating concentrations of Na_2S. (3) The frozen CysK stocks (0.8 $mg.ml^{-1}$ CysK, 25% v/v glycerol) were aliquoted into multiple tubes and stored at stored at -80 ºC to eliminate the effects of freeze thawing. These changes resulted in reliable, reproducible enzyme activity data.

All rates for kinetic analysis were taken from the linear section of each reaction (the first five minutes), indicating that the steady state for calculating enzyme rate in these stopped assays occurs in the first five minutes across all substrate concentrations (Appendix B.5). Thus, all assays were shortened to measure activity over 10 minutes rather than 20 with time points at 0, 2.5, 5, 7.5 and 10 minutes rather than the original 0, 5, 10, 15 and 20 minutes.

3.1.4 CysK kinetic analysis

Enzyme kinetic curves were collected for both substrates, OAS and Na_2S for the purpose of determining K_M and V_{max} for CysK. These kinetic parameters provide insights into the enzyme's affinity for these substrates and can be used to calculate measures of catalytic efficiency including, k_{cat} and k_{cat}/K_M.

Assays varying the concentration of substrate OAS were conducted as per the final parameters in section 3.1.3.4. Rates ($mM.min^{-1}$) were calculated as per section 2.5.1 and plotted against increasing OAS concentrations (0.2 – 10 mM) at saturating concentrations of Na_2S (10 mM). The resulting non-linear regression Michaelis-Menten plot ($R^2 = 0.7428$, Figure 3.4, red line) does not follow a linear increase of rate as substrate concentration rises, however, showing a sigmoidal rate increase. This indicates an alternate kinetic model may be more accurate for CysK. Subsequently, a non-linear

regression allosteric sigmoidal model of catalysis (Equation 2.4) was fit (R^2 = 0.8641, Figure 3.4, blue line) to the data.

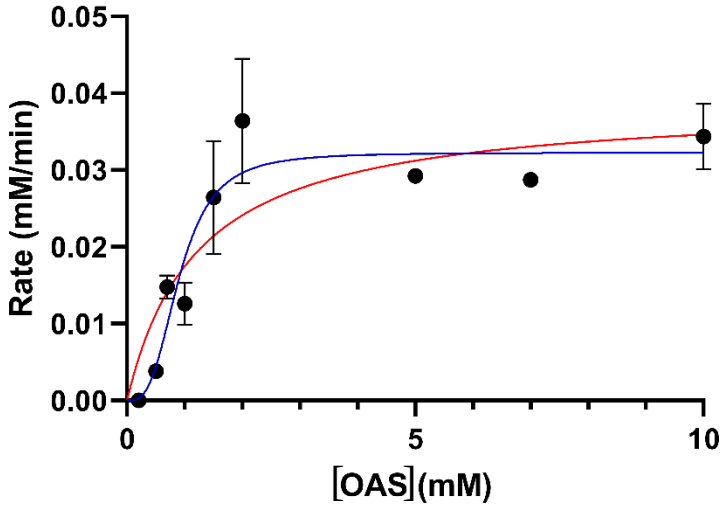

Figure 3.4: CysK activity with varying OAS concentration. Red line shows non-linear regression fit of the Michaelis Menten equation. Blue line shows a non-linear regression fit of an allosteric sigmoidal equation (occurs when the enzyme has cooperative subunits). Na_2S was held at a constant concentration of 10 mM.. Assay reactions were conducted at 37 ºC. All reaction conditions were collected in duplicate. Error bars represent standard error.

Table 3.3: Summary of kinetic parameters for initial OAS data. Values are means calculated from duplicates and are quoted with standard error. k_{cat} values are reported for the CysK dimer.

	Michaelis-Menten	**Allosteric Sigmoidal**
v_{max} ($mM.min^{-1}$)	0.039 ± 0.005	0.032 ± 0.002
K_M (mM)	1.223 ± 0.474	-
K_{half} (mM)	-	0.911 ± 0.104
k_{cat} (s^{-1})	7036 ± 902	5844 ± 362
k_{cat}/K_M ($mM.s^{-1}$)	5753 ± 1475	6417 ± 796
h	-	3.076 ± 0.953
R^2	0.7428	0.8641

The allosteric sigmoidal model, is a co-operative model, which occurs in enzymes with multiple binding sites and is defined by increased affinity of an active site for a ligand, when a ligand binds to another active site (Libretexts, 2020b, 2020a). An enzyme that demonstrates cooperativity is defined as allosteric and can demonstrate either positive or negative cooperativity. Positive cooperativity occurs when a ligand binding to an enzymes active site increases the affinity of one of the enzymes alternate active sites for a ligand, ultimately causing a rapid and co-ordinated increase in the reaction rate as the ligand concentration increases (an allosteric sigmoidal model) (Libretexts, 2020b, 2020a).

Whereas, negative cooperativity occurs when the ligand binding causes a decreased affinity in one of the enzymes alternate active sites for the ligand, ultimately causing a slowed reaction rate (an allosteric hyperbolic model) (Libretexts, 2020b, 2020a). Figure 3.4 shows an allosteric sigmoidal kinetic profile with a good fit ($R^2 = 0.8641$, Figure 3.4, blue line), and characteristic of this model, low enzyme activity at low OAS substrate concentration with a rapid and immediate increase in activity to the V_{max} as OAS concentration increases. The kinetic parameters quoted for the allosteric sigmoidal model also display significantly less error than the Michaelis-Menten kinetic model (Table 3.3). Thus, indicating OAS exhibits positive cooperativity in *N. gonorrhoeae's* CysK dimer.

OASS-A enzymes display a wide variety of kinetic profiles in relation to OAS. Similar to the *N. gonorrhoeae* OASS-A (CysK) characterised here, the OAS kinetic profile for *Datura innoxia* OASS isozyme C (three OASS isozymes A-C were isolated) at low concentrations of OAS, exhibits positive cooperativity (allosteric sigmoidal model). However, although we did not measure activity at OAS concentrations higher than 10 mM, OAS does exhibit competitive inhibition at concentrations higher than 25 mM in *D. innoxia* (Kuske *et al.*, 1994). Interestingly, both *Phaseolus vulgaris* and *Phaseolus polyanthus* OASS-A display a standard Michaelis-Menten relationship to OAS (Bertagnolli & Wedding, 1977), in which the reaction rate increases linearly in relation to substrate concentration until a maximal point at which activity levels off at V_{max} (Libretexts, 2020c). Thus, resulting in an asymptotic rectangular hyperbolic curve. Alternatively, the *S. typhimurium* OASS-A enzyme, exhibits substrate inhibition for OAS at concentrations above 7.5 mM where enzyme activity decreases (Cook & Wedding, 1976; Tai *et al.*, 1993). Assays where the concentration of Na_2S was varied were conducted as per the final parameters in section 3.1.3.4. Rates ($mM.min^{-1}$) were calculated as per section 2.5.1 and plotted against increasing Na_2S concentrations (0.2 – 12 mM) at saturating concentrations of OAS (10 mM). The first six Na_2S concentrations (0.2 - 2 mM)

show virtually no enzyme activity (Figure 3.5), therefore not adhering to the typical Michaelis-Menten kinetic model (R^2 = 0.5380, Figure 3.5, red line). The sigmoidal

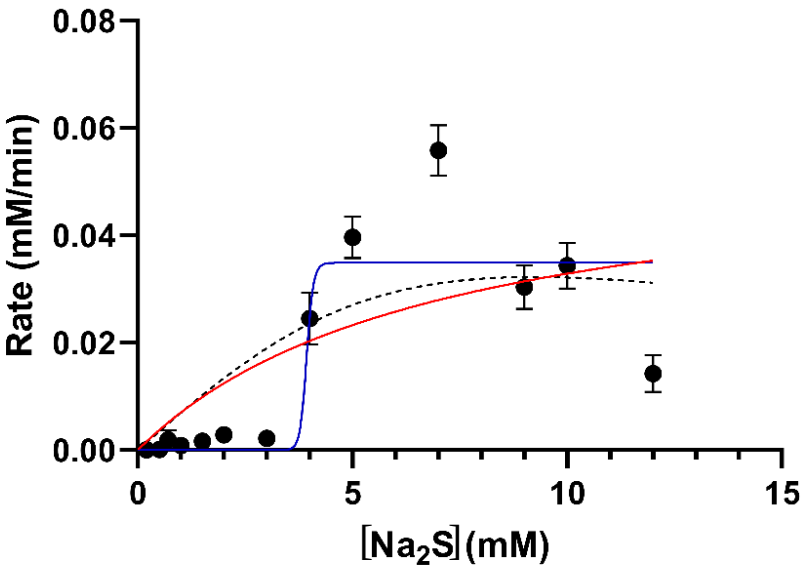

Figure 3.5: CysK activity with varying Na_2S concentration. Kinetic mechanisms modelled for varying Na_2S concentrations. Red line shows a non-linear regression fit of Michaelis-Menten kinetic model. Dotted black line shows a non-linear regression fit of substrate inhibition kinetic model. Blue line shows a non-linear regression fit of an allosteric sigmoidal (cooperativity) kinetic model. All models fit using the same data. OAS was held at a constant concentration of 10 mM (saturating). CysK was freshly thawed for these assays. Assay reaction was conducted at 37 ºC. All reaction conditions were collected in duplicate. Error bars represent standard error.

shape of the rates from 0.2 – 7 mM Na_2S suggest similar positive cooperativity to the OAS kinetic profile. Hence, an allosteric sigmoidal model (R^2 = 0.7728, Figure 3.5, blue line) was fit, giving a K_{half} and V_{max} of 3.933 ± 224.517 mM and 0.035 ± 0.003 mM.min^{-1}, respectively (Table 3.4). Despite the improved fit, the distinct lack of a plateau, indicated some form of inhibition was present at Na_2S concentrations higher than 7 mM. Therefore, a substrate inhibition model (R^2 = 0.6190, Figure 3.5, dotted black line) was fit to the data, giving a K_M and v_{max} of 14014.449 ± 4.743x10^7 mM and 97.924 ± 331330.28 mM.min^{-1}, respectively (Table 3.4). Given the error present for the K_{half} in the allosteric sigmoidal model exceeds both the K_{half} value quoted, and the concentration ranges plotted, this was deemed not scientifically relevant. Combined with the relatively poor goodness of fit (R^2 = 0.7728), it was clear this model was not accurate or scientifically relevant. The K_M and V_{max} values quoted for the substrate inhibition model are incredibly large and exceed the concentration ranges plotted by a huge margin, indicating these to also not be scientifically relevant. Despite these conclusions, it is possible both positive cooperativity and substrate inhibition are occurring in this kinetic profile.

Table 3.4: Summary of kinetic parameters for Na_2S data fit with Michaelis-Menten, allosteric sigmoidal and substrate inhibition models. Values are means calculated from duplicates and are quoted with standard error. k_{cat} values are reported for the CysK dimer.

	Michaelis-Menten	**Allosteric Sigmoidal**	**Substrate Inhibition**
$\mathbf{v_{max}}$ **(mM.min^{-1})**	0.056 ± 0.027	0.053 ± 0.003	97.924 ± 331330.028
$\mathbf{K_M}$ **(mM)**	7.021 ± 6.676	-	14014.449 ± 4.743x10^7
$\mathbf{K_{half}}$ **(mM)**	-	3.933 ± 224.517	
$\mathbf{K_i}$	-	-	0.006 ± 20.589
$\mathbf{k_{cat}}$ **(s^{-1})**	10132 ± 4891	6319 ± 543	17738023 ± 6x10^{10}
$\mathbf{k_{cat}/K_M}$ **(mM.s^{-1})**	1443 ± 1393	1607 ± 276	1266 ± 8565045
h	-	50.66 ± 171493.243	-
$\mathbf{R^2}$	0.5380	0.7728	0.6190

Therefore, the substrate inhibition and allosteric sigmoidal model equations were combined (Equation 2.6) and fit to the data (R^2 = 0.9573, Figure 3.6). This model fit the data relatively well, however, the Hill co-efficient value indicates the inaccuracy of the model. A hill co-efficient of 4.159 ± 0.854 (Table 3.5) suggests the enzyme is functioning as a tetramer, which is incorrect as CysK has been established as a dimer through gel filtration as per section 3.1.2. It was impossible to fit any simple model of substrate inhibition, Michaelis-Menten or allosteric sigmoidal kinetics to the profile. The initially allosteric sigmoidal curve did not smoothly approach an asymptote, instead abruptly decreasing due to substrate inhibition. It is this abrupt decrease in activity past 7 mM Na_2S that makes it difficult to fit any particular model to the data. Due to this, the kinetic constants obtained from the combined allosteric sigmoidal with substrate inhibition model are not particularly accurate, as was the case with both the *P. vulgaris* OASS-A and *D. innoxia* OASS (isozyme A and C) enzymes (Bertagnolli & Wedding, 1977; Kuske *et al.*, 1994).

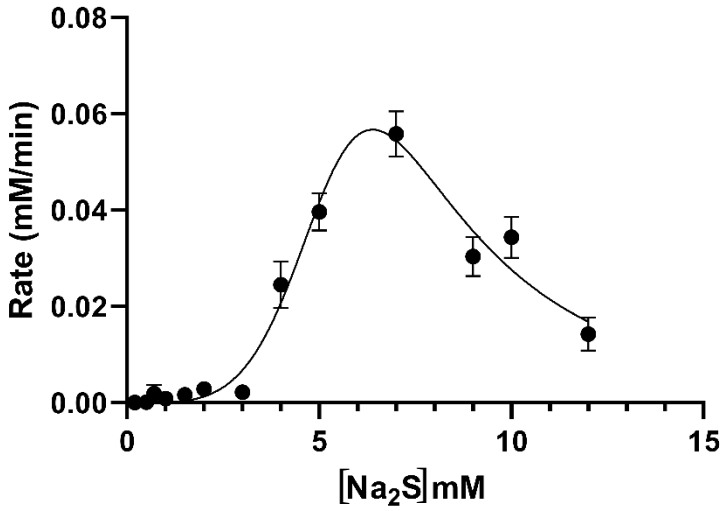

Figure 3.6: Constrained non-linear regression fit of an allosteric sigmoidal substrate inhibition model for Na_2S. OAS was held at a constant concentration of 10 mM (saturating). CysK was freshly thawed for these assays. Assay reaction was conducted at 37 ºC. All reaction conditions were collected in duplicate. Error bars represent standard error.

Interestingly, the *P. vulgaris* OASS-A, shows substrate inhibition after reaching its maximal rate at approximately 1.5 mM S^{2-}. However, positive cooperativity (an allosteric sigmoidal model) is observed at concentrations lower than 0.3 mM (Bertagnolli & Wedding, 1977). Alongside this, *D. innoxia* OASS (isozyme C) exhibits an allosteric sigmoidal (positive cooperativity) response to S^{2-} at concentrations below approximately 0.18 mM with substantial substrate inhibition after 0.2 mM S^{2-} concentration (Kuske *et al.*, 1994). Both, the OASS isoenzyme C from *D. innoxia* and the OASS-A from *P. vulgaris* display very similar kinetic profiles to *N. gonorrhoeae's* for Na_2S, initially an allosteric sigmoidal model, followed by strong substrate inhibition once the maximal rate is reached (Bertagnolli & Wedding, 1977; Kuske *et al.*, 1994). Alternatively, *P. polyanthus* OASS-A shows no allosteric sigmoidal (positive cooperativity) response to S^{2-}, however, fits a substrate inhibition model (Bertagnolli & Wedding, 1977). *S. typhimurium* OASS also shows substantial substrate inhibition after 0.25 mM S^{2-} (Cook & Wedding, 1976). Although the organisms *P. polyanthus'* OASS-A and *S. typhimurium's* OASS do not fit the same kinetic profile as *N. gonorhoeae's* OASS-A (Figure 3.6), both display substrate inhibition in relation to S^{2-}. Substrate inhibition by Na_2S is observed across many species OASS-A enzymes.

Substrate inhibition occurs with concentrations of Na_2S higher than 7 mM (Figure 3.6). In earlier assays CysK activity was analysed with varying OAS concentrations with Na_2S held constant at 10 mM. We therefore recollected rate data for CysK with varying OAS

concentrations at 7 mM Na_2S to give a more accurate kinetic representation of CysK's utilisation of OAS, removing the potential substrate inhibition that may have been contributing in Figure 3.4. Rates ($mM.min^{-1}$) were calculated as per section 2.5.1 and plotted against increasing OAS concentrations (0.2 – 10 mM) at a Na_2S concentration of 7 mM. The allosteric sigmoidal model of catalysis was fit to the data ($R^2 = 0.9795$, Figure 3.7).

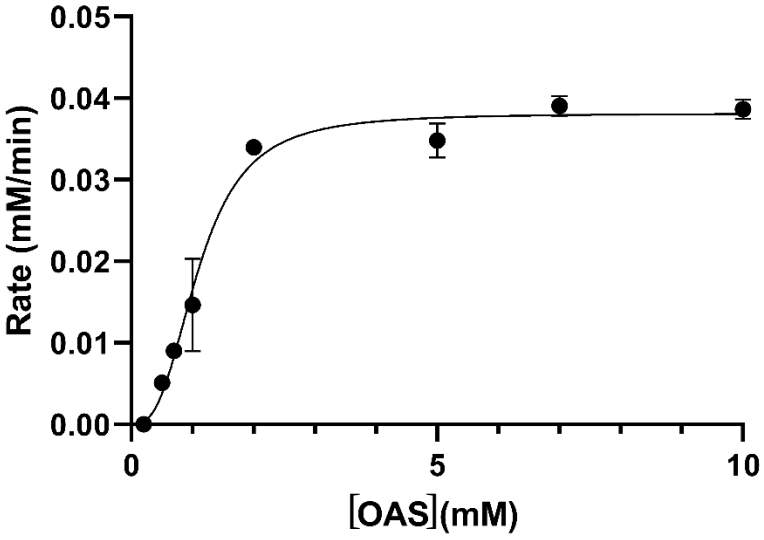

Figure 3.7: CysK activity with varying OAS concentration in the presence of 7 mM Na_2S. Allosteric sigmoidal (cooperativity) model fit to the data. CysK was freshly thawed for these assays. Assay reaction was conducted at 37 ºC. All reaction conditions were collected in duplicate. Error bars represent standard error.

Table 3.5: Summary of enzyme kinetic parameters for substrates OAS and Na_2S. Values are means calculated from duplicates and are quoted with SEM. kcat values are reported for the CysK dimer.

	OAS	**Na_2S**
v_{max} ($mM.min^{-1}$)	0.038 ± 0.001	2.530 ± 4.601
K_M (mM)	-	12.430 ± 8.133
K_{half} (mM)	1.01 ± 0.066	-
K_i	-	5.146 ± 5.012
k_{cat} (s^{-1})	6907 ± 181	458360 ± 833426
k_{cat}/K_M ($mM.s^{-1}$)	6271 ± 329	36875 ± 134097
h	-	4.159 ± 0.854
R^2	0.9795	0.9573

Table 3.6: Comparison of kinetic parameters amongst CysK homologues. Assay methods to measure cysteine produced are varied. $560_{nm}/546_{nm}$ = absorbance of cysteine at 560_{nm} or 546_{nm} wavelength, TNB 412nm = monitoring the disappearance of TNB at 412_{nm} wavelength, Electrode S^{2-} = electrode used to measure depletion of sulphide ions (S^{2-}), - = not reported. k_{cat} values are reported for the CysK dimer.

Organism	K_M or K_{half} (OAS/Na_2S) (mM)	k_{cat} (OAS/Na_2S) (s^{-1})	k_{cat}/K_M (OAS/Na_2S) ($mM.s^{-1}$)	pH, temperature, assay method	Reference
N. gonorrhoeae	1.01/12.43	$6.9x10^3$/458360	6271/36875	7.0, 37 ºC, 560_{nm}	This thesis
P. vulgaris	3.83/0.28	-	-	7.6, 25 ºC, Electrode S^{2-}	(Bertagnolli & Wedding, 1977)
P. polyanthus	0.75/0.18	-	-	7.6, 25 ºC, Electrode S^{2-}	(Bertagnolli & Wedding, 1977)
D. innoxia (isozyme A)	5.3/260	-	-	7.6, 34 ºC, 546_{nm}	(Kuske *et al.*, 1994)
D. innoxia (isozyme C)	5.1/80.5	-	-	7.6, 25 ºC, 546_{nm}	(Kuske *et al.*, 1994)
S. typhimurium	2.135/0.130	-	-	7.6, 25 ºC, Electrode S^{2-}	(Cook & Wedding, 1976)
S. typhimurium	1/0.006	-	$1.4x10^8/2.4x10^{10}$	7.0, 25 ºC, Electrode S^{2-} /TNB 412_{nm}	(Tai *et al.*, 1993)

The difference in the K_M for Na_2S and the K_{half} for OAS (12.43 mM Na_2S vs. 1.01 mM OAS) suggests CysK has a higher affinity for the OAS substrate. The K_M (or K_{half}) values for OAS are comparable with those collected from other CysK homologues (Table 3.6). Interestingly the range of K_M values collected for Na_2S across CysK homologues is extensive, most likely due to difficulties encountered in fitting any single kinetic model to the Na_2S profile. Thus, no accurate comparisons can be made between the *N. gonorrhoeae* K_M for Na_2S and other CysK homologues.

The catalytic turnover (k_{cat}) values were derived from the V_{max} as per section 2.6, assuming a dimer of CysK monomers for comparison with literature values. k_{cat} values for the CysK homologues in Table 3.6 could not be found. The specificity constant (k_{cat}/K_M) values were calculated as per section 2.6. The k_{cat}/K_M values for CysK OAS and Na_2S are $6.271x10^3$ and $3.688x10^4$, respectively. k_{cat}/K_M values of $\geq 10^8$ $M.s^{-1}$ indicate an enzyme is diffusion limited, thus, k_{cat}/K_M values of $10^3/10^4$, indicate CysK is not diffusion limited (Schurr & Schmitz, 1976). These values are however, 100,000 and 1,000,000-fold lower than the literature values found for *S. typhimurium* (Tai *et al.*, 1993). However, due to the issues encountered when fitting a model to the Na_2S kinetic profile, conclusions

cannot be drawn from many of these comparisons without further experimental interrogation of the kinetics.

Interestingly, there is a 10-fold k_{cat}/K_M increase for Na_2S compared to OAS. This, however, cannot be attributed to CysK having a greater affinity for Na_2S, as based on K_M/K_{half} values CysK has a higher affinity for OAS. The discrepancy in this explanation is a result of the difficulty in fitting a model to the Na_2S kinetic profile. K_M values tend to reflect concentrations of substrate observed in the intracellular environment. There are currently no reported values for S^{2-} or OAS concentration for *Neisseria* species. In *B. subtilis,* the intracellular concentrations of OAS have been reported to vary between ~20 – 200 µM, depending on whether cells were grown in the presence of methionine or cystine (cystine causes lower intracellular concentrations of OAS) (Tanous *et al.,* 2008). Assuming a similar intracellular concentration in *N. gonorrhoeae,* this would give a low intracellular concentration to K_M ratio for OAS (20-200 µM vs. 1010 µM, intracellular concentration vs. OAS K_M). This ratio would suggest CysK would not be saturated with OAS, likely limiting activity of CysK *in vivo* (Davidi *et al.,* 2016). The lack of literature values for any bacterial intracellular S^{2-} values does not allow for any conclusions about the effect Na_2S concentrations may have on *in vivo* CysK activity.

Many studies in the literature confirm that CysK uses a bi-bi ping-pong mechanism (also known as a non-sequential mechanism) (Cook & Wedding, 1976; Tai *et al.,* 1993; Rabeh & Cook, 2004; Joshi *et al.,* 2019). Based on this reaction mechanism seen in CysK homologues, we predict that CysK most likely has a bi-bi ping-pong mechanism, which is in keeping with the proposed enzyme:α-aminoacrylate intermediate during nucleophilic attack of the sulphide (Joshi *et al.,* 2019). However, it has been reported that S^{2-}, the inorganic anion, does not have a binding site within the CysK enzyme as a substrate, instead likely adding to the α-aminoacrylate intermediate immediately upon diffusion into the active site. An anion binding site has been confirmed with Cl^- ions present in CysK, causing an inhibited enzyme, however, this allosteric binding site was non-specific, accepting a wide array of anions to bind (Tai *et al.,* 2001). The role of S^{2-} in competitive substrate inhibition has been found across many species, including *D. innoxia, P. vulgaris, P. polyanthus* and *S. typhimurium* (Cook & Wedding, 1976; Bertagnolli & Wedding, 1977; Tai *et al.,* 1993; Kuske *et al.,* 1994). The partial competitive inhibition observed in the Na_2S kinetic profile of *N. gonorrhoeae's* CysK is typical of allosteric inhibitors,

indicating that at high S^{2-} concentrations, S^{2-} binds to an allosteric site, resulting in a partially inhibited enzyme (Tai *et al.*, 2001). Thus, a slightly alternative mechanism to the typical bi-bi ping-pong mechanism is proposed where the S^{2-} binds to an allosteric anion-binding site, causing a less active enzyme, however, despite binding of S^{2-} to the allosteric site or not, the overall reaction mechanism remains ping-pong (Tai *et al.*, 2001). The presence of an allosteric anion binding site explains the partial substrate inhibition we observe for Na_2S.

3.1.4.1 Variation of thiosulphate concentration

Many bacteria have both OASS isoforms, OASS-A/CysK that utilises bisulphide and OASS-B/CysM that utilises thiosulphate producing *S*-sulphocysteine that is converted to L-cysteine via an unknown mechanism (Figure 1.2, black dotted line in the bottom left). Many bacteria have both isoforms for utilisation in either aerobic or anaerobic conditions, however, all *Neisseria* species have only a single OASS enzyme variant. The single *Neisseria* OASS enzyme appears more homologous to the OASS-A/CysK isoform (Hicks & Mullholland, 2018), and from the data presented above is capable of utilising Na_2S as a substrate. Yet *N. gonorrhoeae* lacks the ability to produce sulphide via sulphate reduction (Hicks & Mullholland, 2018) and can grow on thiosulphate in the absence of cysteine. We therefore hypothesised that CysK from *N. gonorrhoeae* was a dual-functioning enzyme capable of utilising both thiosulphate and sulphide for the final step in cysteine biosynthesis. Thus, the ability of *N. gonorrhoeae* CysK to use thiosulphate as substrate was tested in a stopped assay as per section 2.7. Multiple concentrations (1, 2, 5, 10, 15, 20 and 50 mM) of thiosulphate were tested in the presence of 10 mM OAS (saturating).

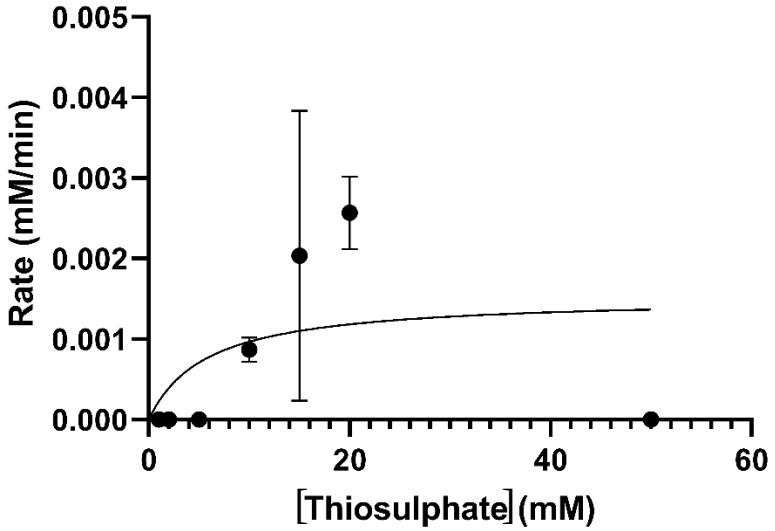

Figure 3.8: Thiosulphate CysK activity assay non-linear regression fit of a Michaelis-Menten model. OAS concentration was held at 10 mM. Assay reactions were conducted at 37 ºC. CysK was freshly thawed. Error bars represent standard error.

Non-linear regression fit of a Michaelis-Menten model gave a v_{max} and K_M of 0.00153 ± 0.0009 mM.min^{-1} and 5.780 ± 11.476 mM, respectively. The error in the K_M is greater than the K_M itself and takes it to below 0. This, alongside the exceptionally low V_{max}, which is outside the values measured indicates there was no enzyme activity detected for any thiosulphate concentration, thus, indicating CysK from *N. gonorrhoeae* cannot use thiosulphate as a substrate (Figure 3.8).

3.1.5 CysK kinetics Conclusions and future directions

The CysK substrates OAS and Na_2S both display positive cooperativity (allosteric sigmoidal) kinetics, however, Na_2S also displays partial competitive substrate inhibition. This coincides with the potential presence of an allosteric anion-binding site on the CysK enzyme proposed by (Tai *et al.*, 2001). *N. gonorrhoeae* CysK is unable to utilise thiosulphate as a substrate indicating the enzyme may not be a dual-functioning enzyme.

Future work includes investigating the effect higher OAS concentrations has on the kinetics of CysK. This will help elucidate the presence of any substrate inhibition that may occur, which may also be explained by the presence of the allosteric binding site, where the α-carboxylate of OAS binds to the allosteric binding site (Tai *et al.*, 2001). Collecting curves of the established reaction with increasing concentrations of Cl^- anions to observe the potential inhibition is also important for understanding the reaction mechanism of CysK. Understanding the reaction mechanism is crucial for computational inhibitor screening to identify lead compounds for CysK inhibition.

3.2 Structural characterisation of CysK from *N. gonorrhoeae*

3.2.1 *O*-acetylserine sulphydrylase/CysK

O-acetylserine sulfhydrylase (CysK/OASS-A, EC:2.5.1.47) is a key enzyme in the biosynthesis of cysteine in bacteria and plants. OASS-A is a member of the tryptophan synthase β-superfamily (Fold type II) and the β-family of PLP dependent enzymes (Mino & Ishikawa, 2003; Guédon & Martin-Verstraete, 2007; Takumi & Nonaka, 2016). Although structures of CysK from other bacteria have been characterised, there has been no investigation into the structure of CysK from *N. gonorrhoeae*.

We propose CysK is a valid target for the design of new antimicrobial compounds for treatment of gonorrhoea. To effectively do this, we require a high-resolution structure of CysK (Reichau *et al.*, 2011), which in turn can be used for computational inhibitor screening to identify leading compounds for future development. As there is currently no determined structure of CysK from *N. gonorrhoeae*, we aimed to purify, crystallise and determine the structure of CysK using X-ray crystallography.

3.2.2 Crystallisation of CysK

Prior to the beginning of this master's research, Annmaree Warrender and I grew diffracting CysK protein crystals and collected three datasets from a 2.3 Å crystal as per section 2.9. The crystal was obtained from crystallisation condition: 0.1 M HEPES pH 7.5, 4% polyethylene glycol 400 (v/v), 2.5 M ammonium sulphate.

3.2.3 CysK data processing

The data collected was initially indexed in space group 19 ($P2_12_12_1$) and a single dataset (number 17) used for processing. However, using solely dataset 17 in this space group, I was unable to solve the structure, with R values not improving during refinement with the best final model having an R_{work}/R_{free} score of 0.2300/0.3083. The space group was subsequently determined to have been incorrectly assigned using *zanuda* (Lebedev & Isupov, 2014) from the CCP4 suite (Winn *et al.*, 2011). The data was subsequently reindexed in space group 4 ($P12_11$) (based on *zanuda*_output), the unit cell dimensions changed to match dataset 16 and the two datasets (16 and 17) were integrated and scaled using XDS (Kabsch, 2010). Reflections were merged, resolution cut back to 2.49 Å, and a FreeR flag dataset for refinement and dataset quality statistics generated (Table 3.7) using AIMLESS from the CCP4 suite (Winn *et al.*, 2011). AIMLESS and *phenix.xtriage*

analysis of twinning and tNCS indicated the dataset had a low percentage of twinning fraction (0.02), therefore, no attempt to detwin the dataset was made. The following data quality thresholds are met by the determined data quality statistics; $CC_{1/2} \geq 0.3$ (0.834), $I/\sigma I \geq 2.0$ (2.6), $R_{merge} \leq 0.8$ (0.654) and overall completeness >95% (99.9%) (values in the highest resolution shell are reported) indicating the data is of good quality. This data was used for downstream processing.

Table 3.7: Data collection statistics for CysK. Statistics for highest resolution shell are shown in brackets. Data statistics generated by AIMLESS and *phenix.tableone*.

Data Statistic	**Apo structure**	
Space group	$P12_11$	
Cell dimensions		
a/b/c (Å)	102.74/62.18/105.67	
α/β/γ (º)	90/90.082/90	
Mosaicity	0.00	
Monomers in asymmetric unit	4	
Resolution range (Å)	47.53-2.49	(2.58-2.49)
Numbers of observed reflections	330233	(32079)
Number of unique reflections	47132	(4605)
R_{merge}	0.056	(0.654)
R_{pim}	0.023	(0.266)
$CC_{(1/2)}$	0.999	(0.834)
Mean of I/σI	19.2	(2.6)
Completeness	100.0	(99.9)
Multiplicity	7.0	(7.0)
Wilson B factor (Ang^2)	60.19	

3.2.4 Solving the CysK structure

Various CysK homologues present in the PDB were selected to be potential candidates for molecular replacement with good sequence similarity (≥ 30%) and conservation of secondary structural features (Figure 3.9). Based on this information, the *M. tuberculosis* CysK structure (3ZEI) (Poyraz *et al.*, 2013) was chosen as the search model for molecular replacement as it exceeded the minimum requirements of sequence similarity (57%) and the majority of the structure was built (97%).

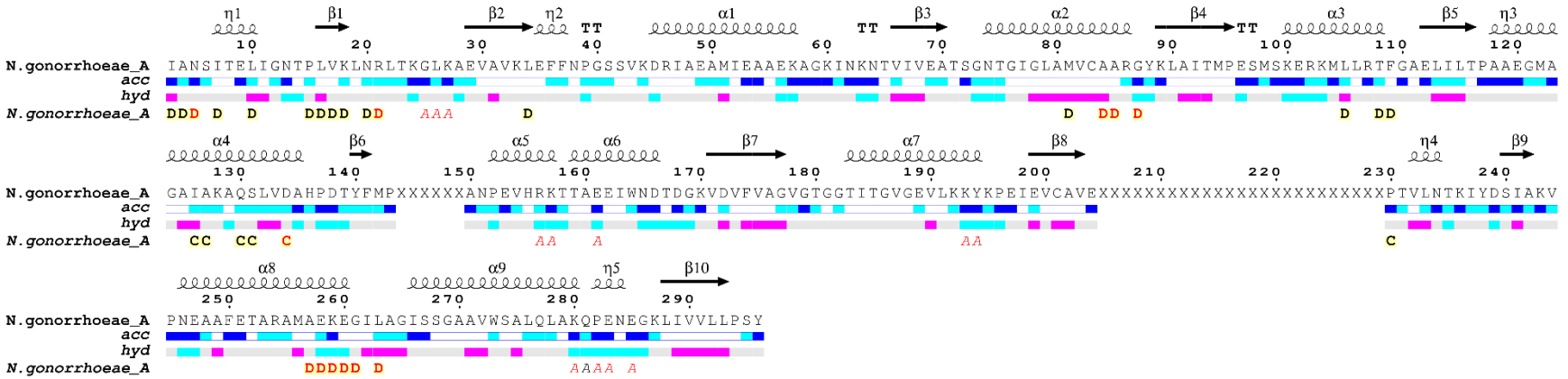

Figure 3.9: ENDscript analysis of the secondary structure of CysK from *N. gonorrhoeae*. For each residue solvent accessibility (acc) and hydrophobicity (hyd) are labelled below the sequence. acc is rated as blue being accessible, cyan less accessible, and white being completely buried from solvent (red being not calculated). hyd is ranked as cyan being hydrophilic, purple being hydrophobic and white being neutral. Secondary structure elements are labelled in grey above the peptide sequence, with helices, β-strands, and β-turns, represented by linked loops, arrows and TT, respectively. Letters indicate noncrystallographic interaction with chain denoted by letter. Refer to (Appendix D.1 Contents of the asymmetric unit for CysK) for chain labelling of the monomers in the ASU. Chain A was used for analysis. Figure generated using ENDscript 2.0 (Robert & Gouet, 2014).

The Matthew's coefficient was used to predict the number of monomers in the asymmetric unit (ASU) (Matthews, 1968). The most likely number of monomer copies present was determined to be four, calculated with a predicted molecular weight of 32.726 kDa for CysK from Protparam as per section 2.4.5. Thus, the CysK monomer (3ZEI) was used as a search model for molecular replacement with four monomers in the ASU (*phenix.phaser*). Phaser found a solution with good TFZ and LLG scores of 19.6 and 687.620, respectively (McCoy *et al.*, 2007).

The CysK model was built using the *autobuild.phenix* programme. The programme was supplied with the *phenix.phaser* output model and map, reflection file (with FreeR flag dataset) and the CysK amino acid sequence. Initially, default settings were used (Appendix D.2 Initial input settings for phenix.autobuild), except waters were not placed in the refinement. The building reached a threshold where the R_{free} and R_{merge} values were not improving. Therefore, default settings with minor alterations were used for the final rounds of structure building, where waters were not placed in the refinement, and rebuild in place was set to false (Appendix D.3 Final input settings for phenix.autobuild). The latter step allows the programme to edit the structure file based on the sequence file, as well as build outside the model (if there is unmodelled density present). The structure went through six iterative building rounds and three cycles of refinement. The resulting structure had a good R_{work}/R_{free} score for a starting model of 0.2305/0.3060. In the asymmetric unit, 4 monomers were built, with two forming a homodimer, while the two remaining monomers were positioned either side of the homodimer. The majority of each monomer was built by automated building using *phenix.autobuild,* however, there were large sections of the protein's amino acid sequence missing. The sections missing from Pro-137-Asn-151 and Glu-204-Ser-240 in each monomer were manually built in COOT.

3.2.5 Analysis of the CysK structure

The final structure model for CysK has a R_{work}/R_{free} of 0.2099/0.2623 (Table 3.8). Structure and map files for the CysK model are listed in (Appendix D.4 CysK structural files). There was no density to support the C-terminal tail from Leu-297 onwards including the hexahistidine-tag in any of the chains within the ASU, or the first two residues of each monomer. There was also no density to support Pro-143-Asn-151 or Glu-204-Tyr-238 (± 2 residues in some chains) across all four monomers in the ASU. The overall structure of CysK is moderately well built, with an average monomer length of 254.5 residues (254.5/312, 81.6% built) (Appendix D.5 CysK chain statistics).

The CysK monomer consists of an N-terminal domain spanning residues Val43-Pro143 and a C-terminal domain spanning residues Ile11-Ser42 and Asn151-Tyr296. The N-terminal domain is potentially extended further than residue Pro143, however, due to resolution restrictions and the potential flexibility of this region, there is a gap in the structure from Arg144-Ala150. The C-terminal domain also has a gap in the residue sequence from Glu204-Ile229, and the C-terminal tail extends further beyond Tyr296, however, due to both resolution and the flexibility of the C-terminal tail, these are the limits of the C-terminal domain.

Table 3.8: CysK final model quality statistics. Statistics generated by *phenix.tableone.*

Data statistic	**CysK**
R_{work}	0.2099
R_{free}	0.2623
No. of protein residues	1038
Total number of non-hydrogen atoms	7967
Macromolecules	7674
Solvent	293
RMS	
Bonds (Å)	0.021
Angles (º)	1.54
Average B value (Å)	64.25
Macromolecules	64.18
Solvent	66.08
Ramachandran analysis	
No. of residues in favoured region (%)	97.33
No. of residues in allowed region (%)	2.38
No. of residues in outlier region (%)	0.30
Rotamer outliers (%)	0

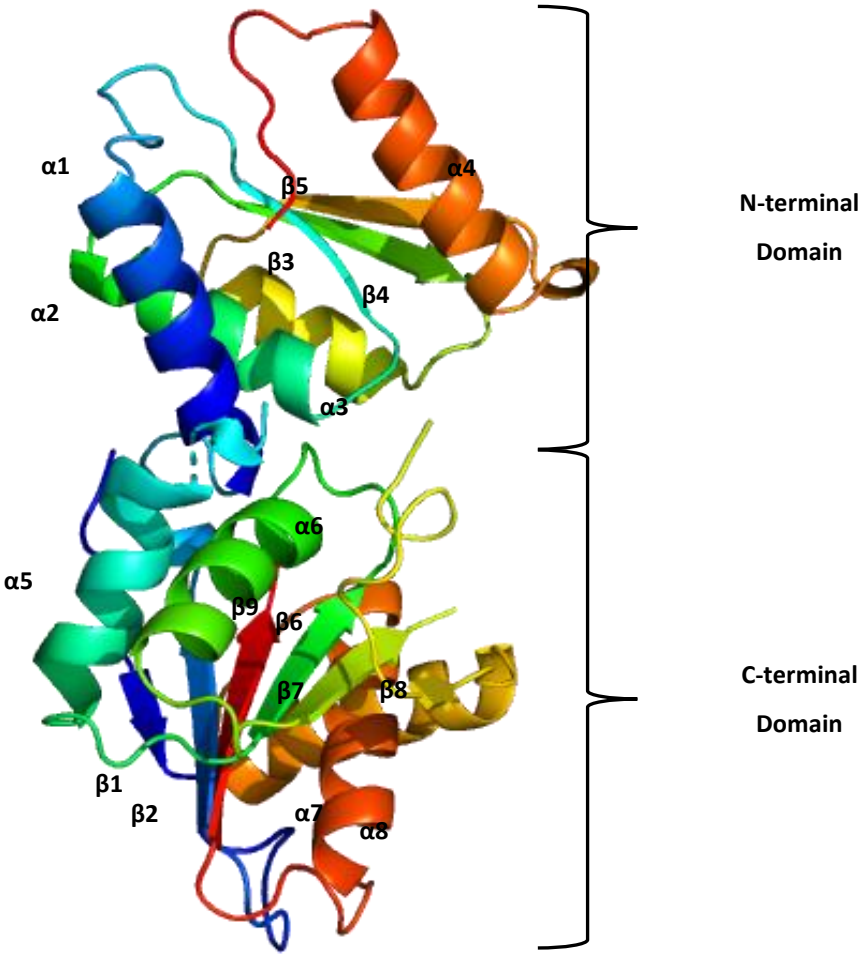

Figure 3.10: Structure of the CysK monomer from *N. gonorrhoeae*. N and C terminal domains outlined on the figure. Each domain is coloured from the N-terminus (blue) to the C-terminus (red). Helices are labelled with α. β-sheets are labelled with β. Figure generated in PyMOL.

3.2.5.1 Analysis of the CysK dimer

The CysK dimer has a height of 46.2 Å, and a width of 61.7 Å and has two-fold symmetry. The monomer-monomer formation of the dimer is a result of multiple hydrogen bonds and hydrophobic interactions between the monomers. A small portion of the dimer surface area is buried at the monomer-monomer interface, with 2840 $Å^2$ of a total dimeric surface area of 22230 $Å^2$ (12.8%) (calculated as per section 2.12.4). The calculated free energy for the dissociation (ΔG^{diss}) of the dimer is 10.7 $kcal.mol^{-1}$, demonstrating that the dimeric arrangement is thermodynamically stable. CysK has been confirmed to elute as a dimer by gel filtration chromatography (Figure 3.2).

3.2.5.2 Analysis of the CysK N-terminal domain

The N-terminal domain consists of a central three-stranded parallel β-sheet which is flanked by three α-helices on one side and a single α-helix on the other side (Figure 3.9, Figure 3.10 and Figure 3.11). Tyr-140 and Phe-141 are indicated to be the beginning of another β-sheet (STRIDE, (Frishman & Argos, 1995)), however, due to the gap from

Arg144-Ala150, this cannot be determined in this structure. The domain begins with an α-helix (α1, Val43-Ala58), and a meandering loop (Gly59-Val66) links to the first central β-sheet (β3, Ile67-Thr71). A sharp turn (Ser72-Gly73) links to the second α-helix (α2, Asn74-Arg86). The second β-sheet begins (β4, Lys90-Pro95), running parallel to β3 after a sharp turn (Gly87-Lys89). From β4 to α3 (Lys100-Phe109) there is a sharp turn (Glu96-Ser99). From α3 there is another sharp turn (Gly110-Ala111) to the third of the central parallel β-sheets (β5, Glu112-Thr116). A single residue sharp turn (Pro-117) leads to the α-helix on the other side of the central parallel β-sheets (α4, Ala118-Ala135). From here, a meandering loop (His136-Thr139) looks to be linking to a fourth central parallel β-sheet that is suggested to begin at Tyr-140 (STRIDE, (Frishman & Argos, 1995)). The linkage between the N-terminus and the C-terminus is missing as one of the residue gaps (Arg144-Ala150). The C-terminal domain begins at Asn151, however, there is also a small section of the C-terminal domain from residues Ile11-Ser42.

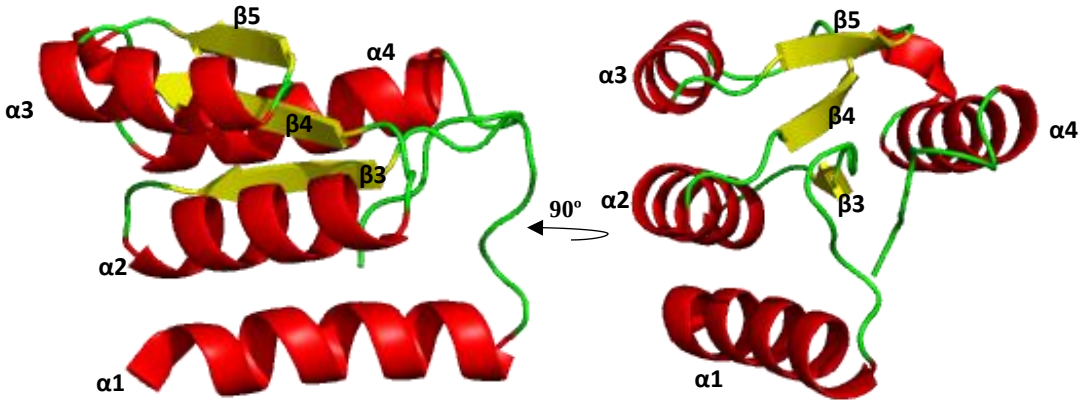

Figure 3.11: Structure of the CysK N-terminal domain from *N. gonorrhoeae*. Helices are coloured red and labelled with α. β-sheets are coloured yellow and labelled with β. Loops and turns are coloured green. Figure generated in PyMOL.

3.2.5.3 Analysis of the CysK C-terminal domain

The C-terminal domain consists of a central six-stranded mixed β-sheet with two α-helices on either side (Figure 3.9, Figure 3.10 and Figure 3.12). The domain begins with a loop (Ile11-Pro15) to the first β-sheet (β1, Leu16-Lys18) and continues with a meandering loop (Leu19-Ala28) to the second central β-sheet (β2, Glu29-Leu34). There is a short 3_{10} (Glu35-Phe37) and sharp turn (Asn38-Ser42) linking to the beginning of the N-terminal domain.

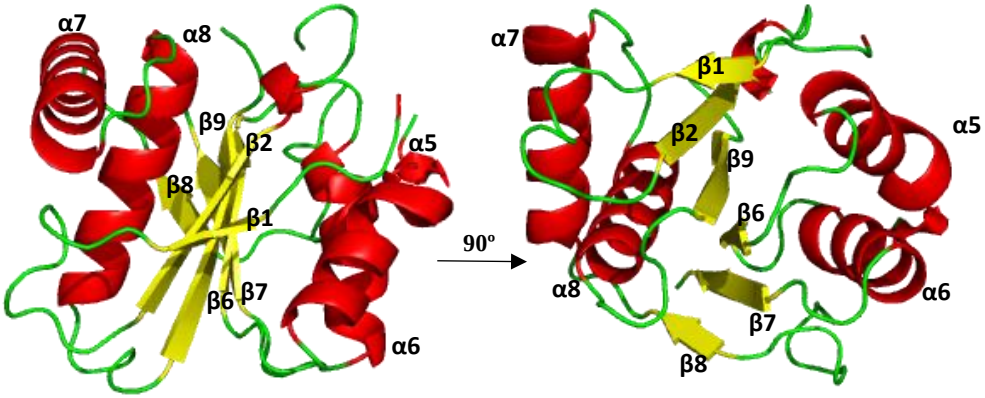

Figure 3.12: Structure of the CysK C-terminal domain from *N. gonorrhoeae*. Helices are coloured red and labelled with α. β-sheets are coloured yellow and labelled with β. Loops and turns are coloured green. Figure generated in PyMOL.

The C-terminal domain continues from Asn151, and the first α-helix of the domain begins (α5, Pro152-Thr167). A loop (Asp168-Asp172) links to the third central β-sheet (β6, Val173-Gly177). The second α-helix (α6, Thr183-Tyr194) is linked to β6 by a short loop (Val178-Gly182) which includes the majority of the PLP interacting 179-GTGGT-183 motif. A turn (Lys195-Ile198) continues from α6 to the fourth central β-sheet (β7, Glu199-Val203) where the residue sequence ends at the Glu204-Ile229 gap. The C-terminal domain continues with a meandering loop (Pro230-Asp239) to the fifth central β-sheet (β8, Ser240-Ala242). A tight turn (Lys243-Pro245) links to the domains third α-helix (α7, Asn246-Glu260), which links to the domains fourth α-helix (α8, Ile266-Lys280) via a turn (Gly261-Gly265). A meandering loop (Gln281-Gly286) connects to the final β-sheet of the domain (β9, Lys287-Leu293), after which the C-terminal domain ends with a loop (Pro294-Tyr296). The C-terminal tail is missing 16 residues in this structure, however, this is consistently found across CysK structures in the PDB (Salsi *et al.*, 2010; Poyraz *et al.*, 2013), and is most likely a result of the C-terminal tail's flexibility.

3.2.5.4 Structure of the CysK active site

The functional enzyme forms a homodimer of ~75.452 kDa and characteristic of the Fold type II family, the active site of the enzyme is made up of residues all from one subunit (Liang *et al.*, 2019). Alignment of the CysK protein sequence from *N. gonorrhoeae* with other bacterial homologues, demonstrates moderate sequence similarity compared to other proteobacterial and plant species (average 54.20% sequence similarity), but shows strong conservation of the PLP co-factor interacting residues Lys-44, Val-40, Ser-266, the asparagine loop at Asn-74, the substrate carboxylate binding Gln-145 and the PLP interacting 179-GTGGT-183 motif (except in *B. abortus*) (Figure 3.13). The active site

residues 71-TSGNTG-76 (Joshi *et al.*, 2019) (except the moderately conserved Serine) and 223-GIGA-226 (Joshi *et al.*, 2019) are also strongly conserved in the six species across the ranges 68/72-72/76 and 222/228-225/231, respectively (Figure 3.13). The closest structural relatives of *N. gonorrhoeae* CysK are from *M. tuberculosis* (Poyraz *et al.*, 2013) and *H. influenzae* (Salsi *et al.*, 2010) with root mean square deviation values after

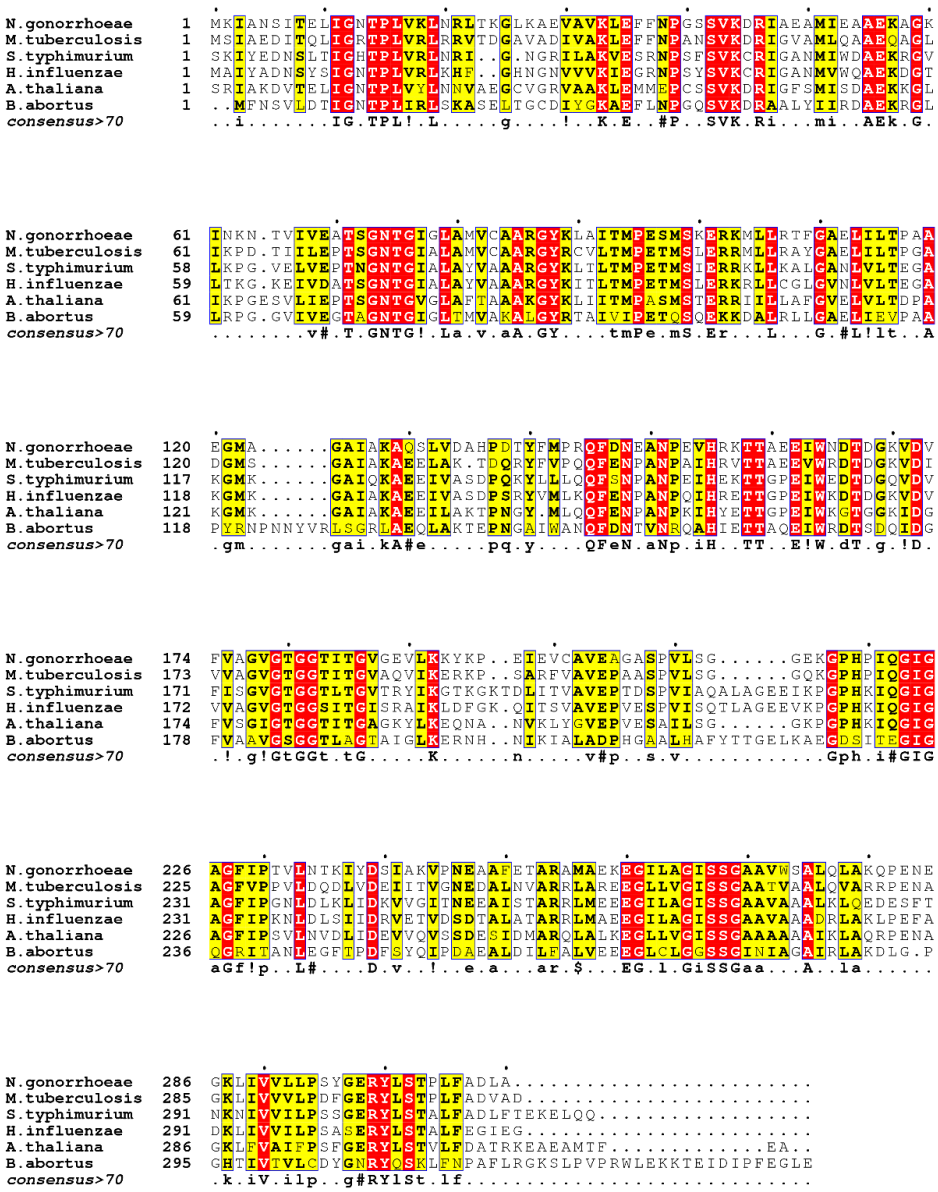

Figure 3.13: CysK protein sequence alignment. The *N. gonorrhoeae* FA1090 CysK amino acid sequence was aligned to the following CysK homologues; *M. tuberculosis* (65.7% sequence similarity); *S. typhimurium* (55.05% sequence similarity); *H. influenzae* (55.84% sequence similarity); *A. thaliana* (55.02% sequence similarity) and *B abortus* (39.41% sequence similarity). Highly conserved residues are highlighted in red, whilst less conserved residues are highlighted in yellow. Sequence alignment created using Clustal Omega. Figure created using ESPript 3.

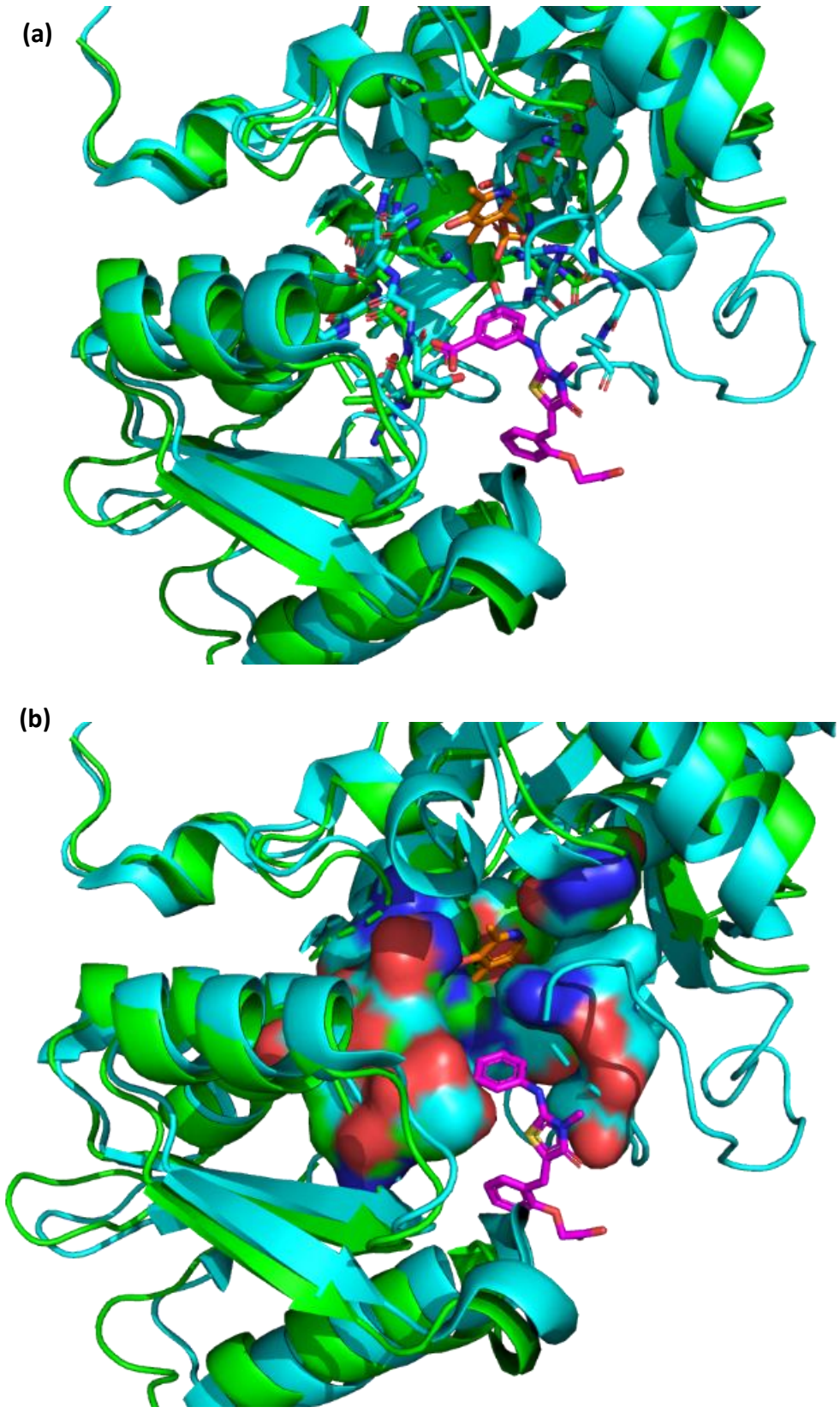

Figure 3.14: Structural overlay of *N. gonorrhoeae* and *M. tuberculosis* CysK monomers. (a) active site and PLP interacting residues shown in licorice-stick format. (b) active site and PLP interacting residues shown as the surface of the active site cleft. *N. gonorrhoeae* structure shown in green. *M. tuberculosis* structure shown in cyan. PLP shown in orange. AWH (3-((Z)-((Z)-5-(4-Fluorobenzylidene)-3-methyl-4-oxothiazolidin-2-ylidene) amino) benzoic Acid) shown in magenta. Red sections of the surface of the active site cleft indicate negative potential. Blue sections of the surface of the active site cleft indicate positive potential. Figure generated in PyMOL.

structural superposition of 1.1 Å (229 equivalent C-atoms) and 1.274 Å (219 equivalent C-atoms), respectively. The active site residues 71-TSGNTG-76 and 223-GIGA-226 are strongly conserved in *N. gonorrhoeae* and have been identified through sequence alignment (Figure 3.13). However, as a function of resolution constraints and the flexibility of the loop, residues 223-GIGA-226 are not visible in the CysK structure. Alignment of the *N. gonorrhoeae* and *M. tuberculosis* CysK structures indicate the 71-TSGNTG-76 active site residues from *N. gonorrhoeae* have the same conformation as *M. tuberculosis* CysK (Figure 3.15).

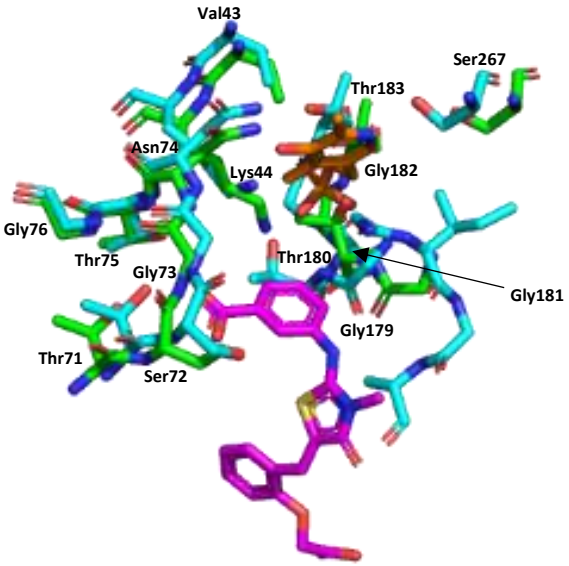

Figure 3.15: Alignment of *N. gonorrhoeae* and *M. tuberculosis* CysK active site and PLP interacting residues, in licorice-stick format. Active site residues 71-TSGNTG-76 and PLP interacting residues; Val-43, Lys-44, Asn-74, Ser-267 and 179-GTGGT-183 motif from *N. gonorrhoeae* are labelled. *M. tuberculosis* active site residues 223-GIGA-226 on the right are not labelled. *N. gonorrhoeae* monomer D residues shown in green. *M. tuberculosis* residues shown in cyan. PLP shown in orange. AWH (3-((Z)-((Z)-5-(4-Fluorobenzylidene)-3-methyl-4-oxothiazolidin-2-ylidene) amino) benzoic Acid) shown in magenta. Figure generated in PyMOL.

Overall, the active site residues and PLP interacting residues that form the active site cleft align in a very similar conformation in *N. gonorrhoeae* and *M. tuberculosis* structures (Figure 3.14, Figure 3.15 and Figure 3.16). Despite the absence of the 223-GIGA-226 active site residues from the *N. gonorrhoeae* CysK structure (Figure 3.15), it is clear the structures form a very similar active site cleft. The binding of AWH (3-((Z)-((Z)-5-(4-Fluorobenzylidene)-3-methyl-4-oxothiazolidin-2-ylidene) amino) benzoic Acid) into the *M. tuberculosis* active site gives a good indication of how *O*-acetylserine would bind into the active site of CysK in *N. gonorrhoeae.* AWH is a novel thiazolidine inhibitor of OASS, designed by (Poyraz *et al.*, 2013), which is bound in the active site of the *M. tuberculosis* CysK.

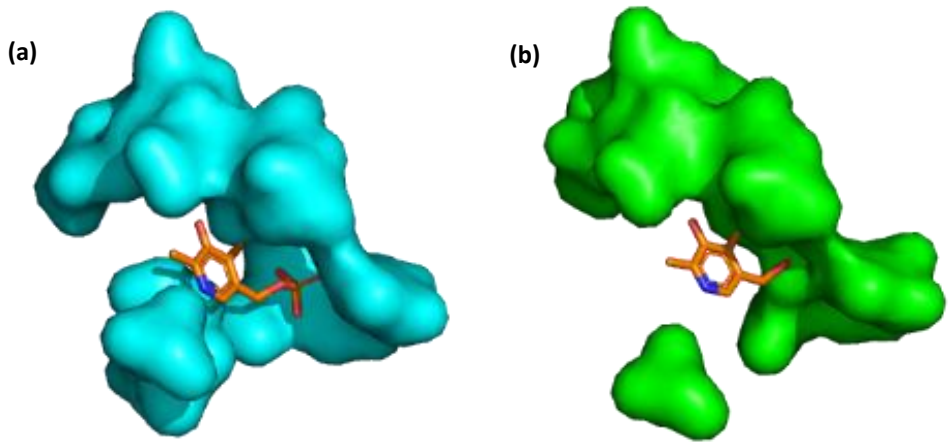

Figure 3.16: CysK active site cleft formed by the active site (71-TSGNTG-76 and 223-GIGA-226) and PLP interacting (Val-43, Lys-44, Asn-74, Ser-267 and 179-GTGGT-183 motif) residues from *M. tuberculosis* (a) and *N. gonorrhoeae* (b). PLP shown in orange. Note the region missing in the *N. gonorrhoeae* structure in (b) corresponds to the missing GIGA flexible loop in the active site. Figure generated in PyMOL.

Structural alignment of the *M. tuberculosis* OASS-A/CysK enzyme with our isolated OASS isoform from *N. gonorrhoeae* indicates, our enzyme is also an OASS-A/CysK enzyme rather than the alternate isoform OASS-B/CysM which has a larger active site. Due to the strong structural similarity between *N. gonorrhoeae* and *M. tuberculosis* CysK enzymes (Figure 3.14, Figure 3.15 and Figure 3.16), it is assumed that the overall surface structure between the two enzymes will be the same if the *N. gonorrhoeae* structure was not missing active site residues (223-GIGA-226) and Glu204-Pro230 stretch. Therefore, to confirm the OASS enzyme from *N. gonorrhoeae* is a true OASS-A/CysK isoform, we compared the structure of *M. tuberculosis* CysK (3ZEI (Poyraz *et al.*, 2013)) with the OASS-B/CysM isoform from *E. coli* (2BHT (Claus *et al.*, 2005)) (Figure 3.17).

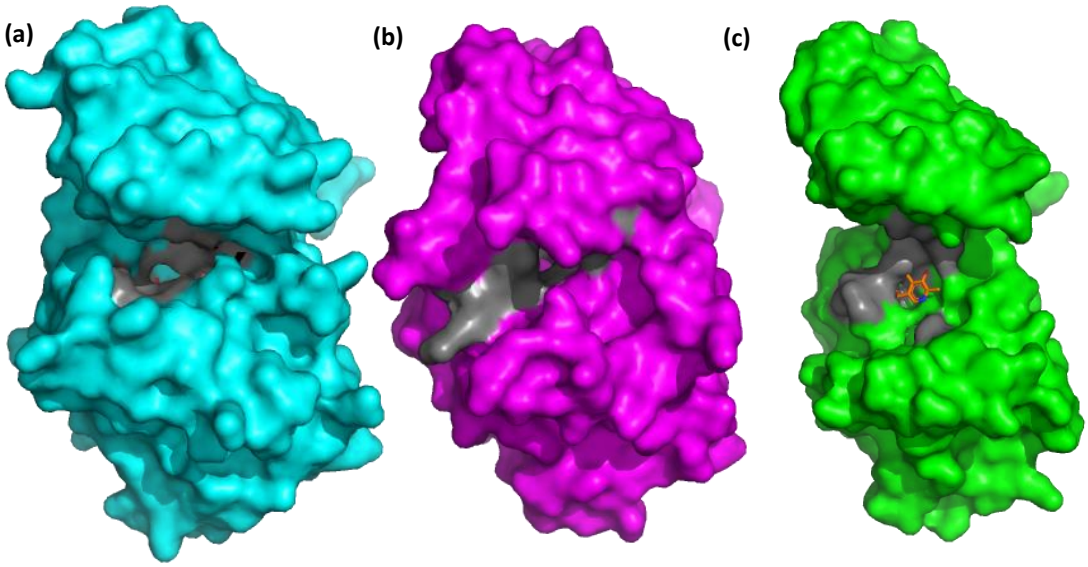

Figure 3.17: CysK and CysM monomers from *M. tuberculosis, E. coli* and *N. gonorrhoeae* focused on the active site cleft. (a) CysK from *M. tuberculosis.* (b) CysM from *E. coli.* (c) CysK from *N. gonorrhoeae*. Active site cleft forming residues are shown in grey. PLP shown in orange.

The active site residue loop (Arg211-Asp227) from CysM extends further than the active site in CysK (Figure 3.17) showing a larger active site capable of accommodating the larger thiosulphate molecule compared to the smaller active site seen in CysK only capable of accommodating sulphide. This is largely due to the three residues found at the beginning of the CysM active site loop, Arg210, Arg211, and Trp212, whereas CysK has significantly smaller residues at a similar position, Lys210, Ser211, and Gly212 (Claus *et al.*, 2005). The *N. gonorrhoeae* CysK is missing a large section of its active site cleft due to the Glu204-Pro230 stretch absent from the structure as a function of resolution and flexibility of this loop.

3.2.5.5 Interaction of the CysK active site with PLP

The heavily conserved PLP interacting residues Val-43, Lys-44, Asn-74, Ser-267 and the 179-GTGGT-183 motif are present within the CysK crystal structure, however, although co-purified with PLP there is no density to support PLP bound in the active site. Interactions with PLP are assumed to be highly conserved across CysK enzymes from many organisms as these residues are highly conserved (Figure 3.13). In *M. tuberculosis*, the 3-hydroxyl group of PLP hydrogen bonds to the side chain of Asn-74 within the highly conserved sequence Glu69-Gly76. This highly conserved sequence is present in *N. gonorrhoeae* from Thr71-Gly76 (Figure 3.13) and so should share the same interaction. Ser-267 which hydrogen bonds to PLP's pyridine nitrogen in *S. typhimurium* (Rabeh & Cook, 2004) is also highly conserved. Many related OASS-A enzymes show essentially

the same interactions with the PLP cofactor (Schnell *et al.*, 2007), so we assume this will be the same in *N. gonorrhoeae*.

The PLP interacting residues from each monomer of the dimer seen in the ASU (Monomer A and D, Appendix D.2) were overlaid with the corresponding residues from the *M. tuberculosis* CysK structure (Figure 3.18 and Figure 3.19) to investigate active site architecture.

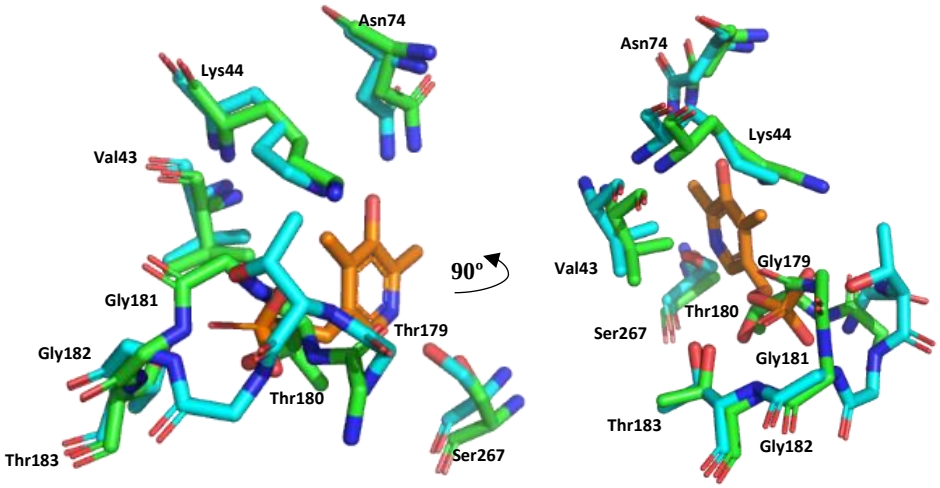

Figure 3.18: Aligned PLP interacting residues from *N. gonorrhoeae* monomer A and *M. tuberculosis* CysK monomer with PLP present, in licorice-stick format. This is monomer A from the ASU (Appendix D.2). *N. gonorrhoeae* CysK is shown in green. *M. tuberculosis* CysK is shown in cyan. PLP is shown in orange. *N. gonorrhoeae* residues are labelled. Right diagram is the left diagram rotated 90º. Figure generated in PYMOL.

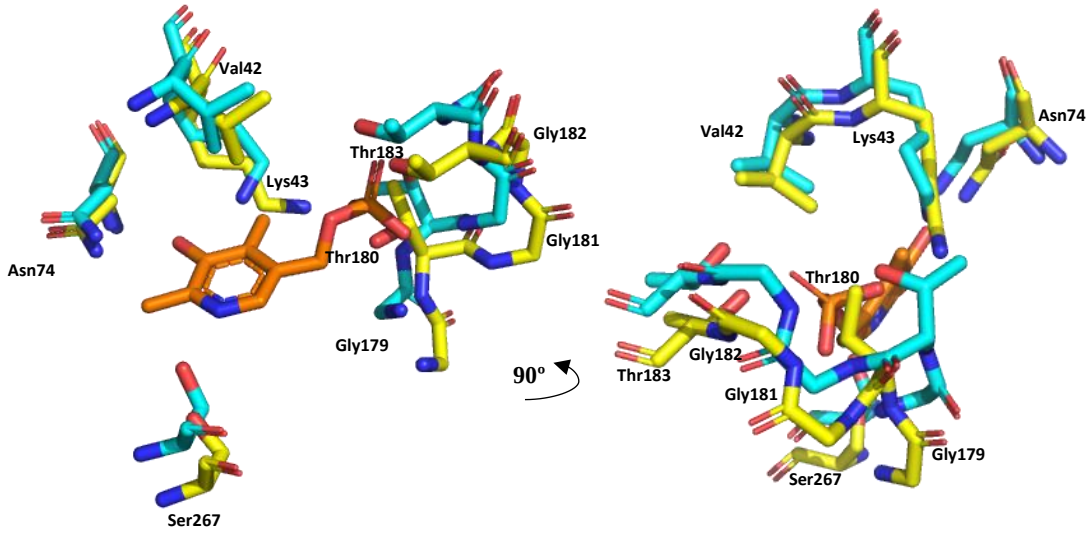

Figure 3.19: Aligned PLP interacting residues from *N. gonorrhoeae* monomer D and *M. tuberculosis* CysK monomer with PLP present, in licorice-stick format. This is monomer D from the ASU (Appendix D.2). *N. gonorrhoeae* CysK is shown in yellow. *M. tuberculosis* CysK is shown in cyan. PLP is shown in orange. *N. gonorrhoeae* residues are labelled. Right diagram is the left diagram rotated 90º. Figure generated in PYMOL.

The 179-GTGGT-183 motif in monomer A is blocking the PLP binding site and is in a significantly different conformation to the same motif in the *M. tuberculosis* CysK structure (Figure 3.18). This would indicate that the monomer is in an inactive

conformation as CysK is PLP dependent and it is unable to bind with the PLP interacting residues here. Conversely, in monomer D, this same motif is in a different conformation that is not preventing binding of the PLP co-factor (Figure 3.19). The Thr-178 sidechain appears particularly close to the phosphate of the PLP. However, considering the slightly different conformation of Lys-43, Gly-179, Thr-180 and the different relative positions of the PLP interacting residues there is still room for the PLP co-factor to bind as this PLP molecule is aligned to the *M. tuberculosis* PLP interacting residues. This indicates monomer D is in an active conformation. To confirm monomer A is correct in the structure, the residue map was checked in WINCOOT, indicating there is no density supporting the 179-GTGGT-183 motif in the same conformation as monomer D (active conformation) (Figure 3.20).

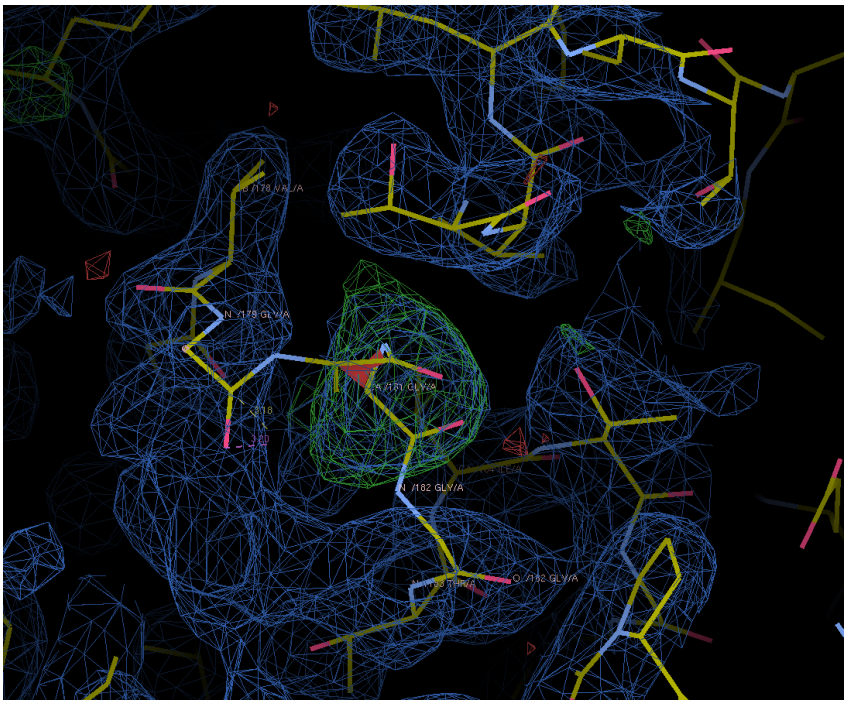

Figure 3.20: Monomer A electron density residue map with 179-GTGGT-183 motif in the same conformation as monomer D. Oxygen is shown in red. Nitrogen is shown in blue. Carbon is shown in yellow. Figure generated in WINCOOT. 2Fo-Fc and Fo-Fc map contoured at one and three σ, respectively.

This indicates our structure of the *N. gonorrhoeae* CysK dimer has one monomer in an active conformation and the other in an inactive conformation.

3.2.5.6 *N. gonorrhoeae* CysK structure conclusions and future directions

N. gonorrhoeae CysK has all of the highly conserved PLP interacting (Val-43, Lys-44, Asn-74, Ser-267, 179-GTGGT-183 motif) and active site (71-TSGNTG-76 and 223-GIGA-226) residues, all of which form the active site cleft.

Interestingly, in the *N. gonorrhoeae* CysK structure we see two different conformations of the PLP interacting loop motif 179-GTGGT-183 in adjacent monomers in the dimer. In monomer A the conformation blocks PLP from being able to bind, and in monomer D is an active form, capable of PLP binding. The other monomer, however, was in an alternate conformation that accommodated the binding of PLP. Therefore, it was surmised that one monomer within the *N. gonorrhoeae* CysK dimer is in an inactive conformation whilst the other is in an active conformation.

Comparison of the active site cleft also supports the conclusion that this OASS isoform is the OASS-A/CysK isoform. However, due to the residues missing from the crystal structure (Glu204-Pro230), which also contain the active site residues 223-GIGA-226, this comparison between the CysM (*E. coli*) and CysK (*M. tuberculosis*) active site clefts cannot conclusively state our OASS is CysK. However, this combined with the structural similarity between *M. tuberculosis* CysK and *N. gonorrhoeae* OASS, allows us to conclude we have isolated OASS-A, a CysK isoform from *N. gonorrhoeae.*

As a result of comparing the active site cleft from CysK (*M. tuberculosis*) with CysM (*E. coli*), a higher resolution structure is required to conclusively state our enzyme is the OASS-A/CysK isoform by structural comparison of the active site to a OASS-B/CysM isoform active site. Future research will also involve co-crystallisation of our CysK with substrates OAS and Na_2S in the active site to allow determination of the interactions between monomers and their active site conformations. Crystallisation in the presence of chloride could also elucidate the potential presence of an allosteric anion binding site within the dimer as seen in other CysK enzymes (Tai *et al.*, 2001).

3.3 Investigating Cysteine Synthase Complex formation in *N. gonorrhoeae*

3.3.1 The Cysteine Synthase Complex

The cysteine synthase bienzyme complex was first discovered during purification of CysE and CysK from *S. typhimurium* (Kredich & Tomkins, 1966; Kredich *et al.*, 1969). Complex formation has since been confirmed across many other species including *E. coli* (Mino *et al.*, 2000; Benoni *et al.*, 2017b), *H. influenzae* (Salsi *et al.*, 2010) and various plant species (Yi *et al.*, 2013). The CSC is an unusual protein complex, as most form to shuttle substrates/products from one enzyme to another. The CSC is different as it forms via binding of the CysE C-terminal tetrapeptide into the active site of CysK, halting all CysK activity and thus, cysteine production (Kredich *et al.*, 1969; Mino *et al.*, 2000; Salsi *et al.*, 2010; Yi *et al.*, 2013; Benoni *et al.*, 2017b; Hicks & Mullholland, 2018). One hypothesis for the formation of the CSC is for modulation of sulphur flux within bacterial metabolism (Hell & Wirtz, 2002; Wirtz *et al.*, 2012). The key residues required for binding of the CysE tail to the CysK active site were determined via screening a tetrapeptide library for binding ability, which was monitored by CysK activity and PLP fluorescence (Campanini *et al.*, 2005). It was established that a C-terminal isoleucine is both essential for binding and inhibition of CysK and is well-conserved across CSC forming organisms (Campanini *et al.*, 2005; Huang *et al.*, 2005; Salsi *et al.*, 2010; Benoni *et al.*, 2017b). The C-terminal tetrapeptide sequence in *N. gonorrhoeae* CysE was confirmed to have the conserved isoleucine with a four-residue sequence DFMI (Oldham, 2020), therefore it was predicted that CysK and CysE from *N. gonorrhoeae* are able to form the CSC. Formation of this complex has not yet been characterised in *N. gonorrhoeae*.

3.3.2 Monitoring CSC formation by fluorescent spectroscopy

Evaluation of CSC formation has been successful in studies by (Kumar *et al.*, 2011), (Campanini *et al.*, 2005) and (Wang & Leyh, 2012). This is a result of measuring the fluctuations in fluorescence linked to the binding of the CysE tail into the CysK active site and alternate conformations of the co-factor, PLP. Within CysK, the co-factor PLP is covalently attached to a conserved Lysine in the active site (Lys-44 in *N. gonorrhoeae* CysK) which forms a fluorescent protonated internal aldimine (Figure 1.9) (Wang & Leyh, 2012). This protonated internal aldimine has two tautomers, the ketoenamine and the enolimine, which each have distinct fluorescent spectral features. The ketoenamine

has an excitation wavelength of ~414 nm with an emission spectrum of ~510 nm which changes upon partial closure of the CysK active site (Wang & Leyh, 2012). Within the CysK active site, binding at a subsite that binds the α-carboxyl of substrates causes partial closing of the CysK active site. This closure is proposed to cause the observed ~15 nm blue shift in PLP emission spectra due to a lengthening of the ketoenamine excited-state lifetime (Wang & Leyh, 2012). The C-terminal carboxylate of CysE C-terminal peptides has been shown to bind to the CysK acceptor subsite, causing the same ~15 nm blue shift that substrate binding to the CysK subsite causes. Thus, indicating the CSC formation can be monitored by the ~15 nm blue shift as a result of the change in PLP fluorescence caused by binding of the CysE C-terminal tail or tetrapeptide into the CysK active site.

3.3.3 Binding of CysE to CysK to form the CSC

CysK and CysE were freshly purified by IMAC and gel filtration as per sections 2.4 and 2.13.1, respectively, using the previously described buffer for CysE and a modified buffer for CysK (pH 8.0 rather than 7.0). Both proteins were purified individually for use in CSC formation experiments.

Initially, the two freshly purified enzymes were combined in a quartz cuvette in a 4:1, CysK:CysE molar ratio and mixed manually using a stir rod. This manual mixing resulted in visible protein precipitation. To prevent protein precipitation after addition of CysE, the emission wavelength was measured at addition of CysE without manual mixing (0 min), and two minutes after to allow mixing to occur. Combination of the two enzymes for CSC formation experiments was conducted as per section 2.13.2.2.

CysK and CysE were combined at a variety of molar ratios and emission wavelength scans from 450-600$_{nm}$ were carried out at an excitation wavelength of 400$_{nm}$ (Figure 3.21).

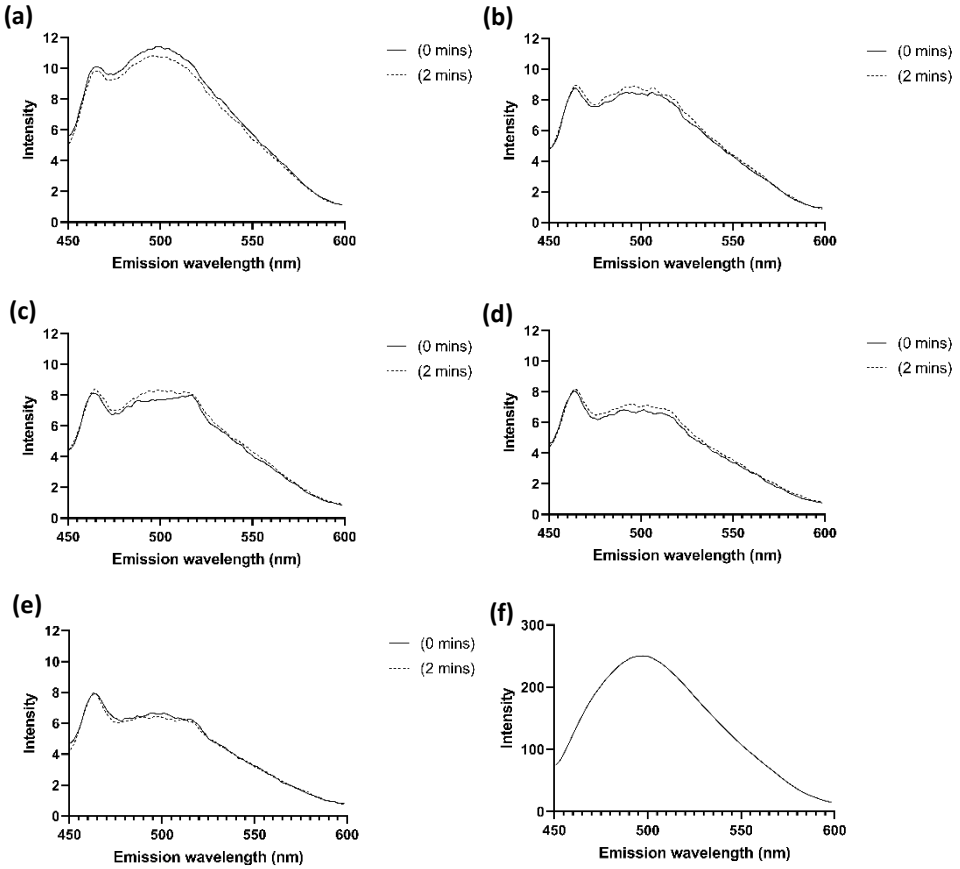

Figure 3.21: Fluorescent spectroscopy emission wavelength scans of CysK:CysE ratios for CSC formation. CysK:CysE (a) 4:1 (b) 2:1 (c) 1:1 (d) 2:3 (e) 1:2 (f) CysK only scan. Measured at room temperature 22 ºC. Excitation wavelength 400_{nm}. Emission wavelength measured between $450\text{-}600_{nm}$.

Table 3.9: Fluorescent spectroscopy emission wavelength measurements of the CysK:CysE ratio for CSC formation. Wavelength of the apex of each peak for each reaction condition are recorded. CysK and CysE were freshly purified. Measurements were taken at room temperature 22 ºC.

CysK:CysE monomeric ratio	**Peak Apex measurements (nm)**	
	0 (min)	**2 (min)**
4:1	498	495
2:1	464.2	Peak 1: 464.8
	-	Peak 2: 497
1:1	Peak 1: 464	Peak 1: 464.8
	Peak 2: 516.6	Peak 2: 498.6
2:3	464	464.2
1:2	463.8	463.4
CysK only	497.6	-

Data processing identified the number of peaks and their corresponding apex wavelength (Table 3.9). The wavelengths in Table 3.9 indicate an approximately 35 nm blueshift in the 2:1, 1:1, 2:3 and 1:2, CysK:CysE mixtures, alongside no shift in the 4:1 mixture.

However, visual interrogation of the spectra (Figure 3.21) shows this supposed blueshift peak at approximately 465_{nm} is present in all spectra at all CysK:CysE ratios. The emission peak at approximately 500_{nm} is also present in all spectra (Figure 3.21). Interestingly, despite the CysK concentration remaining constant, the peak seen at approximately 500_{nm} decreases in intensity as the ratio of CysK:CysE decreases (Table 3.10). The 465_{nm} peak also decreases in intensity until the 1:1, CysK:CysE ratio (Table 3.10).

Table 3.10: Changes in fluorescence peak intensity over varied CysK:CysE ratios. Both 500_{nm} and 465_{nm} peak are shown.

CysK:CysE ratio	500_{nm} Peak		465_{nm} Peak	
	0 min	**2 min**	**0 min**	**2 min**
4:1	11.43	10.81	10.11	9.862
2:1	8.489	8.917	8.757	8.963
1:1	7.997	8.318	8.139	8.410
2:3	6.842	7.191	8.063	8.184
1:2	6.689	6.450	7.917	7.967

As the peak seen at 465_{nm} is not present in the solely CysK fluorescent scan (Figure 3.21f), it is assumed this peak is due to the addition of the CysE protein. However, further fluorescent wavelength scans of solely CysE need to be conducted to confirm this.

The absence of a peak at 485 nm indicates no 15 nm blueshift in the fluorescence spectra, thus, showing the CSC has not formed in this experiment. A possible explanation for the CSC not forming, is the presence of *O*-acetylserine (OAS), which is able to dissociate the complex at OAS concentrations upwards of 50 µM (Kredich *et al.*, 1969; Wang & Leyh, 2012; Benoni *et al.*, 2017a). OAS is a common metabolite present in *E. coli* (Sajed *et al.*, 2016), thus, making it possible that OAS from *E. coli* expression strain BL21 (DE3) could co-purify with CysK or CysE, therefore preventing CSC formation. However, OAS is unstable at pH values greater than 7.6 (Kredich & Tomkins, 1966), where it will non-enzymatically and rapidly convert to *N*-acetylserine, which is unable to bind to CysK (Kredich & Tomkins, 1966). Given CysK purification for this experiment was conducted at room temperature in potassium phosphate buffers with a constant pH of 8.0, there was likely little to no *O*-acetylserine present, and can therefore be ruled out as the cause of the CSC not forming.

3.3.4 Binding of a CysE C-terminal tetrapeptide to CysK

A four amino acid peptide corresponding to the last four amino acids of the CysE C terminal tail was synthesised with the sequence DFMI to test for binding to CysK. A four amino acid peptide was chosen as in previous studies this was shown to bind to the enzyme and inhibit activity (Salsi *et al.*, 2010; Kumar *et al.*, 2011).

CysK and the tetrapeptide were freshly thawed for use in fluorescence spectroscopy and experiments were conducted as per section 2.13.2.3. CysK and the tetrapeptide were combined at a variety of molar ratios and emission wavelength scans from 450-600$_{nm}$ were carried out at an excitation wavelength of 386.2$_{nm}$ (Figure 3.22). The excitation wavelength for these CysK:CysE tetrapeptide fluorescent wavelength scan experiments differ from the CysK:CysE protein fluorescent wavelength scan experiments above as the preliminary excitation wavelength scan completed as per section 2.13.2.3 indicated a different excitation wavelength (386.2$_{nm}$). All measurements were conducted whilst mixing with a magnetic stirrer, and no precipitation was observed. Processed data indicated the number of peaks and their corresponding apex wavelength (Table 3.11). These apex wavelengths indicate an initial redshift (~30 nm) from the initial emission wavelength measured (471 nm) in the 4:1, CysK:CysE tetrapeptide mixture. All other CysK:CysE tetrapeptide ratios indicate essentially no change in wavelength as they fluctuate within the 490-500 nm range in a seemingly random pattern. Interestingly, despite the CysK concentration remaining constant, visual interrogation of the fluorescent spectra (Figure 3.22) indicate the intensity of the peaks in the 490-500$_{nm}$ range increases as the CysK:peptide ratio decreases (Table 3.12).

The absence of a 15 nm blueshift in the fluorescence spectra indicates there has been no binding of the tetrapeptide to CysK, therefore partial closure of the CysK active site has not occurred and, no change in PLP fluorescence has occurred. Thus, further indicating the CSC does not from in *N. gonorrhoeae.* In this experiment, the presence of OAS due to carryover during expression in *E. coli* may be possible. CysK used in this experiment was purified in potassium phosphate buffers at pH 7.0 at which, OAS is more stable and does not rapidly convert to NAS (Kredich & Tomkins, 1966). Thus, OAS may have been

present in the thawed CysK aliquot at concentrations above 50 µM causing dissociation of any CysE C-terminus tail peptide that may have bound to the CysK active site.

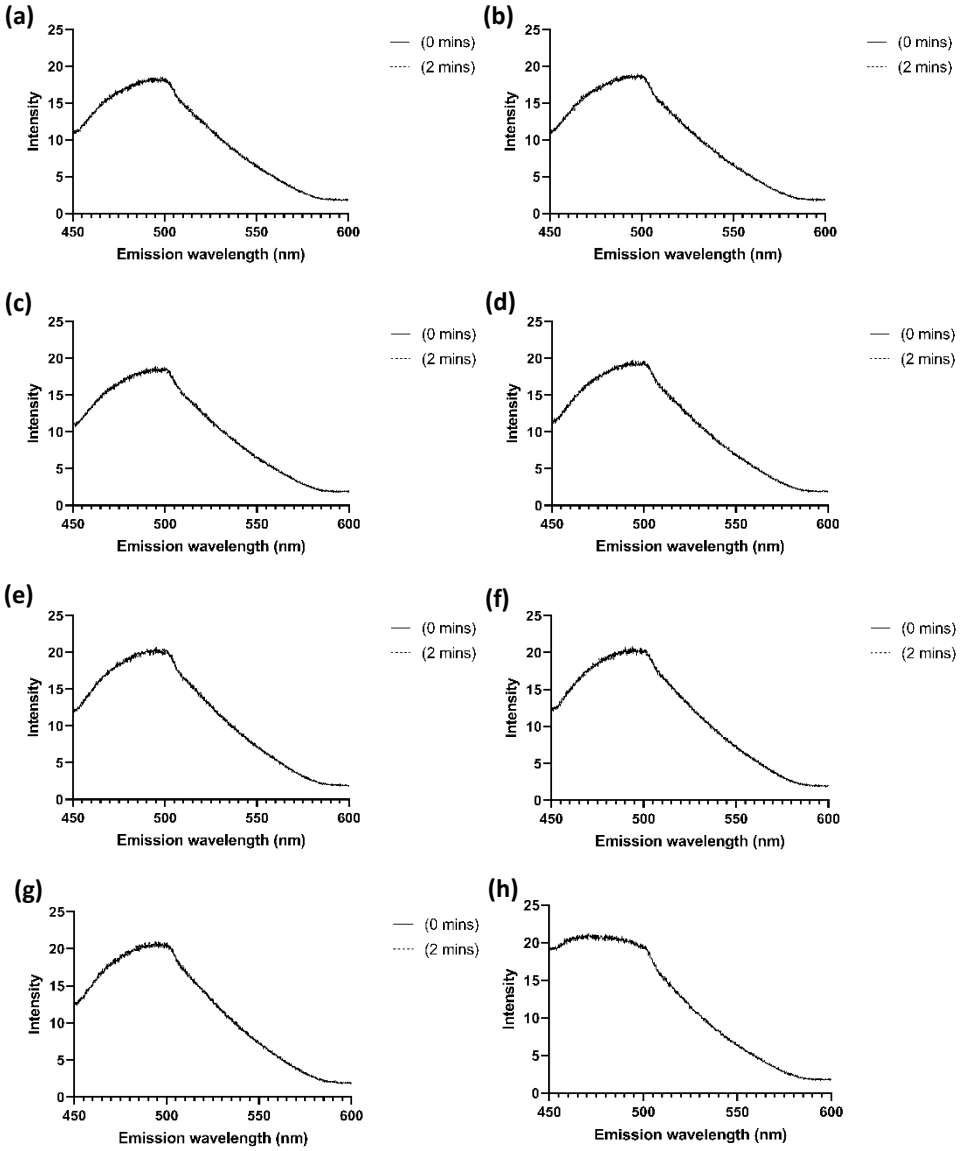

Figure 3.22: Fluorescent spectroscopy emission wavelength scans of CysK:CysE C-terminus tetrapeptide ratios for CSC formation. CysK: CysE C-terminus tetrapeptide (a) 4:1 (b) 2:1 (c) 1:1 (d) 1:2 (e) 1:3 (f) 1:4 (g) 1:5 (h) CysK only. Measured at room temperature 22 ^{o}C. Excitation wavelength 386.2$_{nm}$. Emission wavelength measured in the 450-600$_{nm}$ range.

Table 3.11: Fluorescent spectroscopy emission wavelength measurements of CysK binding to the CysE tetrapeptide. Wavelength of the apex of each peak for each reaction condition are recorded. CysK and CysE C-terminus tetrapeptide were freshly thawed. Measurements were taken at room temperature 22 ºC. Excitation wavelength 386.2_{nm}. Emission wavelength measured in the $450\text{-}600_{nm}$ range.

CysK:CysE C-terminus tail peptide monomeric ratio	Peak Apex measurements (nm)	
	0 (mins)	2 (mins)
4:1	499	498
2:1	497.8	494.8
1:1	494.8	493.6
1:2	500.4	493
1:3	495.2	498.8
1:4	490.2	494.4
1:5	494	495.6
CysK only	471	-

The change in the excitation wavelength for the PLP cofactor between the CysE-CysK and tetrapeptide-CysK experiments (400nm vs 386.2nm) is unexpected and cannot be explained. There are three factors that differ between the CysK:CysE and CysK:CysE C terminus tetrapeptide fluorescence experiments; (1) 25% (*v/v*) glycerol was present in the peptide experiments, due to carryover from freezing CysK in glycerol (2) the CysK and CysE C-terminus tetrapeptide are in potassium buffers at pH 7.0 rather than pH 8.0 for the CysK:CysE experiment and CysE protein was in Tris buffer, and (3) the CysE C terminus tetrapeptide is present rather than the whole CysE enzyme. Despite these factors, the change in excitation and emission wavelength cannot be explained.

Table 3.12: Changes in fluorescence peak intensity over varied CysK:CysE tetrapeptide ratios. $490\text{-}500_{nm}$ peak is shown.

CysK:CysE tetrapeptide ratio	$490\text{-}500_{nm}$ Peak	
	0 mins	2 mins
4:1	18.41	18.58
2:1	18.96	18.89
1:1	18.89	18.68
1:2	19.63	19.57
1:3	20.67	20.48
1:4	20.76	20.59
1:5	20.95	21.00

Both CysK:CysE and CysK:CysE C-terminal tetrapeptide fluorescence spectroscopy experiments show no formation of the CSC occurring, as no 15 nm blue shift caused by

the partial closing of the CysK active site resulting in a change in the PLP fluorescence occured. However, CSC formation has previously been confirmed in other organisms via gel filtration chromatography (Kredich *et al.*, 1969; Kumaran *et al.*, 2009), so we tested the ability of CysE and CysK from *N. gonorrhoeae* to form the CSC by gel filtration chromatography.

3.3.5 Monitoring CSC formation by gel filtration chromatography

Formation of the CSC was also investigated by gel filtration chromatography using freshly purified CysK and CysE as per sections 2.4 and 2.13.1, respectively, using the same buffers as previously mentioned for CysE and modified buffers for CysK (pH 8.0 rather than 7.0). Both proteins were purified individually for use in CSC formation experiments, and analysed using a calibrated gel filtration column. CysE elutes from an Enrich 650 analytical gel filtration column (BioRad) at 12.28 ml, corresponding to a molecular weight of 193.8 kDa, consistent with a CysE hexamer (Figure 3.23a) (Oldham, 2020). CysK elutes at 14.6 ml, corresponding to a molecular weight of 52.862 kDa, consistent with a dimer (Figure 3.23b), which is in keeping with section 3.1.2. CysK and CysE proteins purified in the expected multimeric forms of a dimer and a hexamer, respectively (Figure 3.23a, b).

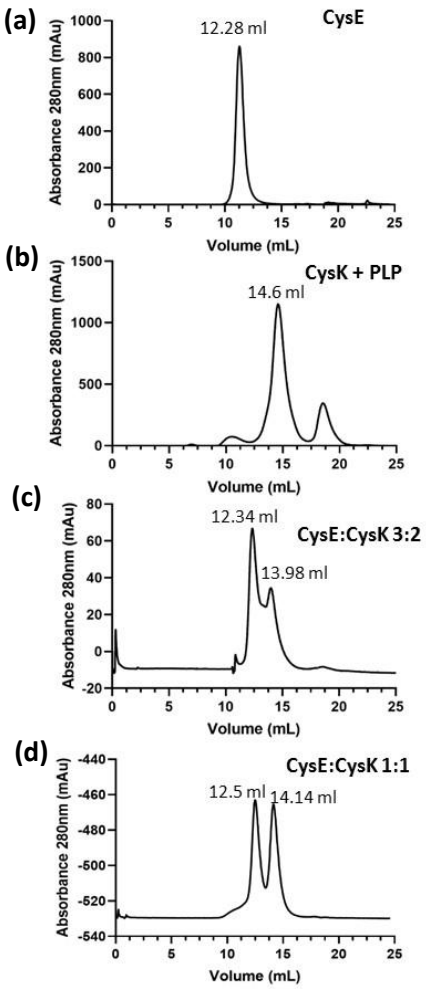

Figure 3.23: Monitoring formation of the CSC by gel filtration chromatography. Elution profiles of CysE (a), CysK (b) and CysE:CysK at molar ratios of 3:2 (c) and 1:1 (d) shown. All peaks are labelled with elution volumes. The absorbance values for the 1:1 ratio are negative as the buffer background was not set to zero after previous use.

To monitor formation of the CSC, CysE and CysK were mixed at a 3:2 and 1:1 molar ratios and analysed by gel filtration chromatography (section 2.13.2.1).

If CysE and CysK formed the CSC we would expect to see an earlier elution peak compared to the CysE and CysK proteins only. A homologous CSC from *E. coli* indicates the CSC is composed of one hexamer and two CysK dimers (3:2 molar ratio) (Benoni *et al.*, 2017b). For *N. gonorrhoeae* this would form a CSC with a predicted molecular weight of ~332 kDa, corresponding to an elution volume of 11.9 ml which is not seen in either Figure 3.12c or Figure 3.12d, indicating the CSC had not formed.

The lack of elution peaks corresponding to the CSC indicates there is no formation of the CSC. The peaks observed at 12.34 and 13.98 mL (Figure 3.23c) correspond to CysE and

CysK, respectively. The peak observed at 12.5 ml and 14.14 mL (Figure 3.23d), also correspond to individual CysE and CysK proteins respectively.

3.3.6 CysK peptide inhibition assays

Given the apparent inability of CysE and CysK to form the CSC, and the inability of the four amino acid CysE C-terminal tetrapeptide to bind to CysK, we investigated if the CysE tetrapeptide could inhibit enzyme activity, which would indicate binding to the enzyme. Tetrapeptide inhibition assays were conducted with the four amino acid peptide that mimics the last four amino acids of the C-terminal tail of CysE. If the tetrapeptide binds into the CysK active site, inhibition of enzyme activity should occur, thus allowing activity assays to indicate potential CSC formation. Assays were set up as per section 2.8. A variety of tetrapeptide concentrations (0.0764, 0.1528, 0.2292, 0.3056, 0.764, 1.528, 7.64, 15.28, 22.92, 30.56, 114.6 and 191 pmol) were trialled in an attempt to collect an IC_{50} curve for peptide inhibition (1.632 µg CysK = 49.75 pmol of CysK monomer) (Figure 3.24).

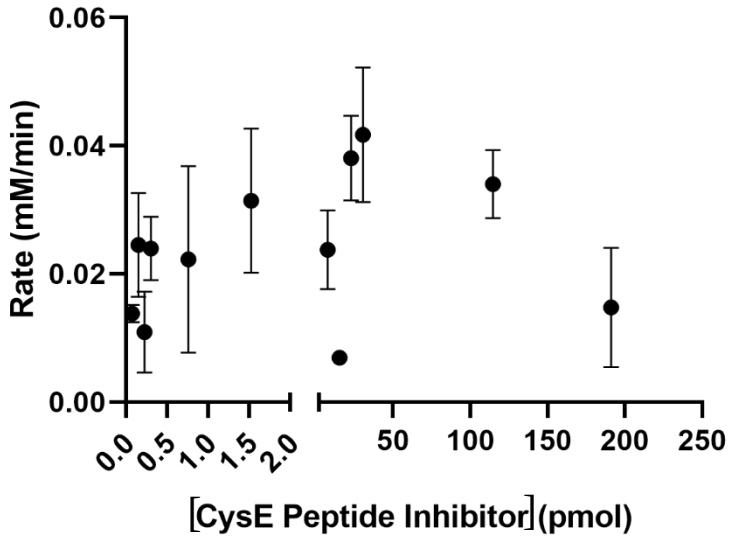

Figure 3.24: Activity of CysK in the presence of the CysE tetrapeptide. Split scale with 30% of the scale showing 0.0764-1.528 pmol varied peptide conditions. Right 70% of the scale portrays activity of 7.64-191 pmol varied peptide conditions. OAS concentration constant at 1 mM. Na_2S concentration constant at 7 mM. All assays were conducted with 49.75 pmol of CysK monomer at 37 ºC with freshly thawed CysK. All reaction conditions were collected in duplicate. Error bars represent standard error.

Figure 3.24 indicates a large variance in activity at varied peptide concentrations, making the fitting of a kinetic model particularly difficult. An accurate IC_{50} curve was not obtained and, given the large error bars, kinetic parameters of an IC_{50} curve cannot be determined. The maximum rates observed in the varied tetrapeptide concentration assays

(at peptide concentrations 22.92 and 30.56 pmol) are within the maximum rates observed in reactions with no tetrapeptide present. This indicates the CysE tetrapeptide does not bind to CysK and inhibit its activity. The OAS concentration was held at 1 mM (1 mM = 1000 µM) in these assays to mitigate the dissociation effect OAS may have on the tetrapeptide binding into the CysK active site. However, dissociation of the CSC can occur at µM concentrations of OAS (upwards of 50 µM OAS) (Kredich *et al.*, 1969; Wang & Leyh, 2012; Benoni *et al.*, 2017a). Therefore, the lack of inhibition seen in these assays may be a result of the presence of dissociating concentrations of OAS, thus, dissociating any tetrapeptide that may have bound to the CysK active site, making it difficult to draw any certain conclusions from these assays.

3.3.7 CSC formation conclusions and future directions

The CysE C-terminus tetrapeptide did not cause inhibition in the activity assay indicating it did not bind to the CysK active site. Both binding of CysK to CysE and CysK to the CysE C-terminus tetrapeptide did not show a change in fluorescence by a blueshift of 15 nm (equivalent to partial closing of the CysK active site creating a change in the PLP fluorescence). Gel filtration CSC formation trials also show no elution peak corresponding to the CSC. These results suggest the CSC does not form within *N. gonorrhoeae.*

Nanomolar concentrations of CysE (7 nM) and CysK (23 nM) (monomer concentrations) from *E. coli* have been used to form the CSC (Benoni *et al.*, 2017b). This *E. coli* CSC had a reported dissociation constant (K_d) of 5 nM (Benoni *et al.*, 2017b), indicating the CysE and CysK subunits have a strong affinity for each other, thus, strongly favouring CSC formation. A similar affinity was assumed of CysK and CysE from *N. gonorrhoeae* when planning the CSC experiments in this research. We have demonstrated that at more concentrated stocks (µM) of CysK and CysE, and lower concentrations of CysK and CysE C-terminus tail peptide (pmol), there is no indication of CSC formation, using multiple methods.

It is possible that the CSC is completely unable to form in *N. gonorrhoeae*. Organisms that have lost the ability to form the CSC would no longer have a CSC inhibited CysK enzyme, allowing increased L-cysteine production. Due to the resulting, unregulated OAS consumption by CysK, down regulation of gene expression in sulphate acquisition genes would occur. Given the high demand for cysteine, to produce reducing compounds

such as glutathione (Seib *et al.*, 2006), it may be advantageous for *N. gonorrhoeae* to not be capable of CSC formation.

It is possible the lack of CSC formation is linked to the inability of *N. gonorrhoeae* to reduce sulphate to sulphide, and that the transcriptional regulator CysB controls two of the deleted genes from this pathway via operon control. *N. gonorrhoeae* OASS has the greatest homology to OASS-A isoform (CysK) as demonstrated via sequence alignment (Hicks & Mullholland, 2018). CysK utilises sulphide as a thiol donor, whereas CysM (OASS-B isoform) utilises directly imported thiosulphate. The inability of CysK to utilise thiosulphate and its ability to form the CSC where CysM cannot (Zhao *et al.*, 2006) suggest that we would be able to from the CSC in *N. gonorrhoeae*. However, all experimental results suggest the contrary.

Further experimentation is required to rule out CSC formation altogether. Peptide inhibition assays and fluorescent spectroscopy will be repeated using a decapeptide corresponding to the last 10 amino acids of the CysE C-terminal peptide to conclude whether our experiments showed no binding of the peptide due to it only being four amino acids in length. Addition of sulphide to the CSC formation in both gel filtration and fluorometric spectroscopy solutions will be trialled as sulphide is shown to promote reassociation of the CSC (Wirtz & Hell, 2006). Co-lysis of the CysK and CysE proteins will be attempted as this method has been established to produce stable complexes for functional and structural studies in challenging protein families including, the human steroid nuclear receptors (SNR) and the HIV-1 pre-integration complex (Levy *et al.*, 2016). Another bacterium, *Brucella abortus* was unable to form the CSC, despite the required residues being present in the CysE C-terminal tetrapeptide (Dharavath *et al.*, 2017). This was due to two CysK residues occupying the active site, thus, preventing the binding of the C-terminal tetrapeptide from CysE (Dharavath *et al.*, 2017). Due to the active site missing from the *N. gonorrhoeae* CysK crystal structure, an improved resolution crystal structure of CysK is required to determine whether this is present in *N. gonorrhoeae* CysK as well.

3.4 Characterisation of the *in vivo* role of CysK by genetic manipulation of *N. gonorrhoeae*

3.4.1 Essentiality of CysK and proposed role *in vivo*

Neisseria species are particularly unique in that they have only one OASS isoform. This isoform has the greatest homology to CysK (OASS-A) and utilises sulphide for cysteine biosynthesis (Hicks & Mullholland, 2018). *N. gonorrhoeae* has an inability to reduce sulphate to sulphide and relies on thiosulphate for cysteine biosynthesis, a substrate which is usually utilised by the alternate OASS isoform CysM. This raises interesting questions regarding the role of CysK in *N. gonorrhoeae*. Whilst not being an essential gene for *N. gonorrhoeae* (Remmele *et al.*, 2014), CysK has been shown to be important for colonisation of epithelial cells in *N. meningitidis* and when knocked out results in both decreased fitness and increased susceptibility to antibiotics (Turnbull & Surette, 2010; Capel *et al.*, 2016).

Many studies are underway with CysK being characterised as an antimicrobial target for other bacterial pathogens (Salsi *et al.*, 2011; Franko *et al.*, 2018; Joshi *et al.*, 2019) and given deleting *cysK* from the genome has inflicted a decrease in fitness and increased susceptibility to antibiotics in other bacterial pathogens (Turnbull & Surette, 2010; Capel *et al.*, 2016), coupled with rapid emergence of antimicrobial resistance in *N. gonorrhoeae,* determining the effects of this knockout in *N. gonorrhoeae* is vital to design of new antimicrobial agents. To determine whether CysK is essential in *N. gonorrhoeae, cysK* gene deletion by homologous recombination in *N. gonorrhoeae* using a plate transformation was trialled.

3.4.2 *N. gonorrhoeae cysK* deletion construct for homologous recombination

A DNA construct was designed and ordered as a geneblock from Twist Bioscience. The construct contained the *N. gonorrhoeae* kanamycin resistance gene (*kanR*) from (Ramsey *et al.*, 2012) flanked by 150 base pairs of DNA sequence homologous to the DNA sequence upstream and downstream of *cysK* in the *N. gonorrhoeae* genome. Included in the construct was a promoter and terminator for the kanamycin resistance gene and the *Neisseria* DNA uptake sequence (DUS) necessary for uptake of DNA (Figure 3.25).

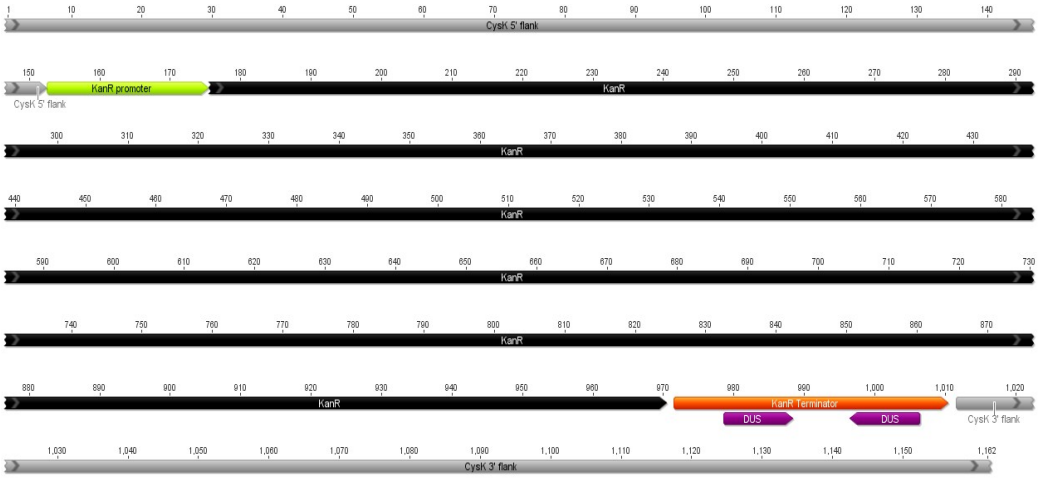

Figure 3.25: DNA construct of the *N. gonorrhoeae cysK* knockout with the kanamycin resistance gene (*kanR*). *kanR* seen in black. 150 bp of DNA sequence homologous to the DNA sequence upstream and downstream of the *cysK* gene in *N. gonorrhoeae* seen in grey. *kanR* promoter seen in green. *kanR* terminator seen in orange. DNA uptake sequences seen in purple. Figure created using Geneious Prime (Biomatter).

Forward and reverse primers for the amplification of the entire DNA construct were designed and ordered as per section 2.14.2. PCR was conducted as per section 2.14.2 to amplify the DNA construct for transformation into *N. gonorrhoeae*. PCR product purity was tested via agarose gel electrophoresis (Figure 3.26) as per section 2.14.1. The gel shows a single distinct band indicating our pure isolated DNA construct.

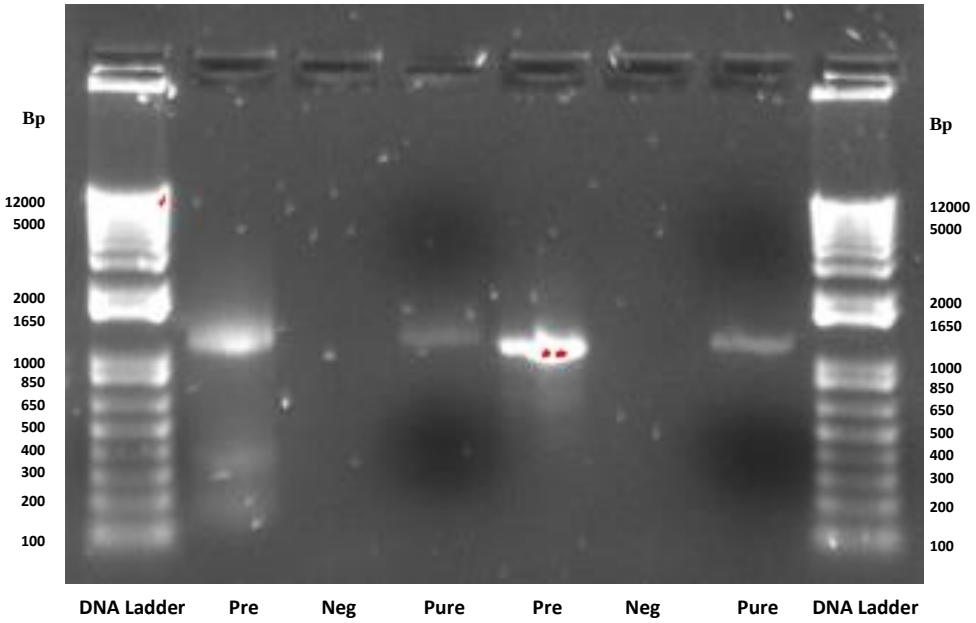

Figure 3.26: PCR amplification and purification results of *cysK* KO construct run on a 1% agarose gel. Pre = PCR product before purification, Neg = negative control with Ultra Distilled water, Pure = purified PCR product, DNA ladder = Invitrogen 1kb+ ladder.

3.4.3 Transformation of *N. gonorrhoeae*

PCR products were prepared for plate transformations and 10 µl of PCR product (20 ng.µl^{-1}) was spotted onto GCB agar plates in two places as per section 2.14.4. Piliated colonies from a fresh GCB agar plate were selected and streaked through the DNA circles for transformation. Single colonies from within these spotted DNA circles were streaked across GCB plates supplemented with 50 µg.ml^{-1} kanamycin and incubated as per section 2.14.4. The plates were checked after a given 48 hours of incubation and no growth was found.

The lack of growth on the kanamycin substituted plates presents three possible conclusions, (1) the gonorrhoea colonies had not successfully been transformed with the DNA PCR products and had therefore not integrated the kanamycin resistance gene into its genome, meaning it could not grow or survive on the kanamycin plate, (2) there was contamination present leading to growth of microbes other than *N. gonorrhoeae* that were therefore unable to transform and could not grow on the kanamycin substituted plates, or (3) *N. gonorrhoeae* could not grow on the kanamycin plates despite successful transformation and hence, uptake of the kanamycin resistance gene into its genome as the *cysK* gene is essential in *N. gonorrhoeae.*

It was determined via colony PCR by Jolyn Pan that conclusion (2) was in fact correct. The colonies present on the initial New Yorker and GCB plates were tested via colony PCR and determined to be contaminants. Therefore, all solutions used from the beginning of PCR process were streaked on GCB plates. The elution buffer from the PCR purification kit (Roche-applied-science) was found to be contaminated. Therefore, *cysK* gene knockout testing was halted until a new purification kit could be obtained.

3.4.4 *cysK* genomic deletion conclusions and future research

No conclusions can be drawn from the *cysK* gene deletion experiments as the presence of contamination means we cannot be certain the colonies streaked onto the kanamycin substituted plates were *N. gonorrhoeae.*

Thus, this experiment will be repeated in future research to determine the effect of knocking out *cysK* on the ability of *N. gonorrhoeae* to grow. It has been found that when a gene knockout is lethal to a bacterium, it is particularly useful to knockdown the gene, causing reduced activity rather than complete removal (Gillaspie *et al.*, 2009). Therefore,

if the *cysK* knockout proves to be lethal, causing *N. gonorrhoeae* to not grow on the kanamycin substituted plates with no contaminants present, a knockdown of the *cysK* gene will be attempted. This will allow more effective study of the effect *cysK* has on the ability of *N. gonorrhoeae* to grow. It has previously been shown a tetracylcine-inducible promoter can be used in *N. gonorrhoeae* (Ramsey *et al.*, 2012). This inducible promoter will be used to replace the *cysK* promoter in *N. gonorrhoeae*, allowing control of the activation of the gene using anhydrotetracycline which is effective at low concentrations without inhibiting growth of the bacterium (Ramsey *et al.*, 2012). Combining the gene knockdown with testing cell adhesion and entry of *N. gonorrhoeae* into human cells using a human cell line, will potentially give further insight into the effect *cysK* has on the ability of *N. gonorrhoeae* to infect its obligate host.

Chapter 4

Conclusions and Future Research

Neisseria gonorrhoeae is the causative agent of the sexually transmitted infection gonorrhoea (Hill *et al.*, 2016; Wi *et al.*, 2017). Rapid development of antibiotic resistance to every available antibiotic for its treatment over the last few decades, has led to increased demand for the development of new antimicrobial agents for future treatment of this disease (Wi *et al.*, 2017). Targeting of amino acid biosynthesis is a promising new avenue for antimicrobial research. The amino acid cysteine's biosynthetic pathway has been demonstrated to be vital for both pathogenicity and virulence in *Neisseria* species (Hatzios & Bertozzi, 2011; Takumi & Nonaka, 2016; Ren *et al.*, 2017; Anderson *et al.*, 2019).

N. gonorrhoeae encounters constant oxidative stress during infection. The ability of this obligate human pathogen to spread to new hosts is wholly dependent on its ability to mitigate and survive the oxidative stress produced by commensal *Lactobacilli* within the urogenital tract and the phagosomes of neutrophils encountered in host immune defence (Seib *et al.*, 2006; Hill *et al.*, 2016). Mitigation of this host derived oxidative stress relies on reducing systems within *N. gonorrhoeae.* Given the necessity of L-cysteine for protein folding, structure and function, formation of vital biomolecules such as biotin, co-enzyme-A, and iron-sulphur clusters and the synthesis of reducing agents, such as glutathione (Carmel-Harel & Storz, 2000; Kredich, 2008; Takumi & Nonaka, 2016; Hicks & Mullholland, 2018), the pathway for *de novo* synthesis of L-cysteine is an ideal target for developing new treatments for *N. gonorrhoeae*. However, both the function of the cysteine biosynthesis pathway and its regulation are not well understood in *N. gonorrhoeae.* In this thesis we have biochemically and structurally characterised one of the key cysteine biosynthetic enzymes, CysK.

CysK is an *O*-acetylserine sulphydrylase that catalyses the final step in cysteine biosynthesis. CysK catalyses the condensation reaction of *O*-acetylserine with sulphide, to form L-cysteine (Rabeh & Cook, 2004; Joshi *et al.*, 2019). The sulphur acquisition and cysteine biosynthesis pathways are regulated on multiple levels in response to the flux of sulphur concentrations (Wirtz *et al.*, 2012). For CysK, this regulation is primarily carried out via CysK:CysE cysteine synthase complex (CSC) formation (Benoni *et al.*, 2017b).

This thesis presents the structure of CysK from *N. gonorrhoeae* at 2.49 Å. In our structure, the key PLP co-factor interacting residues are conserved. However, only part of the active site residues are conserved in the structure where the 223-GIGA-226 residues are not visible. This is a function of low resolution and the flexibility of the active site loop within the crystal structure. Obtaining a structure at a higher resolution with either substrate, S^{2-} or OAS, bound in either the allosteric anion binding site found by (Tai *et al.*, 2001) or the active site, respectively, will allow for better determination of the missing Glu204-Pro230 loop from our structure, as well as a better indication of the mechanism of the enzyme. Each monomer within the homodimer, has an alternate conformation of PLP interacting residues. In monomer A, the 179-GTGGT-183 motif is blocking the PLP co-factor from binding, hence it is assumed this monomer is in an inactive conformation as CysK activity is PLP dependent. Conversely, the monomer D 179-GTGGT-183 motif supports the ability of the PLP co-factor to bind, indicating this monomer is in an active conformation. The presence of these alternate conformations within the homodimer, explains the positive cooperativity displayed within the enzyme's kinetic analysis. We hypothesise binding of substrate into the active site of the active CysK monomer will cause a conformation change in the 179-GTGGT-183 loop of the inactive monomer, allowing PLP to bind, thus changing the inactive monomer to an active conformation. We have also determined the OASS isoform isolated from *N. gonorrhoeae* to be OASS-A/CysK as was hypothesised due to the higher sequence homology to CysK (Hicks & Mullholland, 2018). However, for effective computational inhibitor screening, an understanding of kinetic mechanism is also vital.

CysK from *N. gonorrhoeae* has *O*-acetylserine sulphydrylase activity, with kinetic constants (K_M/K_{half}) of 12.43 (K_M) and 1.01 (K_{half}), for sulphide and *O*-acetylserine, respectively, which are unique when compared with other CysK homologues. We demonstrate an allosteric sigmoidal (positive cooperativity) relationship is present for both substrates at low concentrations. This positive cooperativity is supported by the alternate conformations determined in the monomers of the CysK dimer within our crystal structure. The substrate sulphide also shows allosteric inhibition (partial inhibition), most likely due to the presence of an allosteric anion binding site determined by (Tai *et al.*, 2001). Interestingly, *N. gonorrhoeae* CysK was shown to be unable to utilise thiosulphate, even though the bacteria can grow thiosulphate as a sole sulphur source (Le Faou, 1984) and lack the OASS-B isoform that can utilise thiosulphate (Figure 4.1). This indicates the

CysK from *N. gonorrhoeae* is only capable of using sulphide as a substrate to produce cysteine and is therefore an OASS-A/CysK isoform and not a dual-functioning enzyme. The identification of the isolated OASS isoform from *N. gonorrhoeae* is also supported by our crystal structure analysis. Due to a genomic deletion and remnant pseudogenes corresponding to the sulphate assimilation pathway (Figure 1.2, red), *N. gonorrhoeae* is also incapable of reducing sulphate to sulphide to use in cysteine biosynthesis (Hicks & Mullholland, 2018). Therefore, we propose an alternative pathway for acquiring sulphide from a thiosulphate substrate, involving a sulphurtransferase enzyme, thiosulphate and glutathione (Figure 4.1, grey box on the right).

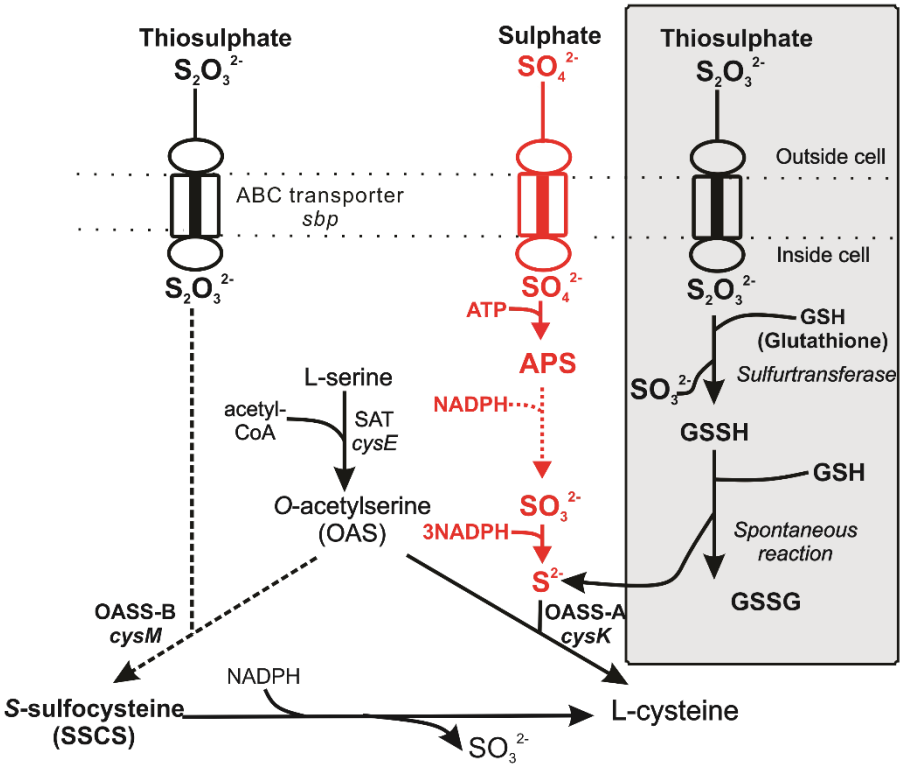

Figure 4.1: Sulphate transport and reduction pathways. Thiosulphate assimilation pathway in other bacteria shown in black on the left with dotted lines. Sulphate reduction pathway absent from *N. gonorrhoeae* shown in red on the right. Hypothesised sulphur acquisition in *N. gonorrhoeae* shown on the right in grey box.

We were unable to get any indication of cysteine synthase complex formation using purified CysK and either CysE or the CysE C-terminus tetrapeptide from *N. gonorrhoeae.* Based on the presence of the isoleucine essential for CSC formation at the end of the C-terminal tail of CysE (Huang *et al.*, 2005), and the flexible nature of the C-terminal tail (Oldham, 2020), we expected the CSC to form or give an indication of CysE tail/tetrapeptide binding to the CysK active site. The primary purpose of the CSC is to promote upregulation of the sulphate acquisition pathway as a response to low sulphur concentrations (Kumar *et al.*, 2011). Given that *N. gonorrhoeae* is unable to reduce sulphate to sulphide, but is capable of growth using thiosulphate as a sole source of sulphur (Le Faou, 1984), there may be no evolutionary advantage to CSC formation. The

lack of CSC formation may provide an advantage to *N. gonorrhoeae,* in that it would allow continuous production of L-cysteine by CysK as it is no longer inhibited by the CysE C-terminus tail binding into its active site. The complex is also unable to form in *E. histolytica*, and is attributed to the CysE forming a trimer rather than a hexamer conformation (Kumar *et al.*, 2011). Despite its inability to store glutathione, *E. histolytica* has high intracellular demands, which it relies on high cysteine concentrations to act as a reducing system to alleviate (Kumar *et al.*, 2011). Conversely, *N. gonorrhoeae* is documented to have high intracellular concentrations of glutathione, however, both organisms would require large amounts of L-cysteine to maintain these high metabolite concentrations. (Remmele *et al.*, 2014) suggests that *de novo* synthesis of cysteine is essential for *N. gonorrhoeae* and that L-cysteine/cystine importation alone, is not sufficient for meeting the L-cystine demands of *N. gonorrhoeae.*

We were unable to conclusively define *cysK* from *N. gonorrhoeae* as essential as contamination interfered with the *cysK* gene deletion experiments. However, if the inability of the streaked *N. gonorrhoeae* to grow on the kanamycin supplemented plates, is seen in future repeats of this experiment, a *cysK* knockdown strain in *N. gonorrhoeae* strain will be created. The promoter of *cysK* in *N. gonorrhoeae* will be replaced with a controllable tetracycline-inducible promoter. This will confirm essentiality by *in vitro* growth experiments in the presence and absence of tetracycline. Combining the gene knockdown with testing cell adhesion and entry of *N. gonorrhoeae* into human cells using a human cell line, will potentially give further insight into the effect *cysK* has on the ability of *N. gonorrhoeae* to infect its obligate host.

We have defined the isolated OASS isoform from *N. gonorrhoeae* as an OASS-A/CysK enzyme through both kinetic and structural analysis. Establishing this is a key point in understanding alternate sulphur acquisition pathways. *N. gonorrhoeae* can grow on thiosulphate as a sole source of sulphur and yet it lacks the enzyme capable of metabolising it. As we have established CysK is inactive at both low and high concentrations of thiosulphate. The apparent inability of the *N. gonorrhoeae* CysK and CysE enzymes to form the CSC is particularly interesting as many other organisms use this to regulate intracellular sulphur flux and cysteine biosynthesis. This suggests it is advantageous for *N. gonorrhoeae* to be unable to regulate either of these situations. However, there is also potential for an alternate mode of regulation. Establishing these alternate sulphur acquisition pathways will help in not only understanding of the

N. gonorrhoeae metabolic pathways but also to develop new potential targets for antimicrobial agents across a vast array of sulphur utilising bacteria.

The results presented here represent a major leap forward in our understanding of both cysteine biosynthesis and sulphur acquisition in *N. gonorrhoeae*. These results are also the basis for future work in identifying potential CysK inhibitors through computational inhibitor screening. Computational inhibitor screening streamlines the inhibitor discovery process via the ability to screen hundreds of thousands of inhibitors, compared to only thousands of inhibitors using typical *in vitro* laboratory based screening. However, computational inhibitor screening also relies on detailed understanding of both the kinetic mechanism and high-resolution protein structures with and without substrates bound. Using the results presented here, computational inhibitor screening is underway by Dr Wanting Jiao at Victoria University of Wellington. Using the structure of CysK presented here and the published structure of *M. tuberculosis* CysK structure with PLP cofactor and a peptide inhibitor bound, we generated a structural model of PLP-bound CysK from *N. gonorrhoeae* for virtual screening. A library of 10 million commercially available compounds that contain drug like features were screened against CysK, using the virtual screening workflow in Schrodinger Suite. The screening has completed and produced 1000 top scored compounds for further examination. Using an established selection workflow, consisting of short MD simulations, 10-20 compounds will be selected for further *in vitro* testing. These will be tested using the assays developed in this thesis. In addition ongoing research to obtain CysK structures with OAS, S^{2-} and Cl^{-} bound will be attempted based on the crystallisation of CysK presented here.

Overall, this research has contributed to a greater understanding of the sulphur acquisition pathway in *N. gonorrhoeae* which may help in elucidation of alternate sulphur acquisition pathways in other microbes. This research has also provided great insight into the previously uncharacterised enzyme, CysK and paved the way for the development of new inhibitors targeting the promising new antimicrobial target in *N. gonorrhoeae*, CysK.

References

Adams, P. D., Afonine, P. V., Bunkóczi, G., Chen, V. B., Davis, I. W., Echols, N., Headd, J. J., Hung, L.-W., Kapral, G. J., Grosse-Kunstleve, R. W., McCoy, A. J., Moriarty, N. W., Oeffner, R., Read, R. J., Richardson, D. C., Richardson, J. S., Terwilliger, T. C., & Zwart, P. H. (2010). PHENIX: a comprehensive Python-based system for macromolecular structure solution. *Acta Crystallographica Section D Biological Crystallography, 66*(2), 213-221.

Anderson, M. T., Mitchell, L. A., Sintsova, A., Rice, K. A., & Mobley, H. L. T. (2019). Sulfur Assimilation Alters Flagellar Function and Modulates the Gene Expression Landscape ofSerratia marcescens. *mSystems, 4*(4).

Balaban, N. (2011). Persistence: mechanisms for triggering and enhancing phenotypic variability. *Current Opinion in Genetics & Development, 21*(6), 768-775.

Benoni, R., Beck, C. M., Garza-Sánchez, F., Bettati, S., Mozzarelli, A., Hayes, C. S., & Campanini, B. (2017a). Activation of an anti-bacterial toxin by the biosynthetic enzyme CysK: mechanism of binding, interaction specificity and competition with cysteine synthase. *Scientific Reports, 7*(1).

Benoni, R., De Bei, O., Paredi, G., Hayes, C. S., Franko, N., Mozzarelli, A., Bettati, S., & Campanini, B. (2017b). Modulation ofEscherichia coliserine acetyltransferase catalytic activity in the cysteine synthase complex. *FEBS Letters, 591*(9), 1212-1224.

Bertagnolli, B. L., & Wedding, R. T. (1977). Purification and Initial Kinetic Characterization of Different Forms of O-AcetylserineSulfhydrylase from Seedlings of Two Species of Phaseolus. *Plant physiology, 60*, 115-121.

Bodie, M., Gale-Rowe, M., Alexandre, S., Auguste, U., Tomas, K., & Martin, I. (2019). Addressing the rising rates of gonorrhea and drug-resistant gonorrhea: There is no time like the present. *Canada Communicable Disease Report, 45*(2/3), 54-62.

Bonner, E. R., Cahoon, R. E., Knapke, S. M., & Jez, J. M. (2005). Molecular Basis of Cysteine Biosynthesis in Plants. *Journal of Biological Chemistry, 280*(46), 38803-38813.

Bulut, H., Moniot, S., Licht, A., Scheffel, F., Gathmann, S., Saenger, W., & Schneider, E. (2012). Crystal Structures of Two Solute Receptors for l-Cystine and l-Cysteine, Respectively, of the Human Pathogen Neisseria gonorrhoeae. *Journal of Molecular Biology, 415*(3), 560-572.

Burkhard, P., Tai, C. H., Jansonius, J. N., & Cook, P. F. (2000). Identification of an allosteric anion-binding site on O-acetylserine sulfhydrylase: structure of the enzyme with chloride bound. *J Mol Biol, 303*(2), 279-86.

Campanini, B., Benoni, R., Bettati, S., Beck, C. M., Hayes, C. S., & Mozzarelli, A. (2015). Moonlighting O-acetylserine sulfhydrylase: New functions for an old protein. *Biochimica et Biophysica Acta (BBA) - Proteins and Proteomics, 1854*(9), 1184-1193.

Campanini, B., Pieroni, M., Raboni, S., Bettati, S., Benoni, R., Pecchini, C., Costantino, G., & Mozzarelli, A. (2014). Inhibitors of the Sulfur Assimilation Pathway in Bacterial Pathogens as Enhancers of Antibiotic Therapy. *Current medicinal chemistry, 22*.

Campanini, B., Speroni, F., Salsi, E., Cook, P. F., Roderick, S. L., Huang, B., Bettati, S., & Mozzarelli, A. (2005). Interaction of serine acetyltransferase withO-acetylserine sulfhydrylase active site: Evidence from fluorescence spectroscopy. *Protein Science, 14*(8), 2115-2124.

Capel, E., Zomer, A. L., Nussbaumer, T., Bole, C., Izac, B., Frapy, E., Meyer, J., Bouzinba-Ségard, H., Bille, E., Jamet, A., Cavau, A., Letourneur, F., Bourdoulous, S., Rattei, T., Nassif, X., & Coureuil, M. (2016). Comprehensive Identification of Meningococcal Genes and Small Noncoding RNAs Required for Host Cell Colonization. *mBio, 7*(4), e01173-16.

Carmel-Harel, O., & Storz, G. (2000). Roles of the Glutathione- and Thioredoxin-Dependent Reduction Systems in theEscherichia ColiandSaccharomyces CerevisiaeResponses to Oxidative Stress. *Annual Review of Microbiology, 54*(1), 439-461.

Claus, M. T., Zocher, G. E., Maier, T. H. P., & Schulz, G. E. (2005). Structure of the O-Acetylserine Sulfhydrylase Isoenzyme CysM from Escherichia coli. *Biochemistry, 44*(24), 8620-8626.

Cook, P. F., & Wedding, R. T. (1976). A reaction mechanism from steady state kinetic studies for O-acetylserine sulfhydrylase from Salmonella typhimurium LT-2. *Journal of Biological Chemistry, 251*(7), 2023-2029.

Criss, A. K., Kline, K. A., & Seifert, H. S. (2005). The frequency and rate of pilin antigenic variation inNeisseria gonorrhoeae. *Molecular Microbiology, 58*(2), 510-519.

Cyr, S. S., Barbee, L., Workowski, K. A., Bachmann, L. H., Pham, C., Schlanger, K., Torrone, E., Weinstock, H., Kersh, E. N., & Thorpe, P. (2020). Update to CDC's Treatment Guidelines for Gonococcal Infection, 2020. *MMWR Morb Mortal Wkly Rep 2020, 69*.

Davidi, D., Noor, E., Liebermeister, W., Bar-Even, A., Flamholz, A., Tummler, K., Barenholz, U., Goldenfeld, M., Shlomi, T., & Milo, R. (2016). Global characterization of in vivo enzyme catalytic rates and their correspondence to in vitrokcatmeasurements. *Proceedings of the National Academy of Sciences, 113*(12), 3401-3406.

Dharavath, S., Raj, I., & Gourinath, S. (2017). Structure-based mutational studies of O-acetylserine sulfhydrylase reveal the reason for the loss of cysteine synthase complex formation in Brucella abortus. *Biochemical Journal, 474*(7), 1221-1239.

Edwards, J. L., & Apicella, M. A. (2004). The Molecular Mechanisms Used by Neisseria gonorrhoeae To Initiate Infection Differ between Men and Women. *Clinical Microbiology Reviews, 17*(4), 965-981.

Edwards, J. L., & Butler, E. K. (2011). The Pathobiology of Neisseria gonorrhoeae Lower Female Genital Tract Infection. *Frontiers in Microbiology, 2*.

El-Benna, J., Hurtado-Nedelec, M., Viviana, Marie, J.-C., Gougerot-Pocidalo, M.-A., & Dang, P. M.-C. (2016). Priming of the neutrophil respiratory burst: role in host defense and inflammation. *Immunological Reviews, 273*(1), 180-193.

Emsley, P., & Cowtan, K. (2004). Coot: model-building tools for molecular graphics. *Acta Crystallographica Section D Biological Crystallography, 60*(12), 2126-2132.

Evans, P. R., & Murshudov, G. N. (2013). How good are my data and what is the resolution? *Acta Crystallographica Section D Biological Crystallography, 69*(7), 1204-1214.

Eyre, D. W., Sanderson, N. D., Lord, E., Regisford-Reimmer, N., Chau, K., Barker, L., Morgan, M., Newnham, R., Golparian, D., Unemo, M., Crook, D. W., Peto, T. E., Hughes, G., Cole, M. J., Fifer, H., Edwards, A., & Andersson, M. I. (2018). Gonorrhoea treatment failure caused by a Neisseria gonorrhoeae strain with combined ceftriaxone and high-level azithromycin resistance, England, February 2018. *Eurosurveillance, 23*(27).

Fifer, H., Cole, M., Hughes, G., Padfield, S., Smolarchuk, C., Woodford, N., Wensley, A., Mustafa, N., Schaefer, U., Myers, R., Templeton, K., Shepherd, J., & Underwood, A. (2018). Sustained transmission of high-level azithromycin-resistant Neisseria gonorrhoeae in England: an observational study. *The Lancet Infectious Diseases, 18*(5), 573-581.

Fisette, P. L., Ram, S., Andersen, J. M., Guo, W., & Ingalls, R. R. (2003). The Lip Lipoprotein from Neisseria gonorrhoeae Stimulates Cytokine Release and NF-κB Activation in Epithelial Cells in a Toll-like Receptor 2-dependent Manner. *Journal of Biological Chemistry, 278*(47), 46252-46260.

Franko, N., Grammatoglou, K., Campanini, B., Costantino, G., Jirgensons, A., & Mozzarelli, A. (2018). Inhibition of O-acetylserine sulfhydrylase by fluoroalanine derivatives. *Journal of Enzyme Inhibition and Medicinal Chemistry, 33*(1), 1343-1351.

Frishman, D., & Argos, P. (1995). Knowledge-based protein secondary structure assignment. *Proteins, 23*(4), 566-79.

Gaitonde, M. (1967). A spectrophotometric method for the direct determination of cysteine in the presence of other naturally occurring amino acids. *Biochemical Journal, 104*(2), 627-633.

Gasteiger, E., Hoogland, C., Gattiker, A., & Duvaud, S. (2005). Protein Identification and Analysis Tools in the ExPASy Server. *In: Walker J.M. (eds) The Proteomics Protocols Handbooks*(Humana Press), 571-607.

George, C. R. R., Enriquez, R. P., Gatus, B. J., Whiley, D. M., Lo, Y.-R., Ishikawa, N., Wi, T., & Lahra, M. M. (2019). Systematic review and survey of Neisseria gonorrhoeae ceftriaxone and azithromycin susceptibility data in the Asia Pacific, 2011 to 2016. *PLOS ONE, 14*(4), e0213312.

Gerbase, A. C., Rowley, J. T., & Mertens, T. E. (1998). Global epidemiology of sexually transmitted diseases. *The Lancet, 351*, S2-S4.

Gillaspie, D., Perkins, I., Larsen, K., McCord, A., Pangonis, S., Sweger, D., Seleem, M. N., Sriranganathan, N., & Anderson, B. E. (2009). Plasmid-Based System for High-Level Gene Expression and Antisense Gene Knockdown in Bartonella henselae. *Applied and Environmental Microbiology, 75*(16), 5434-5436.

Guédon, E., & Martin-Verstraete, I. (2007). Cysteine Metabolism and Its Regulation in Bacteria. In (pp. 195-218). Springer Berlin Heidelberg.

Hampton Research Solutions for Crystal Growth. *TCEP HCl*. Retrieved March, 2021, from https://hamptonresearch.com/uploads/support_materials/HR2-601-862_UG.pdf.

Hatzios, S. K., & Bertozzi, C. R. (2011). The Regulation of Sulfur Metabolism in Mycobacterium tuberculosis. *PLoS Pathogens, 7*(7), e1002036.

Hell, R., & Wirtz, M. (2002). Molecular Biology, Biochemistry and Cellular Physiology of Cysteine Metabolism in *Arabidopsis thaliana*. *The Arabadopsis Book*, 1-19.

Hicks, J. L., & Mullholland, C. V. (2018). Cysteine biosynthesis in Neisseria species. *Microbiology, 164*(12), 1471-1480.

Hill, S. A., Masters, T. L., & Watcher, J. (2016). Gonorrhea-an evolving disease of the new millennium. *Microbial Cell, 3*(9), 371-389.

Hipp, S. S., Lawton, W. D., Chen, N. C., & Gaafar, H. A. (1974). Inhibition of Neisseria gonorrhoeae by a factor produced by Candida albicans. *Applied microbiology, 27*(1), 192-196.

Hopper, S., Wilbur, J. S., Vasquez, B. L., Larson, J., Clary, S., Mehr, I. J., Seifert, H. S., & So, M. (2000). Isolation of Neisseria gonorrhoeaeMutants That Show Enhanced Trafficking across Polarized T84 Epithelial Monolayers. *Infection and Immunity, 68*(2), 896-905.

Hryniewicz, M. M., & Kredich, N. M. (1991). The cysP promoter of Salmonella typhimurium: characterization of two binding sites for CysB protein, studies of in vivo transcription initiation, and demonstration of the anti-inducer effects of thiosulfate. *Journal of Bacteriology, 173*(18), 5876-5886.

Huang, B., Vetting, M. W., & Roderick, S. L. (2005). The Active Site of O-Acetylserine Sulfhydrylase Is the Anchor Point for Bienzyme Complex Formation with Serine Acetyltransferase. *Journal of Bacteriology, 187*(9), 3201-3205.

Jean Kumar, V. U., Poyraz, Ö., Saxena, S., Schnell, R., Yogeeswari, P., Schneider, G., & Sriram, D. (2013). Discovery of novel inhibitors targeting the Mycobacterium tuberculosis O-acetylserine sulfhydrylase (CysK1) using virtual high-throughput screening. *Bioorganic & Medicinal Chemistry Letters, 23*(5), 1182-1186.

Jeelani, G., Sato, D., Soga, T., & Nozaki, T. (2017). Genetic, metabolomic and transcriptomic analyses of the de novo L-cysteine biosynthetic pathway in the enteric protozoan parasite Entamoeba histolytica. *Scientific Reports, 7*(1).

Jennison, A. V., Whiley, D., Lahra, M. M., Graham, R. M., Cole, M. J., Hughes, G., Fifer, H., Andersson, M., Edwards, A., & Eyre, D. (2019). Genetic relatedness of ceftriaxone-resistant and high-level azithromycin resistant Neisseria gonorrhoeae

cases, United Kingdom and Australia, February to April 2018. *Eurosurveillance, 24*(8).

Johnson, C. M., Roderick, S. L., & Cook, P. F. (2005). The serine acetyltransferase reaction: acetyl transfer from an acylpantothenyl donor to an alcohol. *Archives of Biochemistry and Biophysics, 433*(1), 85-95.

Joshi, P., Gupta, A., & Gupta, V. (2019). Insights into multifaceted activities of CysK for therapeutic interventions. *3 Biotech, 9*(2).

Jovanovic, M., Lilic, M., Savic, D. J., & Jovanovic, G. (2003). The LysR-type transcriptional regulator CysB controls the repression of hslJ transcription in Escherichia coli. *Microbiology, 149*(12), 3449-3459.

Kabsch, W. (2010). XDS. *Acta Crystallographica Section D Biological Crystallography, 66*(2), 125-132.

Kertesz, M. A. (2001). Bacterial transporters for sulfate and organosulfur compounds. *Research in Microbiology, 152*(3-4), 279-290.

Kidd, S., & Workowski, K. A. (2015). Management of Gonorrhea in Adolescents and Adults in the United States. *Clinical Infectious Diseases, 61*(suppl 8), S785-S801.

Korshunov, S., Imlay, K. R. C., & Imlay, J. A. (2020). Cystine import is a valuable but risky process whose hazardsEscherichia coliminimizes by inducing a cysteine exporter. *Molecular Microbiology, 113*(1), 22-39.

Kredich, N. M. (2008). Biosynthesis of Cysteine. *EcoSal Plus, 3*(1).

Kredich, N. M., Becker, M. A., & Tomkins, G. M. (1969). Purification and Characterization of Cysteine Synthetase, a Bifunctional Protein Complex, from Salmonella typhimurium. *Journal of Biological Chemistry, 244*(9), 2428-2439.

Kredich, N. M., & Tomkins, G. M. (1966). The Enzymic Synthesis of l-Cysteine in Escherichia coli and Salmonella typhimurium. *Journal of Biological Chemistry, 241*(21), 4955-4965.

Krissinel, E., & Henrick, K. (2007). Inference of macromolecular assemblies from crystalline state. *J Mol Biol, 372*(3), 774-97.

Kumar, S., Raj, I., Nagpal, I., Subbarao, N., & Gourinath, S. (2011). Structural and Biochemical Studies of Serine Acetyltransferase Reveal Why the Parasite Entamoeba histolytica Cannot Form a Cysteine Synthase Complex. *Journal of Biological Chemistry, 286*(14), 12533-12541.

Kumaran, S., Yi, H., Krishnan, H. B., & Jez, J. M. (2009). Assembly of the Cysteine Synthase Complex and the Regulatory Role of Protein-Protein Interactions. *Journal of Biological Chemistry, 284*(15), 10268-10275.

Kuske, C. R., Ticknor, L. O., Guzmán, E., Gurley, L. R., Valdez, J. G., Thompson, M. E., & Jackson, P. J. (1994). Purification and characterization of O-acetylserine sulfhydrylase isoenzymes from Datura innoxia. *Journal of Biological Chemistry, 269*(8), 6223-6232.

Kussell, E., Kishony, R., Balaban, N. Q., & Leibler, S. (2005). Bacterial Persistence. *Genetics, 169*(4), 1807-1814.

Landig, C. S., Hazel, A., Kellman, B. P., Fong, J. J., Schwarz, F., Agarwal, S., Varki, N., Massari, P., Lewis, N. E., Ram, S., & Varki, A. (2019). Evolution of the exclusively human pathogenNeisseria gonorrhoeae: Human-specific engagement of immunoregulatory Siglecs. *Evolutionary Applications, 12*(2), 337-349.

Larsen, B., & Monif, G. R. G. (2001). Understanding the Bacterial Flora of the Female Genital Tract. *Clinical Infectious Diseases, 32*(4), e69-e77.

Le Faou, A. (1984). Sulphur nutrition and metabolism in various species of Neisseria. *Annales de l'Institut Pasteur / Microbiologie, 135*(1, Supplement B), 3-11.

Lebedev, A. A., & Isupov, M. N. (2014). Space-group and origin ambiguity in macromolecular structures with pseudo-symmetry and its treatment with the programZanuda. *Acta Crystallographica Section D Biological Crystallography, 70*(9), 2430-2443.

Lee, R. S., Seemann, T., Heffernan, H., Kwong, J. C., Gonçalves Da Silva, A., Carter, G. P., Woodhouse, R., Dyet, K. H., Bulach, D. M., Stinear, T. P., Howden, B. P., & Williamson, D. A. (2018). Genomic epidemiology and antimicrobial resistance of Neisseria gonorrhoeae in New Zealand. *Journal of Antimicrobial Chemotherapy, 73*(2), 353-364.

Levy, N., Eiler, S., Pradeau-Aubreton, K., Maillot, B., Stricher, F., & Ruff, M. (2016). Production of unstable proteins through the formation of stable core complexes. *Nature Communications, 7*(1), 10932.

Lewis, K. (2010). Persister Cells. *Annual Review of Microbiology, 64*(1), 357-372.

Liang, J., Han, Q., Tan, Y., Ding, H., & Li, J. (2019). Current Advances on Structure-Function Relationships of Pyridoxal 5′-Phosphate-Dependent Enzymes. *Frontiers in Molecular Biosciences, 6*.

Libretexts. (2020a). *Sigmoid Kinetics* [Database]. https://chem.libretexts.org/@go/page/407.

Libretexts. (2020b). *Allosteric Interactions* [Database]. https://chem.libretexts.org/@go/page/41366.

Libretexts. (2020c). *Michaelis-Menten Kinetics* [Database]. https://chem.libretexts.org/@go/page/404.

Liu, X., Mosoian, A., Theresa, Zerhouni‐Layachi, B., Snyder, A., Gary, & Mary. (2006). Gonococcal Lipooligosaccharide Suppresses HIV Infection in Human Primary Macrophages through Induction of Innate Immunity. *The Journal of Infectious Diseases, 194*(6), 751-759.

Lochowska, A., Iwanicka-Nowicka, R., Zaim, J., Witkowska-Zimny, M., Bolewska, K., & Hryniewicz, M. M. (2004). Identification of activating region (AR) of Escherichia coli LysR-type transcription factor CysB and CysB contact site on RNA polymerase alpha subunit at the cysP promoter. *Molecular Microbiology, 53*(3), 791-806.

Madeira, F., Park, Y. M., Lee, J., Buso, N., Gur, T., Madhusoodanan, N., Basutkar, P., Tivey, A. R. N., Potter, S. C., Finn, R. D., & Lopez, R. (2019). The EMBL-EBI search and sequence analysis tools APIs in 2019. *Nucleic Acids Research, 47*(W1), W636-W641.

Maisonneuve, E., & Gerdes, K. (2014). Molecular Mechanisms Underlying Bacterial Persisters. *Cell, 157*(3), 539-548.

Matthews, B. W. (1968). Solvent content of protein crystals. *Journal of Molecular Biology, 33*(2), 491-497.

McCoy, A. J., Grosse-Kunstleve, R. W., Adams, P. D., Winn, M. D., Storoni, L. C., & Read, R. J. (2007). Phasercrystallographic software. *Journal of Applied Crystallography, 40*(4), 658-674.

McPhillips, T. M., McPhillips, S. E., Chiu, H. J., Cohen, A. E., Deacon, A. M., Ellis, P. J., Garman, E., Gonzalez, A., Sauter, N. K., Phizackerley, R. P., Soltis, S. M., & Kuhn, P. (2002). Blu-Ice and the Distributed Control System: software for data acquisition and instrument control at macromolecular crystallography beamlines. *J Synchrotron Radiat, 9*(Pt 6), 401-6.

Meister, A., & Anderson, M. E. (1983). Glutathione. *Annual Review of Biochemistry, 52*(1), 711-760.

Melnikova, D. L., Skirda, V. D., & Nesmelova, I. V. (2019). Effect of Reducing Agent TCEP on Translational Diffusion and Supramolecular Assembly in Aqueous Solutions of α-Casein. *The Journal of Physical Chemistry B, 123*(10), 2305-2315.

Mino, K., & Ishikawa, K. (2003). A novelO-phospho-L-serine sulfhydrylation reaction catalyzed byO-acetylserine sulfhydrylase fromAeropyrum pernixK1. *FEBS Letters, 551*(1-3), 133-138.

Mino, K., Yamanoue, T., Sakiyama, T., Eisaki, N., Matsuyama, A., & Nakanishi, K. (2000). Effects of Bienzyme Complex Formation of Cysteine Synthetase fromEscherichia colion Some Properties and Kinetics. *Bioscience, Biotechnology, and Biochemistry, 64*(8), 1628-1640.

Nozaki, T., Asai, T., Sanchez, L. B., Kobayashi, S., Nakazawa, M., & Takeuchi, T. (1999). Characterization of the Gene Encoding Serine Acetyltransferase, a Regulated Enzyme of Cysteine Biosynthesis from the Protist ParasitesEntamoeba histolyticaand Entamoeba dispar. *Journal of Biological Chemistry, 274*(45), 32445-32452.

Ochman, H., Lawrence, J. G., & Groisman, E. A. (2000). Lateral gene transfer and the nature of bacterial innovation. *Nature, 405*(6784), 299-304.

Oldham, K. (2020). *Cysteine biosynthesis and the role of CysE in Neisseria gonorrhoeae.* Masters thesis, The University of Waikato, Hamilton, New Zealand.

Ostrowski, J., & Kredich, N. M. (1989). Molecular characterization of the cysJIH promoters of Salmonella typhimurium and Escherichia coli: regulation by cysB protein and N-acetyl-L-serine. *Journal of Bacteriology, 171*(1), 130-140.

Ostrowski, J., & Kredich, N. M. (1991). Negative autoregulation of cysB in Salmonella typhimurium: in vitro interactions of CysB protein with the cysB promoter. *Journal of Bacteriology, 173*(7), 2212-2218.

Pinto, R., Leotta, L., Shanahan, E. R., West, N. P., Leyh, T. S., Britton, W., & Triccas, J. A. (2013). Host Cell–Induced Components of the Sulfate Assimilation Pathway Are Major Protective Antigens of Mycobacterium tuberculosis. *The Journal of Infectious Diseases, 207*(5), 778-785.

Poyraz, Ö., Jeankumar, V. U., Saxena, S., Schnell, R., Haraldsson, M., Yogeeswari, P., Sriram, D., & Schneider, G. (2013). Structure-Guided Design of Novel Thiazolidine Inhibitors of O-Acetyl Serine Sulfhydrylase from Mycobacterium tuberculosis. *Journal of Medicinal Chemistry, 56*(16), 6457-6466.

Quillin, S. J., & Seifert, H. S. (2018). Neisseria gonorrhoeae host adaptation and pathogenesis. *Nature Reviews Microbiology, 16*(4), 226-240.

Rabeh, W. M., & Cook, P. F. (2004). Structure and Mechanism of O-Acetylserine Sulfhydrylase. *Journal of Biological Chemistry, 279*(26), 26803-26806.

Ramsey, K. H., Schneider, H., Cross, A. S., Boslego, J. W., Hoover, D. L., Staley, T. L., Kuschner, R. A., & Deal, C. D. (1995). Inflammatory cytokines produced in response to experimental human gonorrhea. *J Infect Dis, 172*(1), 186-91.

Ramsey, M. E., Hackett, K. T., Kotha, C., & Dillard, J. P. (2012). New Complementation Constructs for Inducible and Constitutive Gene Expression in Neisseria gonorrhoeae and Neisseria meningitidis. *Applied and Environmental Microbiology, 78*(9), 3068-3078.

Reichau, S., Jiao, W., Walker, S. R., Hutton, R. D., Baker, E. N., & Parker, E. J. (2011). Potent Inhibitors of a Shikimate Pathway Enzyme from Mycobacterium tuberculosis. *Journal of Biological Chemistry, 286*(18), 16197-16207.

Remmele, C. W., Xian, Y., Albrecht, M., Faulstich, M., Fraunholz, M., Heinrichs, E., Dittrich, M. T., Müller, T., Reinhardt, R., & Rudel, T. (2014). Transcriptional landscape and essential genes of Neisseria gonorrhoeae. *Nucleic Acids Research, 42*(16), 10579-10595.

Ren, X., Eccles, D. A., Greig, G. A., Clapham, J., Wheeler, N. E., Lindgreen, S., Gardner, P. P., & Mackichan, J. K. (2017). Genomic, Transcriptomic, and Phenotypic Analyses of Neisseria meningitidis Isolates from Disease Patients and Their Household Contacts. *mSystems, 2*(6).

Robert, X., & Gouet, P. (2014). Deciphering key features in protein structures with the new ENDscript server. *Nucleic Acids Research, 42*(W1), W320-W324.

Rowley, J., Vander Hoorn, S., Korenromp, E., Low, N., Unemo, M., Abu-Raddad, L. J., Chico, R. M., Smolak, A., Newman, L., Gottlieb, S., Thwin, S. S., Broutet, N., & Taylor, M. M. (2019). Chlamydia, gonorrhoea, trichomoniasis and syphilis: global prevalence and incidence estimates, 2016. *Bulletin of the World Health Organization, 97*(8), 548-562P.

Rusniok, C., Vallenet, D., Floquet, S., Ewles, H., Mouzé-Soulama, C., Brown, D., Lajus, A., Buchrieser, C., Médigue, C., Glaser, P., & Pelicic, V. (2009). NeMeSys: a

biological resource for narrowing the gap between sequence and function in the human pathogen Neisseria meningitidis. *Genome Biology, 10*(10), R110.

Saito, K., Yokoyama, H., Noji, M., & Murakoshi, I. (1995). Molecular Cloning and Characterization of a Plant Serine Acetyltransferase Playing a Regulatory Role in Cysteine Biosynthesis from Watermelon. *Journal of Biological Chemistry, 270*(27), 16321-16326.

Sajed, T., Marcu, A., Ramirez, M., Pon, A., Guo, A. C., Knox, C., Wilson, M., Grant, J. R., Djoumbou, Y., & Wishart, D. S. (2016). ECMDB 2.0: A richer resource for understanding the biochemistry ofE. coli. *Nucleic Acids Research, 44*(D1), D495-D501.

Salsi, E., Bayden, A. S., Spyrakis, F., Amadasi, A., Campanini, B., Bettati, S., Dodatko, T., Cozzini, P., Kellogg, G. E., Cook, P. F., Roderick, S. L., & Mozzarelli, A. (2010). Design ofO-Acetylserine Sulfhydrylase Inhibitors by Mimicking Nature. *Journal of Medicinal Chemistry, 53*(1), 345-356.

Salsi, E., Guan, R., Campanini, B., Bettati, S., Lin, J., Cook, P. F., & Mozzarelli, A. (2011). Exploring O-acetylserine sulfhydrylase-B isoenzyme from Salmonella typhimurium by fluorescence spectroscopy. *Archives of Biochemistry and Biophysics, 505*(2), 178-185.

Sandstrom, I. (1987). Etiology and Diagnosis of Neonatal Conjunctivitis. *Acta Paediatrica, 76*(2), 221-227.

Schnell, R., Oehlmann, W., Singh, M., & Schneider, G. (2007). Structural Insights into Catalysis and Inhibition of O-Acetylserine Sulfhydrylase from Mycobacterium tuberculosis. *Journal of Biological Chemistry, 282*(32), 23473-23481.

Schurr, J. M., & Schmitz, K. S. (1976). Orientation constraints and rotational diffusion in bimolecular solution kinetics. A simplification. *The Journal of Physical Chemistry, 80*(17), 1934-1936.

Seib, K. L., Wu, H.-J., Kidd, S. P., Apicella, M. A., Jennings, M. P., & McEwan, A. G. (2006). Defenses against Oxidative Stress in Neisseria gonorrhoeae: a System Tailored for a Challenging Environment. *Microbiology and Molecular Biology Reviews, 70*(2), 344-361.

Sekowska, A., Kung, H. F., & Danchin, A. (2000). Sulfur metabolism in Escherichia coli and related bacteria: facts and fiction. *J Mol Microbiol Biotechnol, 2*(2), 145-77.

Simons, M. P., Nauseef, W. M., & Apicella, M. A. (2005). Interactions of Neisseria gonorrhoeae with Adherent Polymorphonuclear Leukocytes. *Infection and Immunity, 73*(4), 1971-1977.

Spyrakis, F., Singh, R., Cozzini, P., Campanini, B., Salsi, E., Felici, P., Raboni, S., Benedetti, P., Cruciani, G., Kellogg, G. E., Cook, P. F., & Mozzarelli, A. (2013). Isozyme-Specific Ligands for O-acetylserine sulfhydrylase, a Novel Antibiotic Target. *PLoS ONE, 8*(10), e77558.

Stern, A., Brown, M., Nickel, P., & Meyer, T. F. (1986). Opacity genes in Neisseria gonorrhoeae: control of phase and antigenic variation. *Cell, 47*(1), 61-71.

Stevens, R., Stevens, L., & Price, N. C. (1983). The Satbilities of Various Thiol Compounds used in Protein Purifications. *Biochemical Education 11*(2), 70.

Stipanuk, M. H., Dominy, J. E., Lee, J.-I., & Coloso, R. M. (2006). Mammalian Cysteine Metabolism: New Insights into Regulation of Cysteine Metabolism. *The Journal of Nutrition, 136*(6), 1652S-1659S.

Tai, C.-H., Burkhard, P., Gani, D., Jenn, T., Johnson, C., & Cook, P. F. (2001). Characterization of the Allosteric Anion-Binding Site ofO-Acetylserine Sulfhydrylase†. *Biochemistry, 40*(25), 7446-7452.

Tai, C. H., Nalabolu, S. R., Jacobson, T. M., Minter, D. E., & Cook, P. F. (1993). Kinetic mechanisms of the A and B isozymes of O-acetylserine sulfhydrylase from Salmonella typhimurium LT-2 using the natural and alternate reactants. *Biochemistry, 32*(25), 6433-6442.

Takahashi, H., Watanabe, H., Kim, K. S., Yokoyama, S., & Yanagisawa, T. (2018). The Meningococcal Cysteine Transport System Plays a Crucial Role in Neisseria meningitidis Survival in Human Brain Microvascular Endothelial Cells. *mBio, 9*(6).

Takumi, K., & Nonaka, G. (2016). Bacterial Cysteine-Inducible Cysteine Resistance Systems. *Journal of Bacteriology, 198*(9), 1384-1392.

Tanous, C., Soutourina, O., Raynal, B., Hullo, M. F., Mervelet, P., Gilles, A. M., Noirot, P., Danchin, A., England, P., & Martin-Verstraete, I. (2008). The CymR regulator in complex with the enzyme CysK controls cysteine metabolism in Bacillus subtilis. *J Biol Chem, 283*(51), 35551-60.

Terwilliger, T. C., Grosse-Kunstleve, R. W., Afonine, P. V., Moriarty, N. W., Zwart, P. H., Hung, L.-W., Read, R. J., & Adams, P. D. (2008). Iterative model building, structure refinement and density modification with thePHENIX AutoBuildwizard. *Acta Crystallographica Section D Biological Crystallography*, *64*(1), 61-69.

Thermo Fisher Scientific. (2013). *Instructions Pierce Premium Grade TCEP.HCl* [Online database]. https://www.thermofisher.com/document-connect/document-connect.html?url=https%3A%2F%2Fassets.thermofisher.com%2FTFS-Assets%2FLSG%2Fmanuals%2FMAN0011879_Pierce_PremGrade_TCEP_HCl_UG.pdf&title=VXNlciBHdWlkZTogIFBpZXJjZSBQcmVtaXVtIEdyYWRlIFRDRVAgSENs.

Turnbull, A. L., & Surette, M. G. (2010). Cysteine biosynthesis, oxidative stress and antibiotic resistance in Salmonella typhimurium. *Research in Microbiology, 161*(8), 643-650.

Ulusu, N. N. (2015). Evolution of Enzyme Kinetic Mechanisms. *Journal of Molecular Evolution, 80*(5-6), 251-257.

Unemo, M., Ross, J., Serwin, A. B., Gomberg, M., Cusini, M., & Jensen, J. S. (2020). 2020 European guideline for the diagnosis and treatment of gonorrhoea in adults. *Int J STD AIDS*, 956462420949126.

Unemo, M., & Shafer, W. M. (2014). Antimicrobial Resistance in Neisseria gonorrhoeae in the 21st Century: Past, Evolution, and Future. *Clinical Microbiology Reviews, 27*(3), 587-613.

Vagenende, V., Yap, M. G. S., & Trout, B. L. (2009). Mechanisms of Protein Stabilization and Prevention of Protein Aggregation by Glycerol. *Biochemistry, 48*(46), 11084-11096.

Wang, T., & Leyh, T. S. (2012). Three-stage Assembly of the Cysteine Synthase Complex from Escherichia coli. *Journal of Biological Chemistry, 287*(6), 4360-4367.

Wang, Z., Rejtar, T., Zhou, Z. S., & Karger, B. L. (2010). Desulfurization of cysteine-containing peptides resulting from sample preparation for protein characterization by mass spectrometry. *Rapid Communications in Mass Spectrometry, 24*(3), 267-275.

WHO. (2017). *World Health Organisation (WHO) Global Priority List of Antibiotic-Resistant Bacteria to Guide Research, Discovery, and Development of New Antibiotics*. from https://www.who.int/medicines/publications/WHO-PPL-Short_Summary_25Feb-ET_NM_WHO.pdf.

Wi, T., Lahra, M. M., Ndowa, F., Bala, M., Dillon, J.-A. R., Ramon-Pardo, P., Eremin, S. R., Bolan, G., & Unemo, M. (2017). Antimicrobial resistance in Neisseria gonorrhoeae: Global surveillance and a call for international collaborative action. *PLOS Medicine, 14*(7), e1002344.

Winn, M. D., Ballard, C. C., Cowtan, K. D., Dodson, E. J., Emsley, P., Evans, P. R., Keegan, R. M., Krissinel, E. B., Leslie, A. G. W., McCoy, A., McNicholas, S. J., Murshudov, G. N., Pannu, N. S., Potterton, E. A., Powell, H. R., Read, R. J., Vagin, A., & Wilson, K. S. (2011). Overview of theCCP4 suite and current developments. *Acta Crystallographica Section D Biological Crystallography, 67*(4), 235-242.

Wirtz, M., Beard, K. F. M., Lee, C. P., Boltz, A., Schwarzländer, M., Fuchs, C., Meyer, A. J., Heeg, C., Sweetlove, L. J., Ratcliffe, R. G., & Hell, R. (2012). Mitochondrial Cysteine Synthase Complex Regulates O-Acetylserine Biosynthesis in Plants. *Journal of Biological Chemistry, 287*(33), 27941-27947.

Wirtz, M., & Hell, R. (2006). Functional analysis of the cysteine synthase protein complex from plants: Structural, biochemical and regulatory properties. *Journal of Plant Physiology, 163*(3), 273-286.

Workowski, K. A., & Berman, S. M. (2011). Centers for Disease Control and Prevention Sexually Transmitted Disease Treatment Guidelines. *Clinical Infectious Diseases, 53*(suppl_3), S59-S63.

Yi, H., Dey, S., Kumaran, S., Lee, S. G., Krishnan, H. B., & Jez, J. M. (2013). Structure of Soybean Serine Acetyltransferase and Formation of the Cysteine Regulatory Complex as a Molecular Chaperone. *Journal of Biological Chemistry, 288*(51), 36463-36472.

Zhao, C., Moriga, Y., Feng, B., Kumada, Y., Imanaka, H., Imamura, K., & Nakanishi, K. (2006). On the interaction site of serine acetyltransferase in the cysteine synthase complex from Escherichia coli. *Biochemical and Biophysical Research Communications, 341*(4), 911-916.

Appendices

Appendix A: Cloning information for CysK

A.1 Sequences for CysK (NGO_0340)

CysK (NGO_0340) *Neisseria gonorrhoeae (strain ATCC 700825/FA 1090) location*

CysK FA 1090 nucleotide sequence NC_022240.1 (334792..335724)

ATGAAAATTGCAAACAGCATCACCGAATTGATCGGCAACACGCCTTTGGTC
AAACTGAACCGTTTGACCAAAGGTTTGAAGGCAGAGGTTGCCGTGAAACTG
GAATTTTTTAATCCGGGCAGCAGCGTCAAAGACCGCATTGCCGAAGCAATG
ATCGAGGCCGCCGAAAAAGCGGGAAAAATCAACAAAAACACCGTCATTGT
CGAAGCAACCAGCGGCAATACGGGTATCGGTTTGGCAATGGTATGTGCCGC
ACGCGGCTACAAACTGGCGATTACCATGCCGGAAAGCATGAGCAAAGAGC
GCAAAATGCTGTTGCGCACGTTTGGCGCGGAACTGATTCTAACCCCCGCCGC
CGAAGGTATGGCGGGCGCGATTGCCAAAGCGCAATCCTTGGTGGACGCTCA
TCCAGACACTTATTTTATGCCGCGCCAGTTCGACAATGAGGCAAATCCCGAA
GTCCACCGCAAAACAACCGCCGAGGAAATTTGGAACGATACCGACGGTAAA
GTCGATGTCTTCGTTGCCGGCGTCGGCACGGGCGGTACGATTACCGGCGTG
GGCGAAGTATTGAAAAAATACAAACCCGAAGTTAAAGTGGTTGCCGTCGAG
CCTGAGGCTTCCCCCGTATTGAGCGGCGGCGAAAAAGGCCCGCACCCGATT
CAAGGTATCGGCGCAGGTTTTATTCCGACCGTTTTGAATACCAAAATCTACG
ACAGCATTGCCAAAGTGCCGAACGAAGCGGCTTTTGAAACCGCCCGTGCAA
TGGCGGAAAAAGAAGGCATTTTGGCGGGCATTTCTTCCGGTGCGGCGGTTT
GGAGCGCGTTGCAGCTTGCCAAACAGCCTGAAAACGAAGGCAAGCTGATAG
TCGTGCTGCTGCCTTCTTATGGCGAACGCTATCTCTCTACGCCACTTTTTGCA
GATTTGGCATAA

CysK peptide sequence. C-terminal HexaHis-tag (underlined) 318 residues. 32.726/62.862 kDa (monomer/dimer)

MKIANSITELIGNTPLVKLNRLTKGLKAEVAVKLEFFNPGSSVKDRIAEAMIEAA
EKAGKINKNTVIVEATSGNTGIGLAMVCAARGYKLAITMPESMSKERKMLLRT
FGAELILTPAAEGMAGAIAKAQSLVDAHPDTYFMPRQFDNEANPEVHRKTTAE
EIWNDTDGKVDVFVAGVGTGGTITGVGEVLKKYKPEIEVCAVEAGASPVLSGG
EKGPHPIQGIGAGFIPTVLNTKIYDSIAKVPNEAAFETARAMAEKEGILAGISSGA
AVWSALQLAKQPENEGKLIVVLLPSYGERYLSTPLFADLALEHHHHHH

pET28b description

Table 4.1: Description of the pET28b Vector

Vector	Description
pET28b	*E. coli* expression vector, 5368 bps, N-terminal thrombin cleavage site, Kanamycin resistance, C and N-terminal His-tags, T7-promoter.

GMO approval numbers:

E. coli: GMD101146

N. gonorrhoeae: GMD102338

A.2 Luria Bertani (LB) Agar (1 L)

Combine the following:

5 g Peptone

10 g NaCl

5 g Yeast extract

5 g Agar

1 L of distilled water

Autoclave at 121°C before use.

LB Broth

Same method as LB agar, but no addition of agar.

Appendix B: Protein purification, assay and kinetic information

B.1 Purification buffers for CysK kinetics (Potassium phosphate)

Table 4.2: Purification buffers for CysK kinetics (Potassium phosphate)

	Chemical composition
Lysis buffer	50 mM Potassium phosphate (pH 8.0/7.0) 200 mM NaCl 20 mM Imidazole
Elution buffer	50 mM Potassium phosphate (pH 8.0/7.0) 200 mM NaCl 1 M Imidazole
Gel filtration buffer	50 mM Potassium phosphate (pH 8.0/7.0) 100 mM NaCl

B.2 Purification buffers for CysK crystallography (Tris)

Table 4.3: Purification buffers for CysK crystallography (Tris)

	Chemical composition
Lysis buffer	50 mM Tris (pH 8.0) 200 mM NaCl 20 mM Imidazole
Elution buffer	50 mM Tris (pH 8.0) 200 mM NaCl 1 M Imidazole
Gel filtration buffer	50 mM Tris (pH 8.0) 100 mM NaCl

BioEnrich 650 SEC Calibration Curve

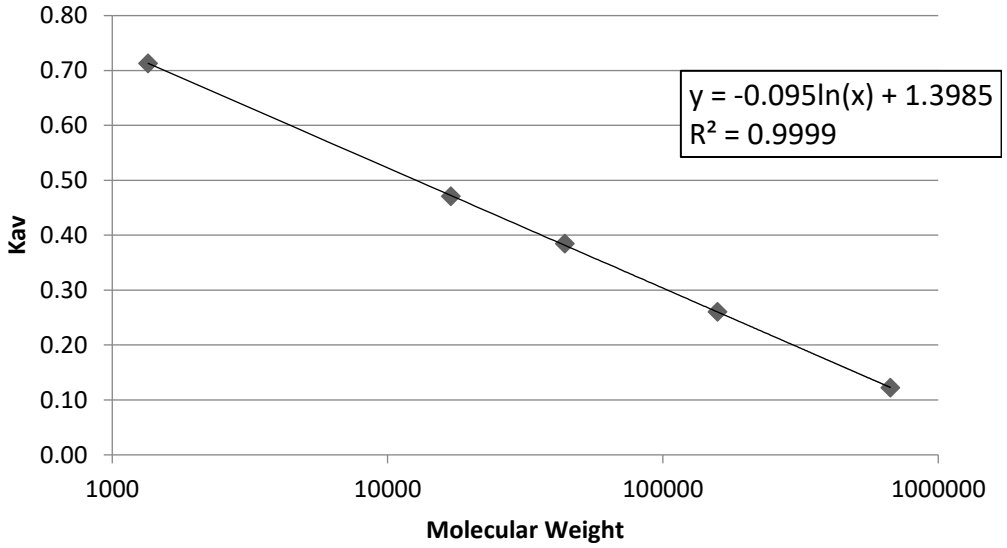

Figure 4.2: Calibration curve of the gel filtration BioEnrich 650 column

L-cysteine Standard Curve

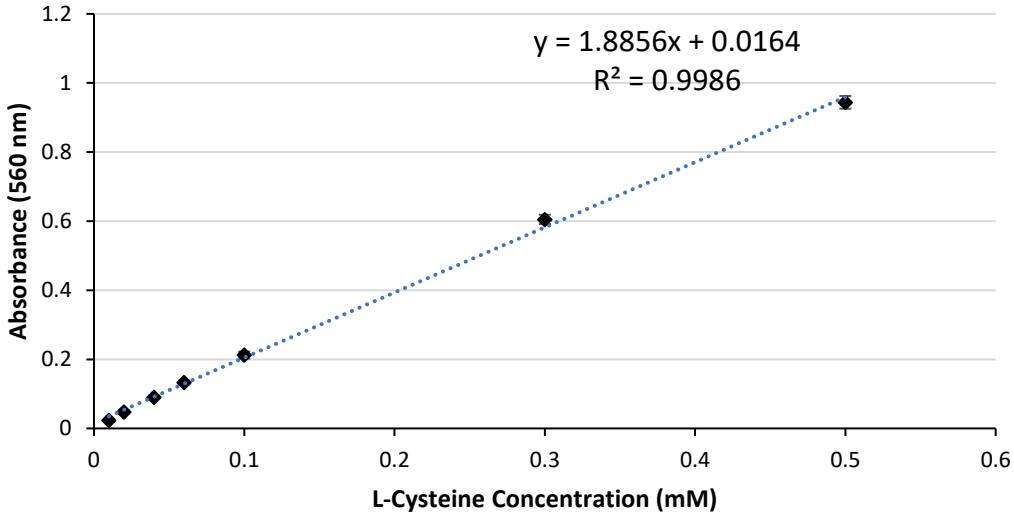

Figure 4.3: L-cysteine standard curve

B.3 SDS-PAGE gel buffer compositions

Quenching buffer (Q4)

250 mM Tris (pH 6.8)

20% glycerol (w/v)

4% SDS (w/v)

10% beta-2-mercaptoethanol (w/v)

0.025% bromophenol blue (w/v)

Tris-glycine SDS buffer

25 mM Tris (pH 8.5)

250 mM glycine

0.1% SDS (w/v)

Fairbanks staining solution

0.05% coomasie blue

25% isopropanol

10% acetic acid

Destaining solution

10% acetic acid

B.4 Required reagents and kinetic assay reagent compositions

***O*-acetylserine (50 mM)**

91.8 mg *O*-acetyl-L-serine hydrochloride

10 ml MQH_2O

***O*-acetylserine (5 mM)**

1 ml *O*-acetylserine (50 mM)

9 ml MQH_2O

Sodium sulphide (50 mM)

71.01 mg Sodium sulphide

10 ml MQH_2O

Sodium sulphide (5 mM)

1 ml Sodium sulphide (50 mM)

9 ml MQH_2O

Sodium thiosulphate (100 mM)

158.11 g

10 ml MQH_2O

Appropriate dilutions were made

Acid Ninhydrin Reagent

250 mg Ninhydrin

6 ml Glacial acetic acid

4 ml Concentrated hydrochloric acid (10 M)

Trichloroacetic acid (20% v/v)

2 g Trichloroacetic acid

10 ml MQH_2O

PLP (Pyridoxal 5'-phopshate, 2mM)

4.94 mg PLP

10 ml MQH_2O

MOPs buffer (100mM, pH 7)

2.093 g MOPs

Make up to 10 ml MQH_2O

DTT (Dithiothreitol)

308.5 mg DTT

Make up to 10 ml with MOPs buffer

pH to 7 with NaOH

CysE C-terminus tail four peptide inhibitor (3820 pmol, 2 mg.ml^{-1})

2 mg CysE four peptide tail

1 ml Potassium phosphate gel filtration buffer

CysE C-terminus tail four peptide inhibitor (382 pmol, 0.2 mg.ml^{-1})

20 µL of 2 mg.ml^{-1} CysE C-terminus four tail four peptide inhibitor

180 µL Potassium phosphate gel filtration buffer

CysE C-terminus tail four peptide inhibitor (38.2 pmol, 0.02 mg.ml^{-1})

20 µL of 0.2 mg.ml^{-1} CysE C-terminus four tail four peptide inhibitor

180 µL Potassium phosphate gel filtration buffer

CysE C-terminus tail four peptide inhibitor (3.82 pmol, 0.002 mg.ml^{-1})

20 µL of 0.02 mg.ml^{-1} CysE C-terminus four tail four peptide inhibitor

180 µL Potassium phosphate gel filtration buffer

L-cysteine (50mM)

60.58 mg L-cysteine

10 ml MQ H_2O

pH to 2.0

L-cysteine (5 mM)

1 ml of 50mM L-cysteine

9 ml MQ H_2O

B.5 Raw assay data

Link to google drive folder:

https://drive.google.com/drive/folders/1ONR57u5S94uNSaFrP2WISeVSQkyPOuAE?usp=sharing

Appendix C: PCR and Gene Knockouts

Agarose gel

50 µl 1xTAE Buffer

0.5 g Agarose

Microwave (30 second bursts till dissolved)

Cool with running water over flask

4 µl Red Safe Stain

Pour into OWL electrophoresis gel caster (ThermoFisher Scientific)

TAE Buffer (50x)

242 g Tris-base

700 ml MQ H_2O

57 ml 100% glacial acetic acid

100 ml 0.5 M EDTA (pH 8.0)

Make up to 1 L with MQ H_2O

TAE Buffer (1x)

50 ml of 50x TAE buffer

Make up to 1 L with MQ H_2O

EDTA (0.5 M)

93.05 g EDTA disodium salt

400 ml MQ H_2O

pH to 8.0 with NaOH

Make up to 500 ml with MQ H_2O

DNA loading buffer (6x)

3ml 30% (v/v) Glycerol

25mg 0.25% (w/v) Bromophenol Blue

25mg 0.25% (w/v) Xylene Cyanol FF

Make up to 10ml with MQ water

GCB Plate

36.25 g GCBase

1.25 g Agar

1 L MQ H_2O

Split into two 500 ml Schott bottles

Autoclaved

500 µl of 50 $mg.ml^{-1}$ kanamycin added to one Schott bottle

Poured into petri dishes and set for ~20 mins

Set plates stored at 4º C

Invitrogen 1kb+ DNA ladder

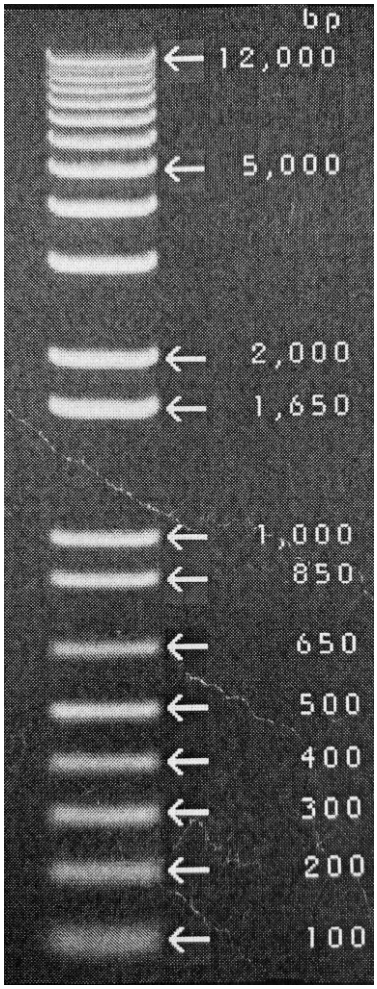

Figure 4.4: Invitrogen 1kb+ DNA ladder used in agarose gel

Appendix D: Crystallisation and Structure solving information

D.1 Contents of the asymmetric unit for CysK

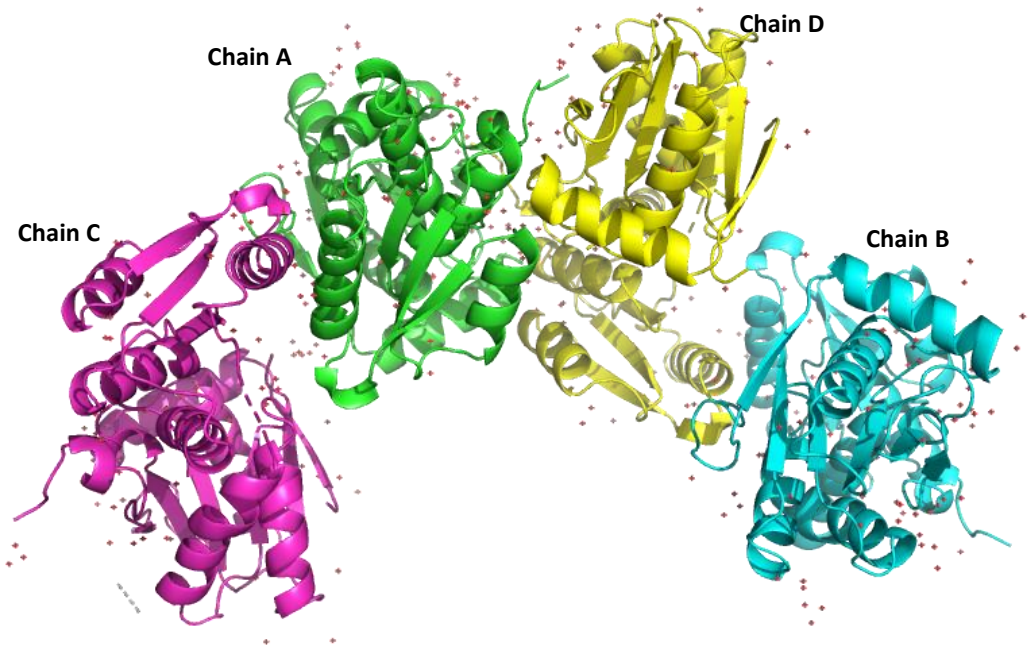

Figure 4.5: Contents of the asymmetric unit for CysK model. Space group $P12_11$. Waters are seen as red crosses. Figure generated in PyMOL.

D.2 Initial input settings for *phenix.autobuild*

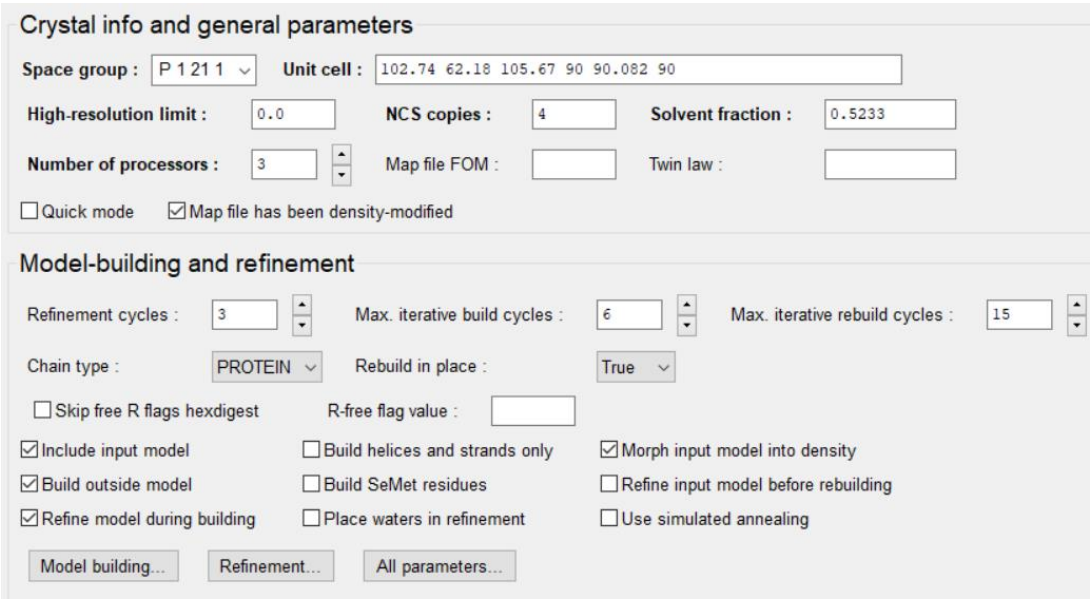

Figure 4.6: Screenshot of initial input settings for *phenix.autobuild* used for building the model of CysK

D.3 Final input settings for *phenix.autobuild*

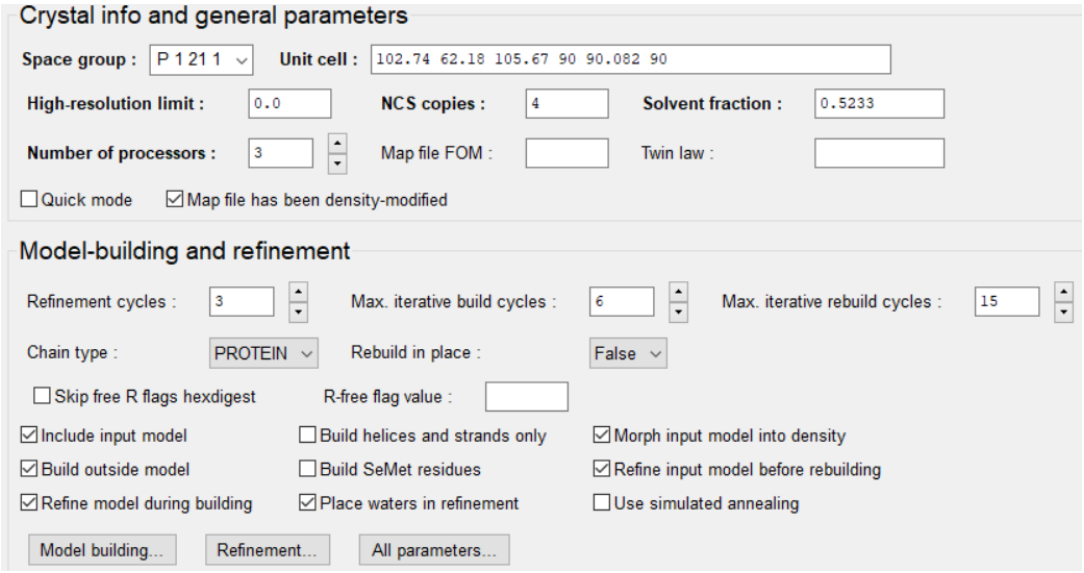

Figure 4.7: Screenshot of initial input settings for *phenix.autobuild* used for building the final model of CysK

D.4 CysK structural files

Link to google drive folder:

https://drive.google.com/drive/folders/1ONR57u5S94uNSaFrP2WISeVSQkyPOuAE?usp=sharing

D.5 CysK chain statistics

Table 4.4: CysK structure statistics for each monomer in the ASU.

Chain	Residue chain built	Residues missing	Total built
A	Ile3-Pro143 Ala150-Glu204 Pro230-Tyr296	51	261/312
B	Ile3-Pro143 Asn151-Glu204 Pro230-Tyr296	52	260/312
C	Ile3-Pro143 Asn151-Gly206 Tyr238-Leu292	64	248/312
D	Ile3-Pro143 Asn151-Ala207 Tyr238-Tyr296	63	249/312